

CPT PaGE

USER'S MANUAL – CPT Interpretation and use

by

S. Stacul, I. Giusti & D. Lo Presti

SUMMARY

1	INTRODUCTION	3
2	INTERPRETATION OF CONTINUOUS MEASUREMENTS	4
2.1	Soil Profile.....	7
2.2	Soil Parameters.....	10
2.3	Output files	13
3	INTERPRETATION OF DISCONTINUOUS MEASUREMENTS	15
3.1	Dissipation tests.....	15
3.1.1	Input file, analysis process and results for the Dissipation Test Module.....	17
3.2	Body wave velocity measurements	18
3.2.1	Input files and analysis process for the S-Waves module.....	18
3.2.2	Output files for the S-Waves module.....	21
3.2.3	Input files and analysis process for the P-Waves Module	21
3.2.4	Output files for the P-Waves module.....	22
4	DESIGN WITH CPT	23
4.1	Liquefaction risk analysis.....	23
4.1.1	Computation of FS_L (Boulanger & Idriss, 2015)	23
4.1.2	Computation of FS_L (Robertson & Wride, 1998)	25
4.1.3	Input data to perform the liquefaction risk analysis.....	26
4.1.4	Output of the liquefaction risk analysis module	26
4.2	Bearing capacity of piles (axial loads)	27
4.2.1	Driven Steel-pipes.....	27
4.2.2	Bored Piles in granular soils (sands).....	31
4.2.3	Load-Settlement curve for the single pile	32
4.2.4	Input data to perform the pile analyses (Driven and Bored Piles)	33
4.2.5	Output of the Driven Piles and Bored Piles modules.....	33
4.3	Settlements of shallow foundations on granular soils	34
4.3.1	Input data to perform the settlement analysis for shallow foundations	35
4.3.2	Output of the Shallow Foundation module	36
5	SPECIAL ISSUES	36
5.1	Small Strain Damping Ratio from Seismic Measurements.....	36
5.2	Unusual soils	37
5.2.1	Input data to estimate the soil effective stress state of shallow layers using a target I_c (1 st method)	39
5.2.2	Output (1 st method)	40
5.2.3	Input data to apply an I_c correction using an available $\Delta I_c(q_t)$ function (2nd method).....	40

5.2.4	Output (2 nd method)	41
5.3	Liquefaction potential from CPTm	41
5.3.1	Computation of FS _L from CPTm (Juang et al., 2006)	41
6	REFERENCE LIST	44
7	ANNEXES:.....	48
7.1	VERIFICATION OF EMPIRICAL EQUATIONS FOR OCR	48
7.2	Lo Presti et al. (2017) – KL in 2017 ICCE – Use in practice of seismic tests.....	51
7.3	Lo Presti et al. (2016) - CPTu in unusual soil.....	51
7.4	Meisina et al. (2017) in 2017 ICCE – Liquefaction risk analysis with mechanical CPT ...	51

1 INTRODUCTION

Various codes are available for the interpretation of both mechanical (CPTm) and piezocone (CPTU) data (i.e. Geostru, 2017; Geologismiki, 2009).

The main peculiarities of this program can be summarised as follows:

- a huge database was used to check the correctness of various interpretation methods. The inferred parameters were compared against those obtained (in the same sites) from laboratory tests. Consequently, the program does not contain all possible approaches but only those that were positively verified;
- as for the liquefaction risk, there is a proliferation of methods. The main problem, is the potential mixing of these methods by the users. This would introduce an additional undesirable bias. This program utilises two methods in their integral and original form. Moreover, the LPI is computed according to its original formulation;
- there is a general disagreement about the use of mechanical CPT (CPTm) for liquefaction risk analysis. Anyway, in many countries, like Italy, huge database exists of CPTm. Therefore, a method is proposed to correct CPTm data so that it is possible to obtain similar safety factors as from CPTU. The method was verified by comparing pairs of CPTm and CPTU carried at close distance from each other;
- interpretation of CPTm is restricted to soil profile and liquefaction risk analysis;
- as for the seismic measurements, the small strain damping ratio is evaluated by means of the Spectral Slope method. S wave velocities are obtained by applying the cross – correlation method. P wave velocities are obtained by considering the peak to peak time delay;
- for those deposits (above the water table), whose effective stress state is controlled by suction, the program gives the possibility of empirically determining the soil suction. The method applies only to homogeneous layers of fine-grained soils.

2 INTERPRETATION OF CONTINUOUS MEASUREMENTS

Pagani Piezocone, gives, as usually, measurements of the tip resistance (q_c), sleeve friction (f_s), dynamic pore pressure (u_2 – measured behind the tip) and deviation from the verticality (tilt angle) every two cm of penetration. The actual penetration rate is also available. As for CPTm, only q_c and f_s are available. The above measurements are called “raw data”. The first step is to upload and plot raw data.

As for CPTu the input file is a comma-separated values (.csv) file. Such a file consists of four columns:

column 1: Depth [cm]
column 2: Tip resistance [MPa]
column 3: Sleeve friction [kPa]
column 4: Pore water pressure [kPa]

You can find an example of a .csv file required to perform a CPTu interpretation in the “Example” folder.

As for CPTm the input file is a comma-separated values (.csv) file. Such a file consists of three columns:

column 1: Depth [cm]
column 2: Tip resistance [MPa]
column 3: Sleeve friction [kPa]

You can find an example of a .csv file of a CPTm in the “Example” folder. CPTm data can be used only to perform a liquefaction risk analysis as described in sections 4.1 and 5.3. Interpretation of CPTm for soil profile and parameter is not included.

The program can read only numerical data. Therefore, before uploading the data - file, it is necessary to specify the number of rows containing alphanumeric characters in order to skip these rows. The N_{kt} Bearing Capacity factor, the water table depth, the Tip net area ratio (a_n) and the Sleeve net ratio (b_n) of the cone are given in the main Tab ‘Data Profiles’. The default values of N_{kt} , a_n and b_n are 14, 0.80 and 0.008 respectively.

Then upload the raw data selecting ‘Input CSV’ in the menu bar and clicking on the ‘Load CPTu DATA’ button.

Once loaded the input file you can press the button “Verify Input” in the main Tab “Data Profiles”. The command “Verify Input” controls that input data are written correctly. To plot the raw data, press the “Plot Input Data Profiles” button (Figure 1).

As a first elaboration the total tip resistance and total sleeve friction are computed according to the following equations:

$$q_t = q_c + (1 - a_n) u_2$$
$$f_t = f_s - b_n u_2$$

where: a_n = tip net area ratio; b_n = sleeve net ratio. These parameters are obtained, for each piezocone, by calibration in a triaxial cell (Pagani 2017). By default, the following values are used: $a_n = 0.80$ $b_n = 0.008$. Anyway, used correlations mainly refer to f_s than to f_t .

Total and effective vertical stresses are computed according to the following equations:

$$\sigma_{VO} = \sum \gamma_{ii} \cdot \Delta z_i$$
$$\sigma'_{VO} = \sigma_{VO} - u_o$$

$$u_o = \gamma_w (z - z_w)$$

where: γ_t (total unit weight of the soil) is obtained by means of the correlation shown later on; $\gamma_w = 10 \text{ kN/m}^3$ (unit weight of water) by default. The water table depth (from ground level) is given by z_w .

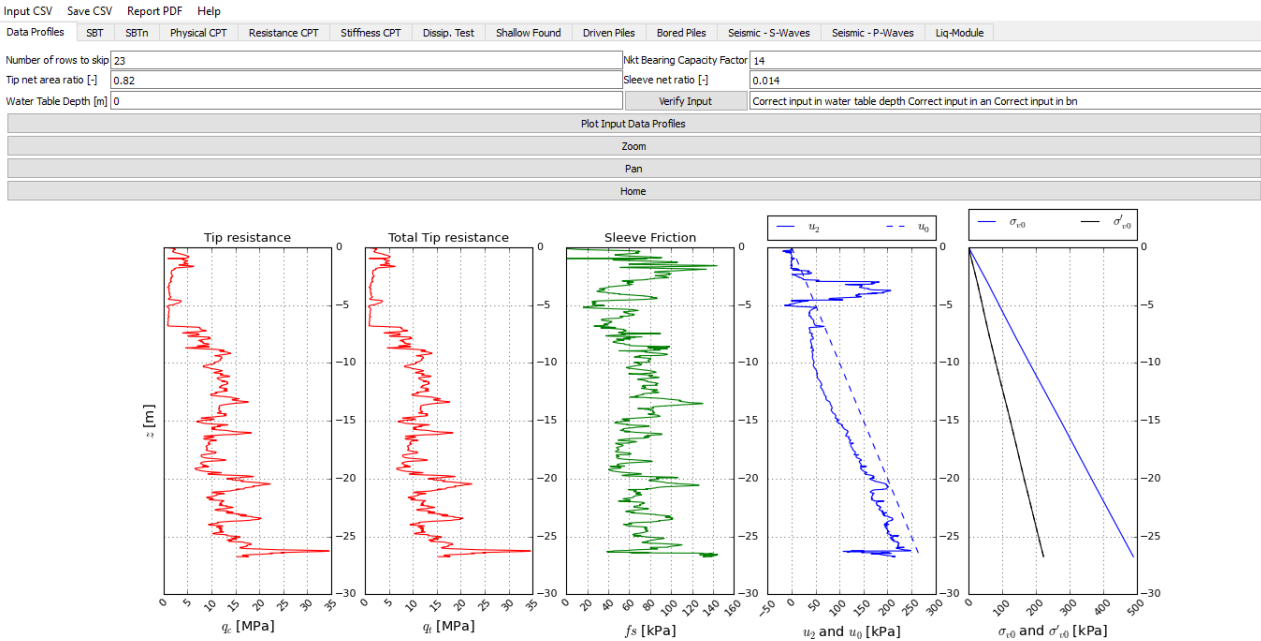


Figure 1. “Input Data Profiles Tab”

In the next Tabs “SBT” (Figure 2), “SBTn” (Figure 3), “Physical CPT” (Figure 4), “Resistance CPT” (Figure 5), “Stiffness CPT” (Figure 6) the user can plot the results of the CPTu interpretation pressing the “Plot ...” button in each tab. The soil classification methods and the set of correlations used to obtain the parameters in these Tabs are fully described in the following two sections (2.1 Soil Profile and 2.2 Soil parameters).

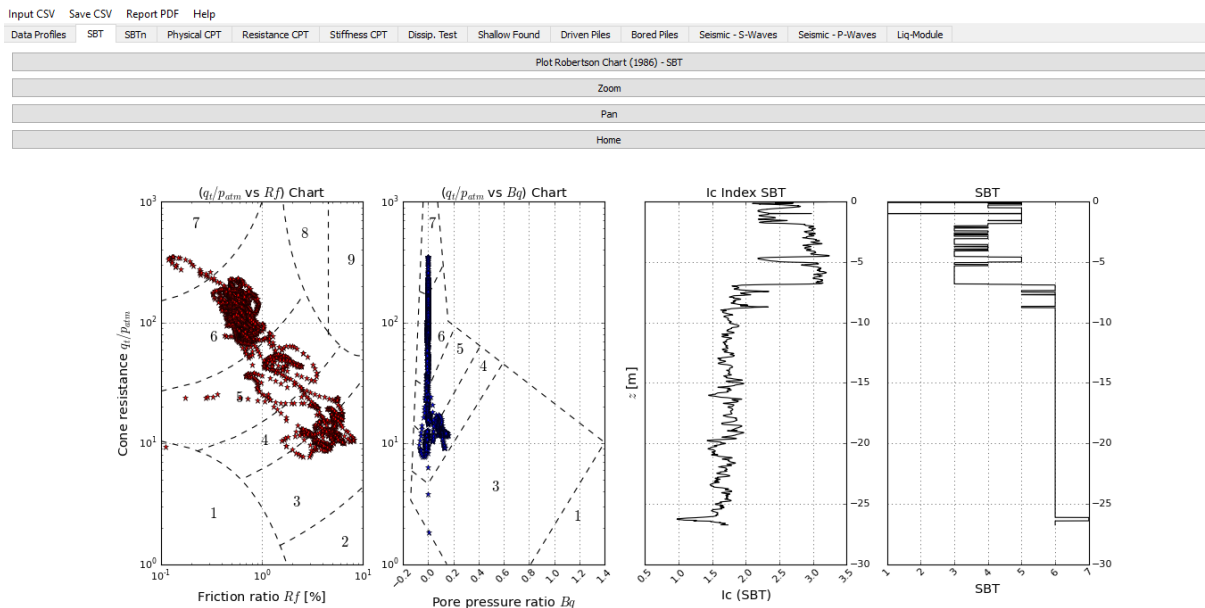


Figure 2. “SBT (Robertson 1986 – Updated by Robertson 2010) Classification Tab”

Input CSV Save CSV Report PDF Help

Data Profiles SBT SBTn Physical CPT Resistance CPT Stiffness CPT Dissip. Test Shallow Found Driven Piles Bored Piles Seismic - S-Waves Seismic - P-Waves Liq-Module

Method [1] I_c target 0 Correction up to depth [m] 0 Apply Method [1]

Method = $a1+a2/qz$ [2] $a1$ 0.05 $a2$ 0.75 Apply Method [2]

Method = $a1*qt^a2$ [2] $a1$ 0 $a2$ 0 Apply Method [2]

Plot Robertson Chart (1990) - SBTn

Zoom

Pan

Home

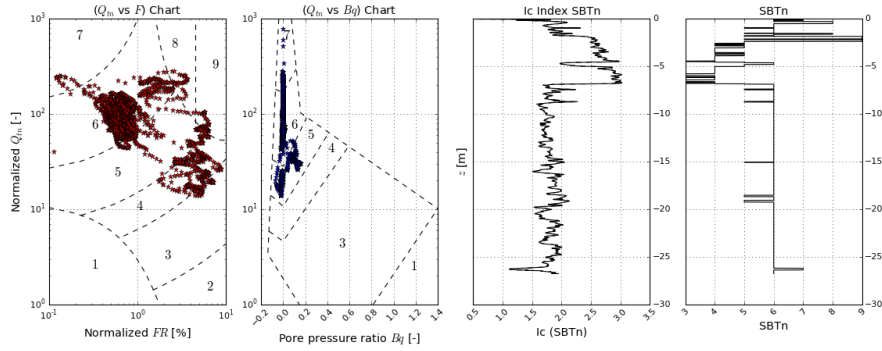


Figure 3. "SBTn (Robertson, 1990) Classification Tab"

Input CSV Save CSV Report PDF Help

Data Profiles SBT SBTn Physical CPT Resistance CPT Stiffness CPT Dissip. Test Shallow Found Driven Piles Bored Piles Seismic - S-Waves Seismic - P-Waves Liq-Module

Plot Physical Properties

Zoom

Pan

Home

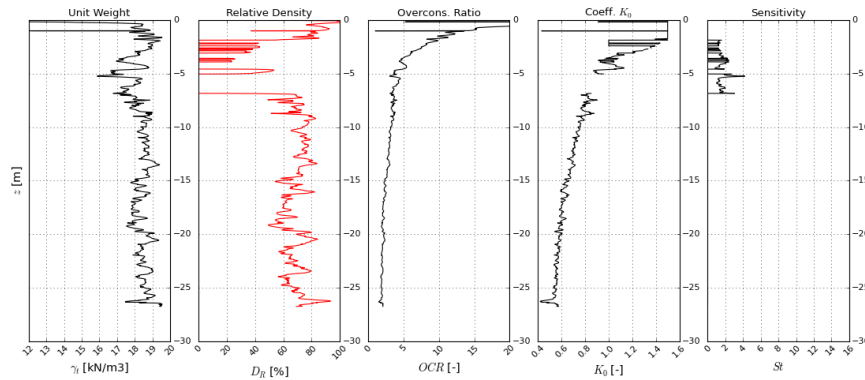


Figure 4. "Physical Properties Tab"

Input CSV Save CSV Report PDF Help

Data Profiles SBT SBTn Physical CPT Resistance CPT Stiffness CPT Dissip. Test Shallow Found Driven Piles Bored Piles Seismic - S-Waves Seismic - P-Waves Liq-Module

Plot Resistance parameters

Zoom

Pan

Home

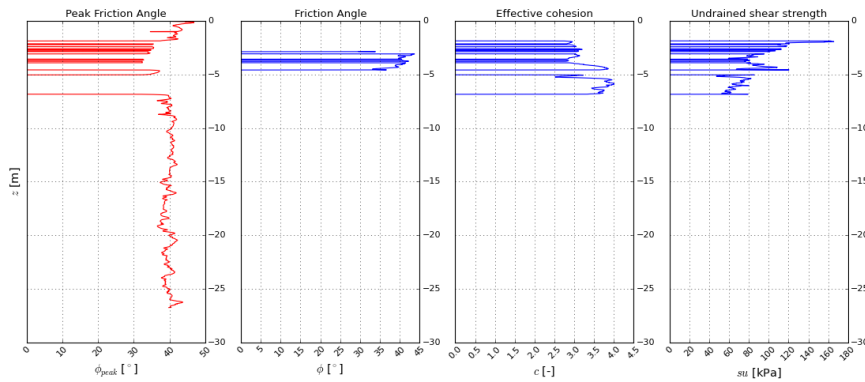


Figure 5. "Resistance parameters Tab"

Input CSV Save CSV Report PDF Help

Data Profiles SBT SBTn Physical CPT Resistance CPT Stiffness CPT Dissip. Test Shallow Found Driven Piles Bored Piles Seismic - S-Waves Seismic - P-Waves Liq-Module

Safety Factor [-] 3 R factor [-] 0.9

Exponent SBTn 3-4 [-] 0.3 Exponent SBTn 5-6-7-8-9 [-] 0.9 Update Gs

Plot Stiffness parameters

Zoom

Pan

Home

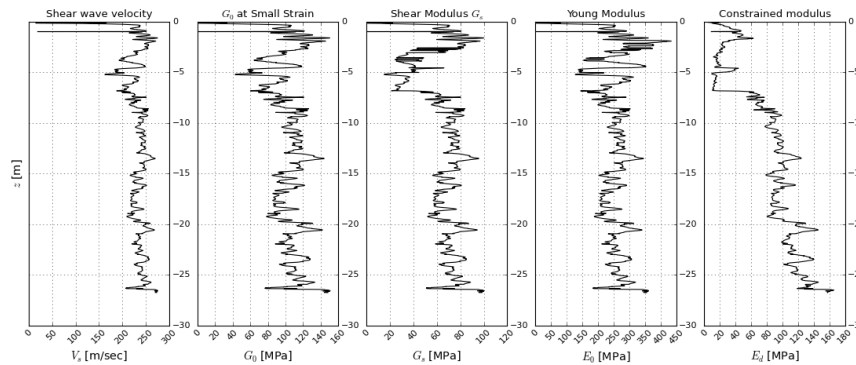


Figure 6. "Stiffness parameters Tab"

2.1 Soil Profile

Soil profile is inferred by using the Robertson et al. (1986) approach as modified by Robertson (2010). The normalized Robertson (1990) approach is also used. Figure 7 and Figure 8 show the classification charts. The most popular classification system, based on total tip resistance q_t and Friction Ratio, has been proposed by Robertson et al. in 1986 (SBT). Friction ratio is evaluated as follows:

$$R_f(\%) = \frac{f_s}{q_t} \cdot 100$$

The advantage of this method is the chance of evaluating soil types immediately during the test, since it does not require the evaluation of normalised parameters. The classification chart by Robertson et al. (1986) includes 12 soil types. The following table shows the Soil Behaviour Type classes as defined by Robertson (1986).

Zone	Soil Behaviour Type
1	Sensitive fine grained
2	Organic material
3	Clay
4	Silty clay to clay
5	Clayey silt to silty clay
6	Sandy silt to clayey silt
7	Silty sand to sandy silt
8	Sand to silty sand
9	Sand
10	Gravelly sand to sand
11	Very stiff fine grained (Overconsolidated or cemented)
12	Sand to clayey sand (Overconsolidated or cemented)

Table 1: Soil Behaviour Type classes proposed by Robertson et al. 1986.

The SBTn classification is made through the use of the classification charts proposed by Robertson (1990). The following normalised quantities have to be evaluated (Figure 7):

$$Q = \frac{q_t - \sigma_{v0}}{\sigma'_{v0}} ; \quad F = \frac{f_s}{q_t - \sigma_{v0}} \cdot 100; \quad B_q = \frac{u_2 - u_0}{q_t - \sigma_{v0}}$$

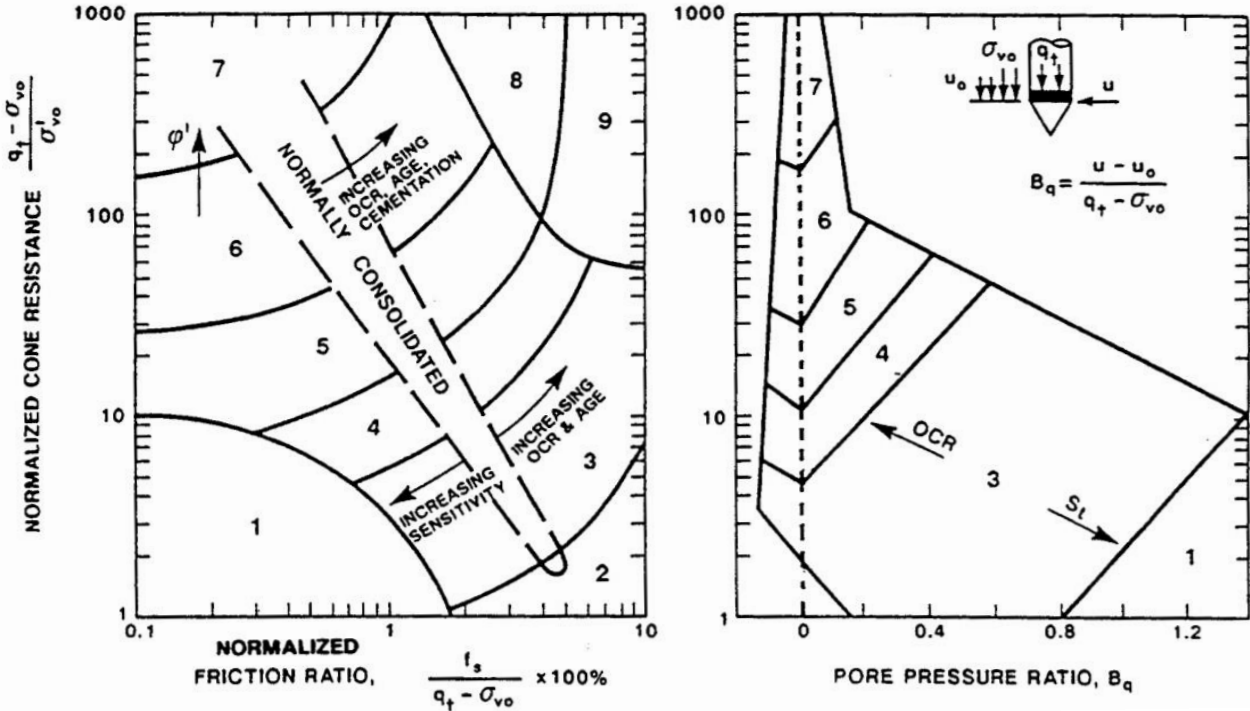


Figure 7: SBTn classification chart proposed by Robertson (1990).

The classification charts by Robertson (1990) include 9 soil types. The class numbers in Figure 7 correspond to:

- 1: sensitive, fine grained
- 2: organic soil-peat
- 3: clays-clays to silty clay
- 4: silt mixtures-clayey silt to silty clay
- 5: sand mixtures-silty sand to sandy silt
- 6: sands- clean sand to silty sand
- 7: gravelly sand to sand
- 8: very stiff sand to clayey sand (heavily overconsolidated or cemented)
- 9: very stiff, fine grained (heavily overconsolidated or cemented)

The evaluation of the Soil Behaviour Type (SBTn) Index I_c is made with the iterative method proposed by Robertson and Wride (1998):

$$I_c = \sqrt{(3.47 - \log Q_{tn})^2 + (\log F + 1.22)^2}$$

$$Q_{tn} = \left(\frac{q_t - \sigma_{v0}}{\sigma_{atm}} \right) \left(\frac{\sigma_{atm}}{\sigma'_{v0}} \right)^n$$

$$n = 0.381 \cdot I_c + 0.05 \cdot \left(\frac{\sigma'_{v0}}{\sigma_{atm}} \right) - 0.15$$

The following table shows the correspondence between I_c values and SBTn classes defined by Robertson (1990).

Soil classification (SBTn)	Zone number (Robertson SBT 1990)	SBT Index values
Organic soils: peats	2	$I_c > 3.60$
Clays: silty clay to clay	3	$2.95 < I_c < 3.60$
Silt Mixtures: clayey silt to silty clay	4	$2.60 < I_c < 2.95$
Sand Mixtures: silty sand to sandy silt	5	$2.05 < I_c < 2.60$
Sands: clean sand to silty sand	6	$1.31 < I_c < 2.05$
Gravelly sand to dense sand	7	$I_c < 1.31$

Table 2: SBTn classes defined by Robertson (1990) and respective I_c values (Robertson and Wride 1998).

The chart proposed by Robertson (2010) is an update of the previous Robertson (1986). The number of classes was reduced to match Robertson (1990) SBTn zones. The classification is made in terms of dimensionless cone resistance, (q_t/p_a with p_a = atmospheric pressure) and R_f . In this case a log scale is used for both axes.

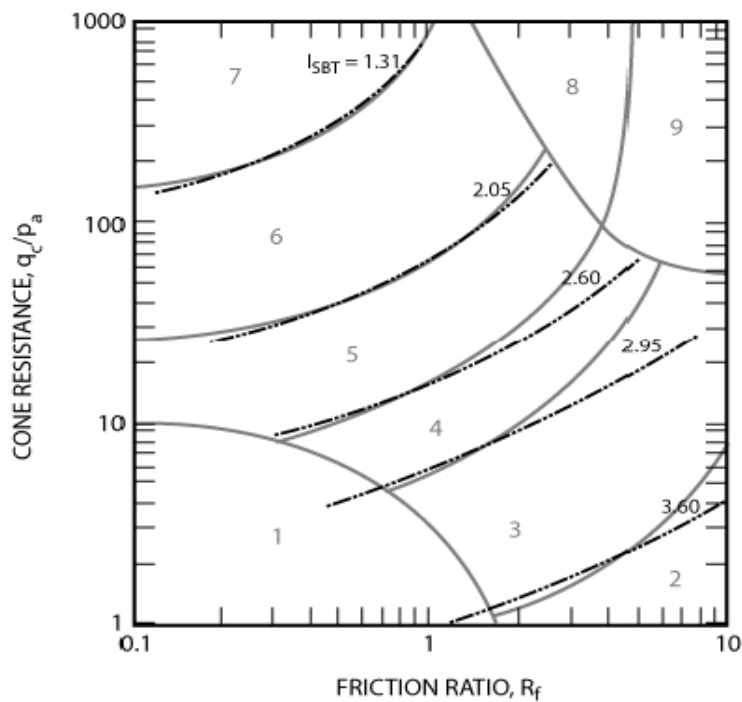


Figure 8: SBT Classification chart proposed by Robertson (2010).

Common SBT description	SBT zone Robertson et al. 1986	SBTn zone Robertson 1990
Sensitive fine grained	1	1
Clay - Organic soil	2	2
Clays: clay to silty clay	3	3
Silt mixtures: Clayey silt and silty clay	4 & 5	4
Sand mixtures: Silty sand to sandy silt	6 & 7	5
Sands: clean sands to silty sands	8	6
Dense sand to gravelly sand	9 & 10	7
Stiff sand to clayey sand - Overconsolidated or cemented	12	8
Stiff fine grained - Overconsolidated or cemented	11	9

Table 3: Robertson (1986) SBT classes and respective Robertson (1990) SBTn classes, as proposed by Robertson (2010).

The SBT index has been evaluated as follows (Robertson, 2010):

$$I_{SBT} = \sqrt{\left(3.47 - \log\left(\frac{q_t}{p_a}\right)\right)^2 + (\log R_f + 1.22)^2}$$

where:

q_t = CPT cone resistance (or corrected cone resistance, q_t)

R_f = friction ratio

f_s = CPT sleeve friction

The non-normalized SBT index (I_{SBT}) is essentially the same as the normalized SBTn index (I_c) but only uses the basic CPT measurements.

2.2 Soil Parameters

The following soil parameters are computed according to the empirical or semi-empirical correlations reported below.

The unit weight is evaluated with the following expression (Mayne, 2012):

$$\gamma_t = 26 - \frac{14}{1 + [0.5 \cdot \log(f_s + 1)]^2}$$

where f_s is in kPa and γ_t is in kN/m^3 .

The relative density is evaluated for SBTn classes 5,6,7 and 8 using the expression proposed by Lancellotta (1983):

$$D_R = 68 \left[\log\left(\frac{q_t}{\sqrt{\sigma_{atm} \sigma'_{v0}}}\right) - 1 \right]$$

where σ_{atm} is the atmospheric pressure expressed with the same unit as σ'_{v0} and q_t .

The overconsolidation ratio is evaluated as follows:

$$OCR = \frac{\sigma'_p}{\sigma'_{v0}}$$

where σ'_p is the preconsolidation pressure. The estimation of σ'_p is made according to the expression proposed by Mayne (2007), applicable for all kind of materials:

$$\sigma'_p = 0.101 p_{atm}^{0.102} G_0^{0.478} \sigma'_{v0}{}^{0.420}$$

Where G_0 is (Robertson P.K.,2009a):

$$G_0 = (q_t - \sigma_{v0}) \cdot 0.0188 \cdot 10^{0.55I_c + 1.68}$$

In Appendix A1, the verification of this method is shown.

The geostatic lateral stress is inferred from the well-known expression (Mayne and Kulhawy, 1982)

$$\frac{\sigma'_{h0}}{\sigma'_{v0}} = K_0 = (1 - \sin \varphi') OCR^{\sin \varphi'}$$

for SBTn classes 1,2,3,4 and 9. On the other hand, for sands the aforementioned expression is used, but the possible maximum value for K_0 is 1.5.

The effective stress friction angle for SBTn classes 5,6,7 and 8 is obtained using the equation proposed by Kulhawy and Mayne (1990):

$$\varphi' (^\circ) = 17.60^\circ + 11^\circ \log \left(\frac{q_t}{\sqrt{\sigma'_{v0} \cdot \sigma_{atm}}} \right)$$

For fine grained soils (SBTn 1,2,3,4,9) the effective stress friction angle is (Mayne and Campanella, 2005):

$$\varphi' = 29.5^\circ B_q^{0.121} (0.256 + 0.336 B_q + \log Q)$$

this expression is applicable for $0.10 < B_q < 1.00$ and $20^\circ < \varphi' < 45^\circ$. For the same kind of materials, the effective cohesion intercept is evaluated as follows:

$$c' \approx 0.02 \sigma'_p$$

While, as far as the undrained friction angle is concerned, the following expression is applicable (SBTn classes 1,2,3,4,9):

$$s_u = \frac{(q_t - \sigma_{v0})}{N_{kt}}$$

where N_{kt} is a Bearing Capacity factor and can be defined by the user. The default value is 14.

The small strain shear modulus is computed from the estimation of the shear wave velocity, V_s , and the unit weight. The expression proposed by Mayne (2006) is considered for V_s :

$$V_s = 118.8 \log(f_s) + 18.5$$

Therefore, G_0 is:

$$G_0 = \rho_t V_s^2$$

$$\rho_t = \frac{\gamma_t}{g}$$

where $g = 9.81 \text{ m/s}^2$ is the gravitational acceleration constant.

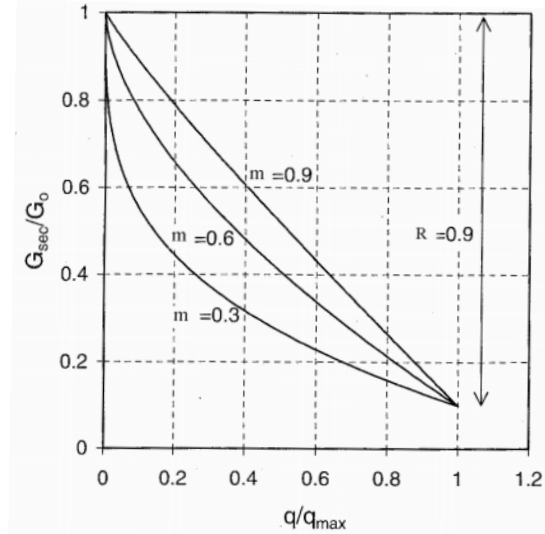
In addition, the small strain shear modulus G_0 can be evaluated using the following expression:

$$G_0 = (q_t - \sigma_{v0}) \cdot 0.0188 \cdot 10^{0.55I_c + 1.68}$$

The shear modulus G is computed according to the Fahey and Carter model (1993):

- SBTn classes 3 and 4 8 (NC or lightly OC fine grained soils): $G = G_0[1 - f^{0.3}]$
- SBTn classes 5,6,7,8 and 9 (overconsolidated clay and sands): $G = G_0[1 - f^{0.9}]$

where $f = q/q_{max}$ is the mobilization factor and can be defined by the user. The assumed default value is 0.33 (i.e. considering a global safety factor of 3.0). The R parameter is considered equal to 0.9.



The Young's modulus E_0 is then obtained with the following expression:

$$E_0 = 2 G_0(1 + \nu)$$

where:

$\nu' = 0.2$ for drained conditions and all material classes

$\nu_u = 0.5$ for undrained conditions and fine-grained soils.

The constrained modulus D' is evaluated as follows (Robertson P.K., 2009a):

$I_c > 2.20$	$D' = \alpha (q_t - \sigma_{v0})$	$\alpha = Q_{tn}$ if $Q_{tn} \leq 14$
		$\alpha = 14$ if $Q_{tn} > 14$
$I_c \leq 2.20$	$D' = (q_t - \sigma_{v0}) \cdot 0.03 \cdot 10^{0.55 I_c + 1.68}$	

2.3 Output files

The results of computations are saved as CSV files in a user-defined folder, using from the main bar *Save CSV* → *Save CPTu results*.

A list of saved files and their contents and structure is reported in the following:

- **filename_CPTu_data.csv** – such a file consists of 18 columns:
 - column 1: z, depth [m]
 - column 2: q_c , tip resistance [MPa]
 - column 3: f_s , sleeve friction [kPa]
 - column 4: u_2 , pore water pressure [kPa]
 - column 5: q_t , total tip resistance [MPa]
 - column 6: u_0 , hydrostatic water pressure [kPa]
 - column 7: Total geostatic vertical stress [kPa]
 - column 8: Effective geostatic vertical stress [kPa]
 - column 9: Q_{tn} , normalized tip resistance [-]
 - column 10: F , normalized friction ratio [%]
 - column 11: B_q , normalized pore pressure parameter [-]
 - column 12: SBTn (Robertson, 1990)
 - column 13: I_c , classification index (Robertson, 1990)
 - column 14: q_t/p_a , cone resistance [-]
 - column 15: f_s/q_t , friction ratio [%]
 - column 16: SBT (Robertson, 1986 – Updated in 2010)
 - column 17: I_c , classification index (Robertson, 1986 – Updated in 2010)
 - column 18: Effective vertical stress corrected [kPa]

- **filename_CPTu_physical.csv** – such a file consists of 6 columns:
 - column 1: z, depth [m]
 - column 2: soil unit weight [kN/m³]
 - column 3: D_r , relative density [%]
 - column 4: OCR, overconsolidation ratio [-]
 - column 5: K_0 [-]
 - column 6: S_t , sensitivity [-]

- **filename_CPTu_resistance.csv** – such a file consists of 5 columns:
 - column 1: z, depth [m]
 - column 2: effective peak friction angle for coarse soils [deg]

- *column 3*: effective peak friction angle for fine-grained soils [deg]
- *column 4*: effective cohesion for fine-grained soils [kPa]
- *column 5*: undrained shear strength [kPa]

- ***filename_CPTu_stiffness.csv*** – such a file consists of 6 columns:
 - *column 1*: z , depth [m]
 - *column 2*: V_s , shear wave velocity [m/s]
 - *column 3*: G_0 , shear modulus at small strain level [MPa]
 - *column 4*: G_s , shear modulus [MPa]
 - *column 5*: E_0 , Young modulus at small strain level [MPa]
 - *column 6*: E_d , constrained modulus [MPa]

3 INTERPRETATION OF DISCONTINUOUS MEASUREMENTS

3.1 Dissipation tests

The dissipation test is an important instrument to characterise soil consolidation parameters and it consists of measuring pore water pressure over time once the tip is halted at a certain depth during a penetration test. The interpretation of piezocone tests is made using the theoretical solution proposed by Teh and Houlsby (1991). They analysed cone penetration test in clay considering the soil as a homogeneous elastic perfectly plastic material obeying the von Mises yield criterion. Their solution is properly adopted when the test is conducted under undrained conditions and the shape of the dissipation curve overlaps the theoretical one (Figure 9, curve C). The data in Figure 9 are shown as normalized excess pore water pressure over time:

$$\frac{\Delta u_t}{\Delta u_i} = \frac{(u_2 - u_0)_t}{(u_2 - u_0)_i}$$

Where t stands for the generic time and i stands for the initial value.

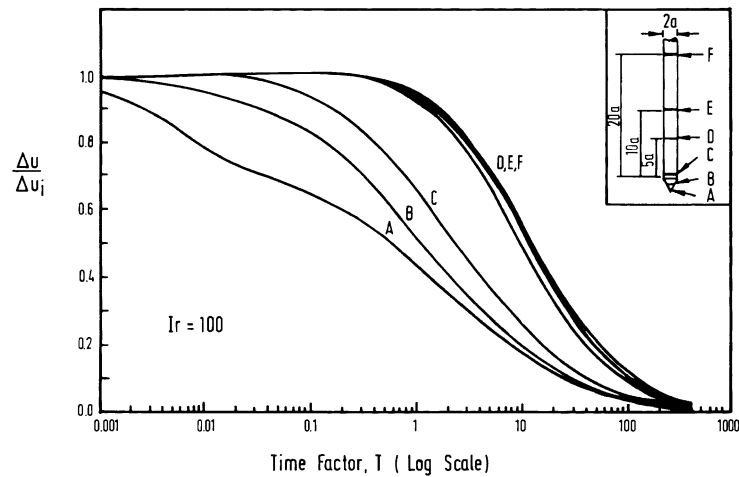


Figure 9: Theoretical dissipation curves at different locations of a 60° cone penetrometer (Teh and Houlsby, 1991)

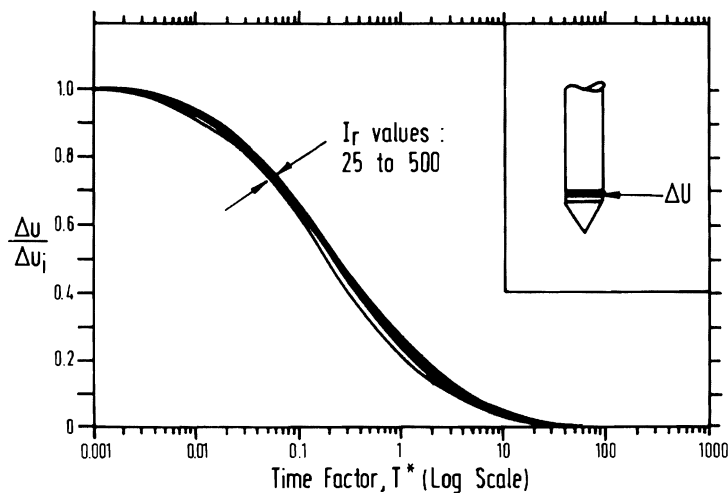


Figure 10: Normalized penetration curves, at u_2 position, plotted against the time factor T^* , for different values of the Rigidity Index.

The solution proposed by Teh and Houlsby is also illustrated in Figure 10, for different values of the rigidity index, with respect to the time factor T^* defined as:

$$T^* = \frac{c_h t}{a_c^2 \sqrt{I_r}}$$

Where c_h is the coefficient of consolidation, t is the elapsed time, a_c is the probe radius, $I_r = \frac{G}{s_u}$ is the rigidity index of the soil.

In this application, the coefficient of consolidation is evaluated identifying the elapsed time corresponding to the 50% dissipation of the excess pore water pressure generated during penetration:

$$c_h = \frac{T_{50} \cdot a_c^2 \cdot \sqrt{I_r}}{t_{50}}$$

where: a_c is the probe radius, $I_r = \frac{G}{s_u}$ is the rigidity index of the soil, t_{50} is the elapsed time corresponding to the 50% of excess pore water pressure dissipation and $T_{50} = 0.245$ is the time factor corresponding to the 50% of dissipation for u_2 measurements. G is the small strain shear modulus and can be estimated from CPTu results or on the base of available seismic measurements. The undrained shear strength is estimated from CPTu results as illustrated previously.

When the shape of the dissipation curve doesn't follow the theoretical one, the solutions proposed by Sully et al. (1999) are adopted to interpret the test for overconsolidated fine grained soils. They subdivided the various non-standard dissipation responses in main classes and proposing plot corrections. This application applies the so-called log-time correction. In particular it is possible to interpret no-standard curves that follow the trends showed in Figure 11. In these cases, the maximum value is taken as the initial value and the time at which this peak occurs is taken as the new zero time of the dissipation record.

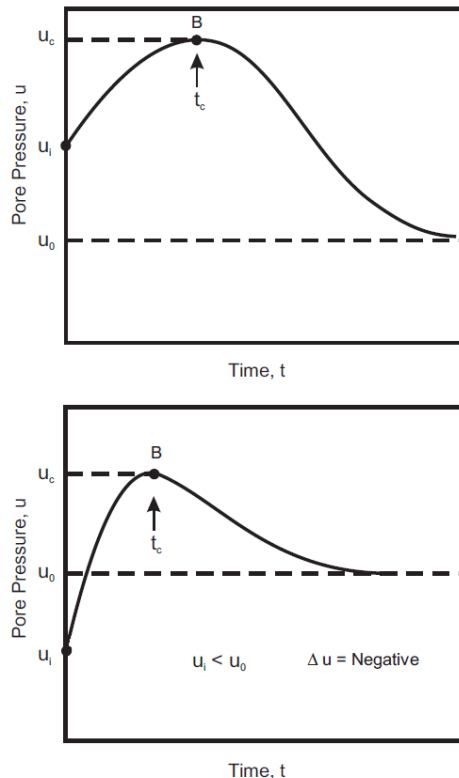


Figure 11: Non-standard dissipation curves (after Sully et al. 1999).

3.1.1 Input file, analysis process and results for the Dissipation Test Module

It is firstly required that you load the CPT test data as described in section 2. Then move in the “Dissip. Test” Tab.

The input files is a .csv files (CSV, comma-separated values file). Such files consist of 2 columns:

column 1: Time [sec];

column 2: Pore water pressure (u_2) [kPa].

You can find an example input file required to perform a Dissipation Test interpretation in the “Example” folder.

Then upload the raw data selecting ‘Input CSV’ in the menu bar and clicking on the ‘Load Dissip’ button.

The following input data is also required:

- *Depth Dissipation Test*: specify here the dissipation test depth (below the ground surface) [meter];

Then you can press the button “Verify depth” in the “Dissip. Test” Tab. The command “Verify depth” controls that input data is written correctly. Finally, you can perform the dissipation test interpretation pressing the ‘Calculate’ button.

The results are automatically shown in this Tab just close to the “Calculate” button, in terms of coefficient of consolidation, c_h (in m^2/s^2) and in terms of t_{50} (in sec) that corresponds to the elapsed time corresponding to the 50% of excess pore water pressure dissipation. After that you can press the “Plot Dissipation test” to display the test interpretation result (Figure 12).

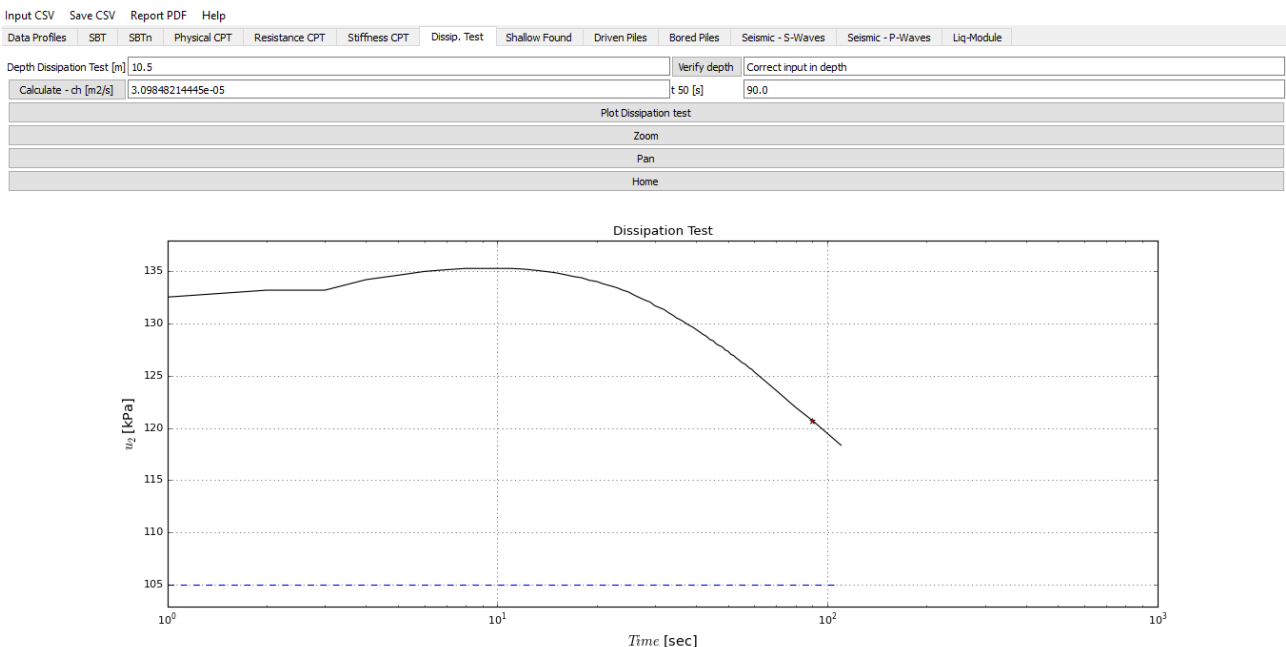


Figure 12. Dissipation test Tab. Interpretation results

3.2 *Body wave velocity measurements*

The Pagani seismic module is equipped with a pair of triaxial accelerometers located at a relative distance from each other of 0.5 m. Therefore, two waveforms are recorded for each hit by the data acquisition system. Usually, a left and a right impulse are given. Therefore, each measurement consists of 4 records or waveforms. Test interpretation is carried out by means of the cross-correlation method, as for the S waves. In other words, the travel time between the two accelerometers is computed from the time delay which maximizes the cross – correlation function between the two recorded waveforms, for each impulse. How to take advantage of the left and right impulse is explained later on. The P wave velocities are computed by considering the peak to peak time delay between the two accelerometric records. In this case only two waveforms from a single impulse are used.

Two different types of source are used for:

- a drop hammer of 10 kg with a special anvil (drop height of about 1.8 m). This source is used for P waves.
- a manual hammer of 5 kg. This hammer is used to hit the aluminum blocks from right or left. The blocks are kept well in contact onto the soil by the penetrometer – legs.

In principle, the first type of source mainly produces PV and SV waves while the second type of source mainly produces PV and SH waves. In any case, the above is a simplification and the generated wave field is usually quite complex.

Butterworth filters are applied only to the shear wave signals.

3.2.1 *Input files and analysis process for the S-Waves module*

The input files are 4 .txt files (ASCII). Such files consist of 1 column:

column 1: Wave amplitude (the first wave amplitude data is at the row number 6). These 6 rows are automatically skipped by the code.

You can find an example of 4 .txt (ASCII) files required to perform a S-wave interpretation in the “Example” folder.

The time step of each record is 0.033 milliseconds and the standard duration of each record is 600 milliseconds with a pre-trigger of 50 milliseconds.

To perform an S-wave analysis load the “Left and Right” records of the two receivers, for a total of 4 records (pressing the “Load Receiver ...” buttons in the “Seismic S-Waves” Tab). The Receiver 1 is the upper one, the Receiver 2 is located 0.50 m below the first one.

The following input data are also required:

- *Depth Receiver 1:* specify here the depth (below the ground surface) of the upper receiver (Receiver 1) [meter];
- *Plate distance:* specify here the horizontal distance between the vertical axis of the SCPT-rods and the plate used to generate the seismic waves [meter]. As default this distance is set equal to 0.50 m;
- *Remove data:* here there are two options ([1] or [2]). If you use the value 1 means that you want to remove data (excluding them from the analysis process) starting from the time 0 and up to a time value

(in milliseconds) that you have to specify in the “Remove time up to” field. If you use the value 2, the entire length of the records will be used in the analysis process. As default this value is set equal to 2;

- *Signal duration*: specify here the time duration of the records in milliseconds. As default this value is set equal to 600 milliseconds.

The use of the fields “Freq 1” and “Freq2” and of the button “Calculate D at small strain level” is not required if you just want to estimate the shear wave velocity (V_s), while is required in the case you want to compute the Damping ratio at small strain levels with the Spectral Slope Method (see section 5.1).

Then press the button “Verify Input” to check and upload the input data, finally press the “Calculate V_s ” button to perform the S-waves analysis and computation of S wave – propagation velocity. The computed V_s value is displayed. After that you can press the “Plot S-Waves Analysis” button and the following plots are shown (see Figure 13):

- *Plot n° 1*: the filtered waveforms of the two receivers are shown. Please note: all the 4 records (2 for each receiver) have been uploaded. The filtered signal called “Rec 1” was obtained after: a) subtracting the Left record with the Right record of the first receiver, b) applying a Butterworth filter. The filtered signal called “Rec 2” was obtained after: a) subtracting the Left record with the Right record of the second receiver, b) applying a Butterworth filter. In the plot n°1 are displayed with the blue and red points the peaks of the “Rec 1” and “Rec 2” signals, that are useful to define the part of the signals that will be used to perform the cross-correlation;
- *Plot n°2*: the same signals as in Plot n°1 are displayed again but the “Rec 2” has been shifted of a time interval equal to the time delay computed from the cross-correlation analysis;

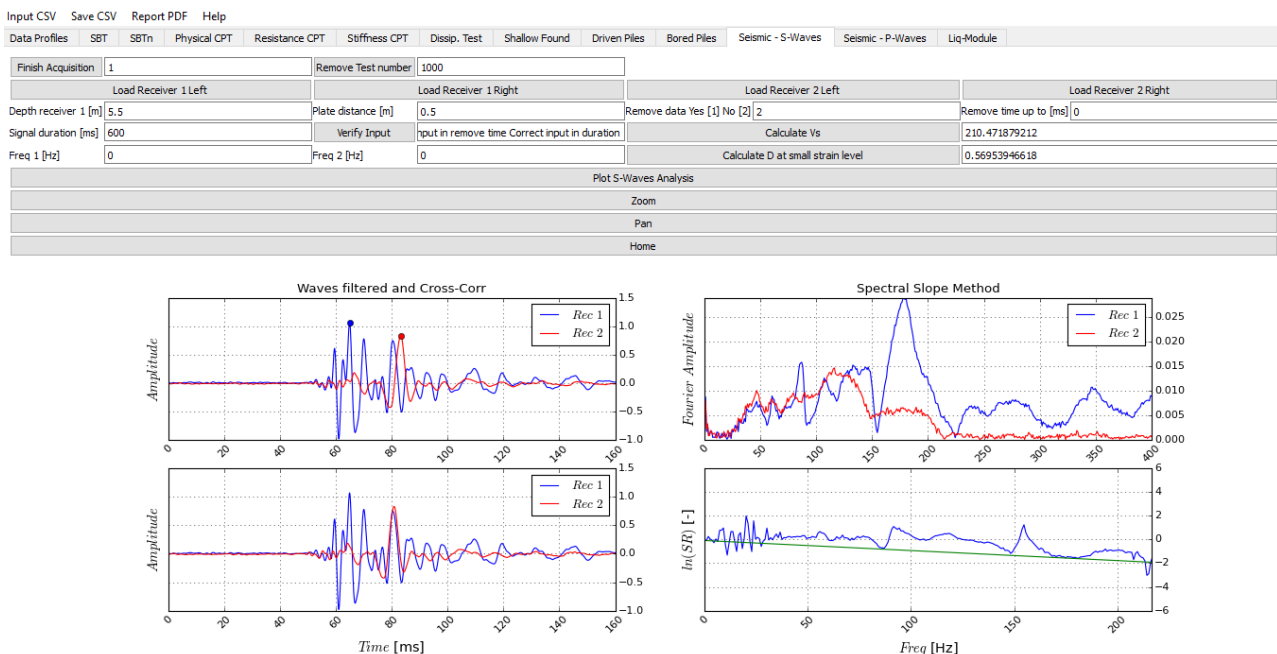


Figure 13. “Seismic S-Waves” Tab

- *Plot n°3 and Plot n°4*: these plots represent the Fourier Spectra (Fourier Amplitude vs Frequency) and the ‘Napierian Logarithm of the Spectral Ratio’ vs ‘Frequency’ relationship, respectively. These are necessary to estimate the Damping ratio at small strain level using the Spectral Slope Method. After pressing the “Calculate Vs” button, a Damping ratio value is displayed. Such a value was obtained using as “Freq1” the frequency value closer to 0 Hz and as “Freq2” the frequency value closer to 120% of the frequency at which the maximum Fourier Amplitude in plot n°3 is reached. The damping is computed with the following expression:

$$D = - \frac{\ln \frac{A_2(Freq_2)}{A_1(Freq_2)} - \ln \frac{A_2(Freq_1)}{A_1(Freq_1)}}{(Freq_2 - Freq_1) * 2\pi * Time Delay}$$

Where the $A_1(f)$ and $A_2(f)$ are the Fourier amplitudes of the signals of the receiver 1 and 2 respectively and displayed in the plot n°3.

In the plot n°4 is shown the Napierian logarithm of the spectral ratio as a function of the frequency and a line having a slope equal to:

$$Slope = - \frac{\ln \frac{A_2(Freq_2)}{A_1(Freq_2)} - \ln \frac{A_2(Freq_1)}{A_1(Freq_1)}}{(Freq_2 - Freq_1)}$$

Tuning the estimate of the Damping ratio at small strain level is possible by selecting a more appropriate and small frequency interval. This involves modifying “Freq1” and “Freq2” values according to the indications provided in the section 5.1. After such a selection of frequency interval, press the “Calculate D at small strain level” button to perform the damping analysis. To update the plots, press again the “Plot S-Waves Analysis” button.

It is possible to perform further analyses of seismic measurements by loading again all the necessary input data as previously described. The main results of each analysis are stored once the user press the button “Calculate Vs”. The following data of each analysis are saved in background:

1. Depth of the middle point of the two receivers’ alignment;
2. Shear wave velocity (Vs);
3. Damping at small strain level (D). Please note that the first estimate of D was computed using as “Freq1” the frequency value closer to 0 Hz and as “Freq2” the frequency value closer to the 120% of the frequency at which the maximum Fourier Amplitude in plot n°3 is reached. To refine this value, you need to follow the indications provided in section 5.1. The stored D value is updated when you change the Freq1 and Freq2 values and press the “Calculate D at small strain level”.

Once you have performed all the analyses press the button “Finish Acquisition” to freeze the results. Only when the acquisition has been stopped you can remove some of the previously performed analyses. To do that please insert the undesired/unsuccessful analysis number in the field close to the “Remove Test number” and press this button. In case you don’t remember the number of the analysis you want to remove you can create a temporary output file from the main bar *Save CSV* → *Save S-Waves*. Once generated the output .csv file you can easily find the number of analysis to remove.

3.2.2 Output files for the S-Waves module

The results of computations are saved as CSV files in a user-defined folder, using from the main bar *Save CSV* → *Save S-Waves*.

The saved file and its content and structure is reported in the following:

- **filename_S_Waves.csv** – such a file consists of 3 columns:
 - *column 1*: z, depth of the middle of the two receivers' alignment [m]
 - *column 2*: V_s , shear wave velocity [m/sec]
 - *column 3*: D, damping ratio at small strain level [%]

3.2.3 Input files and analysis process for the P-Waves Module

The input files are 2 .txt files (ASCII). Such files consist of 1 column:

column 1: Wave amplitude (the first wave amplitude data is at the row number 6). These 6 rows are automatically skipped by the code.

You can find an example of 2 .txt (ASCII) files required to perform a P-wave interpretation in the “Example” folder.

The time step of each record is 0.033 milliseconds and the standard duration of each record is 600 milliseconds with a pre-trigger of 50 milliseconds.

To perform a P-wave analysis load the records of the two receivers, for a total of 2 records (pressing the “Load Receiver ...” buttons in the “Seismic P-Waves” Tab). The Receiver 1 is the upper one, the Receiver 2 is located 0.50 m below the first one.

The following input data are also required:

- *Depth Receiver 1*: specify here the depth (below the ground surface) of the upper receiver (Receiver 1) [meter];
- *Plate distance*: specify here the horizontal distance between the vertical axis of the SCPT-rods and the plate used to generate the seismic waves [meter]. As default this distance is set equal to 1.50 m;
- *Signal duration*: specify here the time duration of the records in milliseconds. As default this value is set equal to 600 milliseconds;
- *Pre-trigger*: specify here the time duration of the pre-trigger in milliseconds. As default this value is set equal to 50 milliseconds.

Then press the button “Verify Input” to check and upload the input data. After that, press the “Calculate V_p ” button to perform the P-waves analysis.

The computed V_p value is displayed. After that you can press the “Plot P-Waves Analysis” button and the following plot is shown (see Figure 14):

- *Plot*: the filtered records of the two receivers are shown. In the plot are displayed with the blue and red points the peaks of the P waves “Rec 1” and “Rec 2” signals, while the blue and the red stars represent the time at which each signal has an amplitude bigger than the 102% of the maximum noise

value recorded during the pre-trigger phase. These two points are useful to evaluate an appropriate time interval where can be found the peaks of the P-waves.

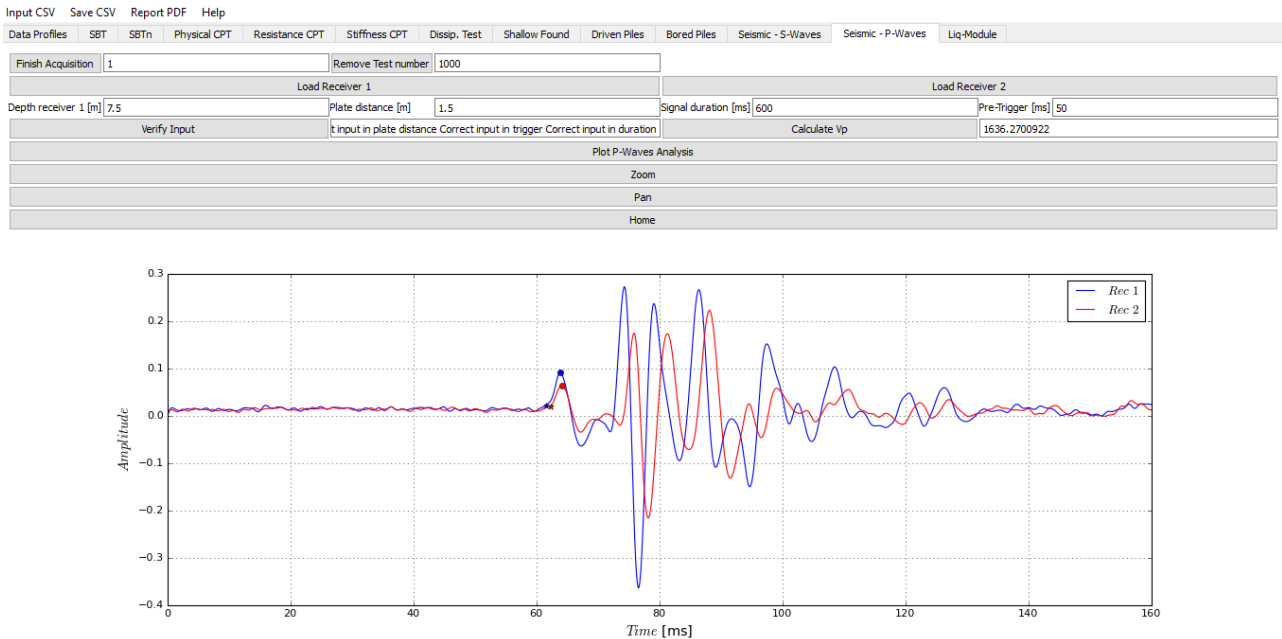


Figure 14. “Seismic P-Waves” Tab

It is possible to perform further analyses loading again all the input data as described previously. The main results of each analysis are stored once the user press the button “Calculate Vp”. The following data of each analysis are saved in background:

1. Depth of the middle point of the two receivers’ alignment;
2. P-wave velocity (Vp);

Once you have performed all the analyses press the button “Finish Acquisition” to freeze the results. Only when the acquisition has been stopped you can remove some of the previously performed analyses. To do that please insert the undesired/unsuccessful analysis number in the field close to the “Remove Test number” and press this button. In case you don’t remember the number of the analysis you want to remove you can create a temporary output file from the main bar *Save CSV* → *Save P-Waves*. Once generated the output .csv file you can easily find the number of analysis to remove.

3.2.4 Output files for the P-Waves module

The results of computations are saved as CSV files in a user-defined folder, using from the main bar *Save CSV* → *Save P-Waves*.

The saved file and its content and structure is reported in the following:

- **filename_P_Waves.csv** – such a file consists of 2 columns:
 - *column 1*: z, depth of the middle of the two receivers’ alignment [m]
 - *column 2*: Vp, P-wave velocity [m/sec]

4 DESIGN WITH CPT

4.1 Liquefaction risk analysis

Liquefaction risk analysis is carried out according to the Boulanger & Idriss (2015) and Robertson & Wride (1998) approaches that give an estimate of the safety factor against liquefaction. This safety factor is inferred from a simplified estimate of the earthquake induced cyclic stress ratio (CSR) and the cyclic resistance ratio (CRR) at various depths. It is assumed that liquefaction occurs at a given depth when the safety factor ($FS_L = CRR/CSR$) is equal to 1. The liquefaction effects at ground level are estimated by means of the LPI (Liquefaction Potential Index) as defined by Iwasaki et al. (1978). LPI is computed as:

$$LPI = \int_0^{20} F_1 W(z) dz$$

Where: $F_1 = 1 - FS_L$ for $FS_L \leq 1$ and $F_1 = 0$ for $FS_L > 1$; $W(z)$ is a depth weighting function given by $W(z) = 10 - 0.5z$; and z is depth in meters below the ground surface.

In other word Penetration tests should be extend down to 20 m at least.

LPI can range from 0 to a maximum of 100 (i.e. where FS_L is zero over the entire 20 m depth). Analyzing SPT data from 55 sites in Japan, Iwasaki et al. (1978) proposed that severe liquefaction should be expected for sites where $LPI > 15$ but not where $LPI < 5$.

4.1.1 Computation of FS_L (Boulanger & Idriss, 2015)

CSR is computed according to the following equation:

$$CSR = 0.65 \frac{\sigma_v}{\sigma'_v} \frac{a_{max}}{g} r_d$$

Where: σ_v , σ'_v total and effective vertical geostatic stresses; a_{max} = peak ground acceleration. In principle should be inferred from seismic response analysis in terms of effective stresses. In practice can be inferred from SRA (seismic response analysis) in terms of total stresses or from the simplified procedures prescribed by technical codes. Italian Building Code recommends assuming $a_{max} = S_S S_T a_{max,R}$ where $a_{max,R}$ = peak ground acceleration for a given site and a given return period (Type A soil). S_S and S_T = stratigraphic and topographic amplification factors respectively, which depend on soil type and topography. In absence of specific SRA, type D soil should be considered. Moreover:

$$r_d = \exp[\alpha(z) + \beta(z) M]$$

This shear stress reduction factor accounts for soil flexibility.

$$\alpha(z) = -1.012 - 1.126 \sin\left(\frac{z}{11.73} + 5.133\right)$$

$$\beta(z) = 0.106 + 0.118 \sin\left(\frac{z}{11.28} + 5.142\right)$$

M = Magnitude.

The soil's cyclic strength (CRR) depends on number of cycles of a given amplitude. In other words, it depends on earthquake duration, i.e. earthquake Magnitude. This is accounted for by the MSF (magnitude scale factor). Moreover, an increase of the mean normal stress inhibits the dilatancy. This aspect, relevant for very high stresses, is accounted for by the K_σ factor.

$$K_\sigma = 1 - C_\sigma \ln\left(\frac{\sigma'_v}{p_{atm}}\right) \leq 1.1$$

$$C_\sigma = \frac{1}{37.3 - 8.27(q_{c1Ncs})^{0.264}} \leq 0.3$$

Where:

$q_{c1Ncs} = q_{c1N} + \Delta q_{c1N}$ i.e. the tip resistance corrected to account for overburden stress and fine content.

$$q_{c1N} = C_N \frac{q_c}{p_{atm}} \quad C_N = \left(\frac{p_{atm}}{\sigma'_v}\right)^m \leq 1.7 \quad m = 1.338 - 0.249 q_{c1Ncs}$$

$$\Delta q_{c1N} = \left(11.9 + \frac{q_{c1N}}{14.6}\right) \exp\left[1.63 - \frac{9.7}{FC+2} - \left(\frac{15.7}{FC+2}\right)\right]$$

Moreover:

$$MSF = 1 + (MSF_{max} - 1) \left[8.64 \exp\left(\frac{-M}{4} - 1.325\right)\right]$$

$$MSF_{max} = 1.09 + \left(\frac{q_{c1Ncs}}{180}\right)^3 \leq 2.2$$

Therefore, the computation of K_σ as well as MSF involves an iterative procedure. Fine content (FC) is inferred from soil classification index (I_c) as follows:

$$I_c = \{[3.47 - \log Q]^2 + [1.22 + \log F]^2\}^{0.5}$$

$$Q = \left(\frac{q_t - \sigma_{v0}}{p_{atm}}\right) \left(\frac{p_{atm}}{\sigma'_{v0}}\right)^n \quad F = \left(\frac{f_s}{q_t - \sigma_{v0}}\right) 100$$

$$FC = 80(I_c + C_{FC}) - 137 \quad 0 \leq FC \leq 100\%$$

The C_{FC} fitting parameter is set equal to 0. The cutoff I_c parameter can also be user defined. The default value is 2.6. Based on Italian data for medium low seismicity areas (Emilia Romagna and Tuscany) it is suggested to assume a value of 2.45. In practice, when this parameter exceeds the fixed cutoff value, the soil is considered non-liquefiable.

The cyclic resistance ratio is computed as follows:

$$CRR = \exp\left[\left(\frac{q_{c1Ncs}}{113}\right) + \left(\frac{q_{c1Ncs}}{1000}\right)^2 - \left(\frac{q_{c1Ncs}}{140}\right)^3 + \left(\frac{q_{c1Ncs}}{137}\right)^4 - C_0\right]$$

Where C_0 is a fitting parameter = 2.6 ± 0.2 .

The safety factor is then computed as follows:

$$FS_L = MSF K_\sigma \frac{CRR}{CSR}$$

The output consists of a profile of FS_L with depth and the LPI (Figure 15).

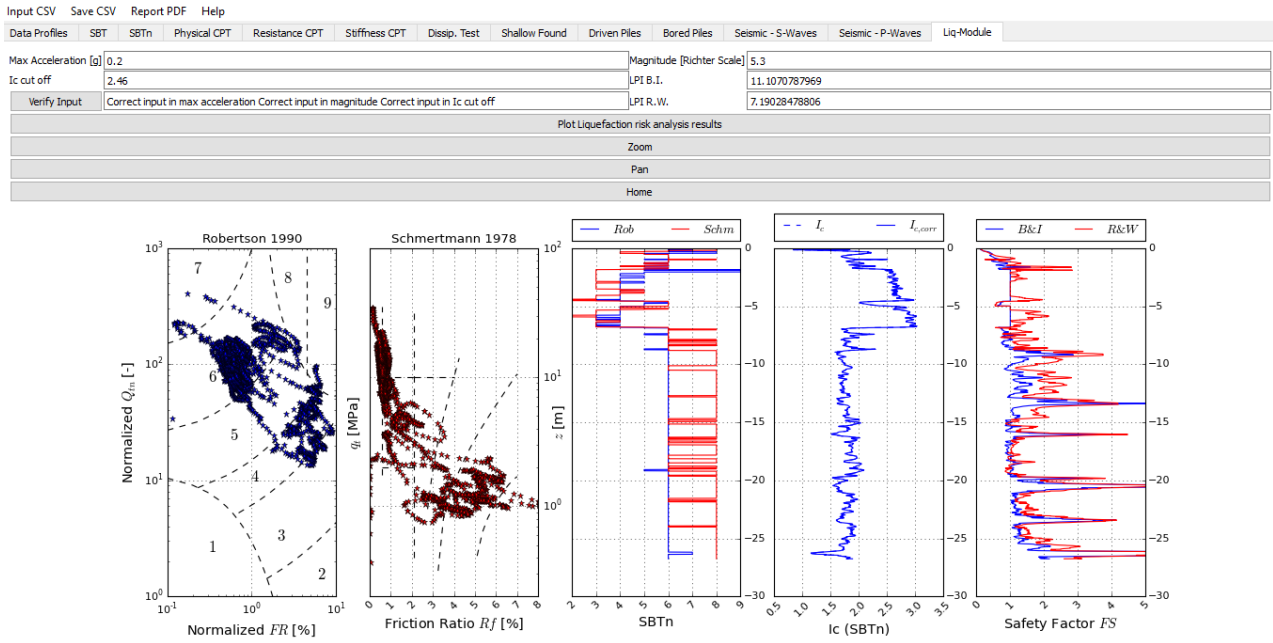


Figure 15. "Liq-Module" Tab

4.1.2 Computation of FS_L (Robertson & Wride, 1998)

The method mainly concerns the estimate of CRR. MSF, K_σ , and r_d are computed according to Youd et al. (2001). CRR is computed according to the following procedure:

$$CRR = 0.833 \frac{(q_{c1N})_{cs}}{1000} + 0.05 \quad \text{if } q_{c1Ncs} < 50$$

$$CRR = 93 \left[\frac{(q_{c1N})_{cs}}{1000} \right]^3 + 0.08 \quad \text{if } q_{c1Ncs} < 160$$

Where $(q_{c1N})_{cs}$ is the cone penetration resistance corrected in order to take into account both the confining stress and the fine content.

To obtain $(q_{c1N})_{cs}$ the following procedure is used:

$$(q_{c1N}) = \frac{q_c}{100} \left(\frac{100}{\sigma'_{v0}} \right)^n$$

$$(q_{c1N})_{cs} = K_c (q_{c1N})$$

$$K_c = 1.0 \quad \text{if } I_c \leq 1.64$$

$$K_c = -0.403I_c^4 + 5.581I_c^3 - 21.63I_c^2 + 33.75I_c - 17.88 \quad \text{if } I_c > 1.64$$

$$I_c = [(3.47 - \log Q)^2 + (1.22 + \log F)^2]^{0.5}$$

$$Q = \frac{q_c - \sigma'_{v0}}{100} \left(\frac{100}{\sigma'_{v0}} \right)^n$$

$$F = \frac{f_s}{q_c - \sigma'_{v0}} 100(\%)$$

The above expressions use [kPa] for both stresses and penetration resistance. The following steps are necessary:

- assume $n = 1.0$ and compute I_c ;
- if $I_c > 2.6$ the soil is classified as clay and the computation can terminate;
- otherwise assume $n = 0.5$. If assuming $n = 0.5$, $I_c < 2.6$, the soil is classified as cohesionless and it is necessary to evaluate the liquefaction potential;
- If assuming $n = 0.5$, $I_c > 2.6$, the soil contains non-plastic silt and computation has to be done with $n = 0.7$.

The safety factor is computed as already shown in the previous section. The same type of output is given when using Boulanger & Idriss method as well as Robertson and Wride approach.

4.1.3 *Input data to perform the liquefaction risk analysis*

It is firstly required that you load the CPT test data as described in section 2. Then move in the “Liq-Module” Tab.

The following input data are required:

- *Max acceleration*: specify here the peak ground acceleration a_{\max} in gravity unit;
- *Magnitude*: specify here the magnitude of the earthquake;
- *Ic cut off*: the default value is 2.6. This value can be user defined, however it is recommended to use values in the range between 2.4 and 2.8.

Then press the “Verify Input” button to upload and check the input data and perform the liquefaction risk analysis. Finally press the “Plot liquefaction risk analysis results” button to display the results.

4.1.4 *Output of the liquefaction risk analysis module*

The results of computations are saved as CSV files in a user-defined folder, using from the main bar *Save CSV* → *Save LIQ results*.

The file saved and its content and structure is reported in the following:

- **filename_liq_output.csv** – such a file consists of 20 columns:
 - *column 1*: z, depth [m]

- *column 2*: q_c , tip resistance [MPa]
- *column 3*: f_s , sleeve friction [kPa]
- *column 4*: Total geostatic vertical stress [kPa]
- *column 5*: Effective geostatic vertical stress [kPa]
- *column 6*: Q , normalized tip resistance [-]
- *column 7*: I_c , classification index
- *column 8*: SBTn (Robertson, 1990)
- *column 9*: q_{c1N} (Boulanger & Idriss, 2015)
- *column 10*: q_{c1Ncs} (Boulanger & Idriss, 2015)
- *column 11*: $CRR_{7.5}$ (Boulanger & Idriss, 2015)
- *column 12*: CSR (Boulanger & Idriss, 2015)
- *column 13*: FS_L (Boulanger & Idriss, 2015)
- *column 14*: cumulative LPI (Boulanger & Idriss, 2015)
- *column 15*: q_{c1N} (Robertson & Wride, 1998)
- *column 16*: q_{c1Ncs} (Robertson & Wride, 1998)
- *column 17*: $CRR_{7.5}$ (Robertson & Wride, 1998)
- *column 18*: CSR (Robertson & Wride, 1998)
- *column 19*: FS_L (Robertson & Wride, 1998)
- *column 20*: cumulative LPI (Robertson & Wride, 1998)

4.2 Bearing capacity of piles (axial loads)

4.2.1 Driven Steel-pipes

For driven steel-pipes in sand or clay the Imperial College method (ICP) is used (Jardine et al., 2005).

Closed-ended piles

Shaft resistance in sand

The shaft resistance Q_s is equal to:

$$Q_s = \pi D \int \tau_f dz$$

Where:

- $\tau_f = (\sigma'_{rc} + \Delta\sigma'_{rd}) \tan \delta_{cv}$;
- δ_{cv} = interface angle of friction at failure (depends on pile roughness and other factors);
- $\sigma'_{rc} = 0.029q_c(\sigma'_{v0}/p_{atm})^{0.13}(h/R)^{-0.38}$ = local radial effective stress. h/R is limited to a minimum value equal to 8;
- R = pile external radius;
- h = distance between the calculation point and the pile-tip;
- $\Delta\sigma'_{rd} = 2G \Delta r/R$ = dilatant increase in local radial effective stress during pile loading;
- $\Delta r = 2R_{cla} \cong 0.02 \text{ mm}$
- $G = q_c[A + B\eta - C\eta^2]^{-1}$ (from Baldi et al., 1989), $A=0.0203$, $B=0.00125$, $C=1.216 \cdot 10^{-6}$;
- $\eta = q_c(p_{atm}\sigma'_{v0})^{-0.5}$.

Base resistance in sand

The base resistance Q_b is equal to:

$$Q_b = q_b \pi D^2 / 4$$

Where:

- $q_b = q_c [1 - 0.5 \log(D/D_{CPT})]$;
- D = pile external diameter;
- $D_{CPT} = 0.036$ m (CPT cone diameter);

A lower limit of $q_b = 0.30q_c$ is suggested for piles with $D > 0.90$ m. q_c is an average value over 1.5 pile diameter above and below the pile tip.

Shaft resistance in clay

The shaft resistance Q_s is equal to:

$$Q_s = \pi D \int \tau_f dz$$

Where:

- $\tau_f = \sigma'_{rf} \tan \delta_f = (K_f/K_c) \sigma'_{rc} \tan \delta_f$;
- δ_f = a value between δ_{peak} (peak interface angle of friction) and $\delta_{ultimate}$ (ultimate interface angle of friction);
- $\sigma'_{rc} = K_c \sigma'_{v0}$ = local radial effective stress after equalization. K_c depends on the yield stress ratio (YSR), h/R and sensitivity S_t expressed by ΔI_{vy} . h/R is limited to a minimum value equal to 8;
- $K_c = [2.2 + 0.016 YSR - 0.87 \Delta I_{vy}] YSR^{0.42} (h/R)^{-0.20}$;
- $\Delta I_{vy} = \log_{10} S_t$;
- If YSR is not available and it is assumed that $YSR \cong OCR$:

$$K_c = [2 - 0.625 \Delta I_{v0}] YSR^{0.42} (h/R)^{-0.20}$$

- K_f/K_c = loading factor $\cong 0.80$ (is constant regardless of the direction of loading or drainage conditions).

Base resistance in clay

The base resistance Q_b is equal to:

$$Q_b = q_b \pi D^2 / 4$$

Where:

- $q_b = 0.8 q_c$ (undrained loading case);
- $q_b = 1.3 q_c$ (drained loading case);

q_c is an average value over 1.5 pile diameter above and below the pile tip.

Open-ended piles

Shaft resistance in sand

The shaft resistance Q_s is equal to:

$$Q_s = \pi D \int \tau_f dz$$

Where:

- $\tau_f = (\sigma'_{rc} + \Delta\sigma'_{rd}) \tan \delta_{cv}$;
- $\sigma'_{rc} = 0.029q_c(\sigma'_{v0}/p_{atm})^{0.13}(h/R^*)^{-0.38}$ = local radial effective stress. h/R^* is limited to a minimum value equal to 8;
- $R^* = (R_{outer}^2 - R_{inner}^2)^{0.5}$.

Base resistance in sand

A rigid basal plug can develop during static loading if these criteria are satisfied:

- 1) $D_{inner} < 0.02 (D_r - 30)$ (D_r = relative density in %);
- 2) $D_{inner} / D_{CPT} < 0.083 q_c/p_{atm}$.

For fully plugged piles develop 50% of the end resistance of closed-ended piles of the same diameter after a pile head displacement of 10%D.

Q_b is equal to:

$$Q_b = q_b \pi R_{outer}^2$$

Where q_b is equal to:

$$q_b = q_c [0.5 - 0.25 \log(D/D_{CPT})]$$

Limiting values:

- 1) the fully plugged capacity should be no less than the unplugged capacity;
- 2) q_b should not fall below $0.15q_c$ (for $D > 0.90$ m).

Unplugged piles are assumed to sustain end bearing on the annular pile base area only with $q_{ba} = q_c$. Contributions from internal shear stresses are not considered.

Q_b is equal to:

$$Q_b = q_{ba} \pi (R_{outer}^2 - R_{inner}^2)$$

Where q_{ba} is equal to:

$$q_{ba} = q_c$$

Shaft resistance in clay

The shaft resistance Q_s is equal to:

$$Q_s = \pi D \int \tau_f dz$$

Where:

- $\tau_f = \sigma'_{rf} \tan \delta_f = (K_f/K_c) \sigma'_{rc} \tan \delta_f$;
- δ_f = a value between δ_{peak} (peak interface angle of friction) and $\delta_{ultimate}$ (ultimate interface angle of friction);
- $\sigma'_{rc} = K_c \sigma'_{v0}$ = local radial effective stress after equalization. K_c depends on the yield stress ratio (YSR), h/R^* and sensitivity S_t expressed by ΔI_{vy} . h/R^* is limited to a minimum value equal to 8;
- $K_c = [2.2 + 0.016 YSR - 0.87 \Delta I_{vy}] YSR^{0.42} (h/R^*)^{-0.20}$;
- $\Delta I_{vy} = \log_{10} S_t$;
- If YSR is not available and it is assumed that $YSR \cong OCR$:
$$K_c = [2 - 0.625 \Delta I_{v0}] YSR^{0.42} (h/R^*)^{-0.20}$$
- K_f/K_c = loading factor $\cong 0.80$ (is constant regardless of the direction of loading or drainage conditions);
- $R^* = (R_{outer}^2 - R_{inner}^2)^{0.5}$.

Base resistance in clay

Plugging during static loading can occur if:

$$1) [D_{inner}/D_{CPT} + 0.45 q_c/p_{atm}] < 36$$

For fully plugged piles develop half of the end resistance of closed-ended piles after a pile head displacement of 10%D.

Q_b is equal to:

$$Q_b = q_b \pi D^2 / 4$$

Where q_b is equal to:

$$q_b = 0.4 q_c \text{ (Undrained loading case)}$$

$$q_b = 0.65 q_c \text{ (Drained loading case)}$$

Unplugged piles sustain end bearing on the annular area of steel only.

Q_b is equal to:

$$Q_b = q_{ba} \pi (R_{outer}^2 - R_{inner}^2)$$

Where q_{ba} is equal to:

$$q_{ba} = q_c \text{ (Undrained loading case)}$$

$$q_{ba} = 1.6q_c \text{ (Drained loading case)}$$

4.2.2 Bored Piles in granular soils (sands)

For bored piles:

Shaft resistance

The shaft resistance Q_s is equal to:

$$Q_s = \pi D \int \tau_f dz$$

Where:

$$\tau_f = \alpha q_c$$

The adopted α values are those suggested by Alsamman (1995) and shown in Figure 16.

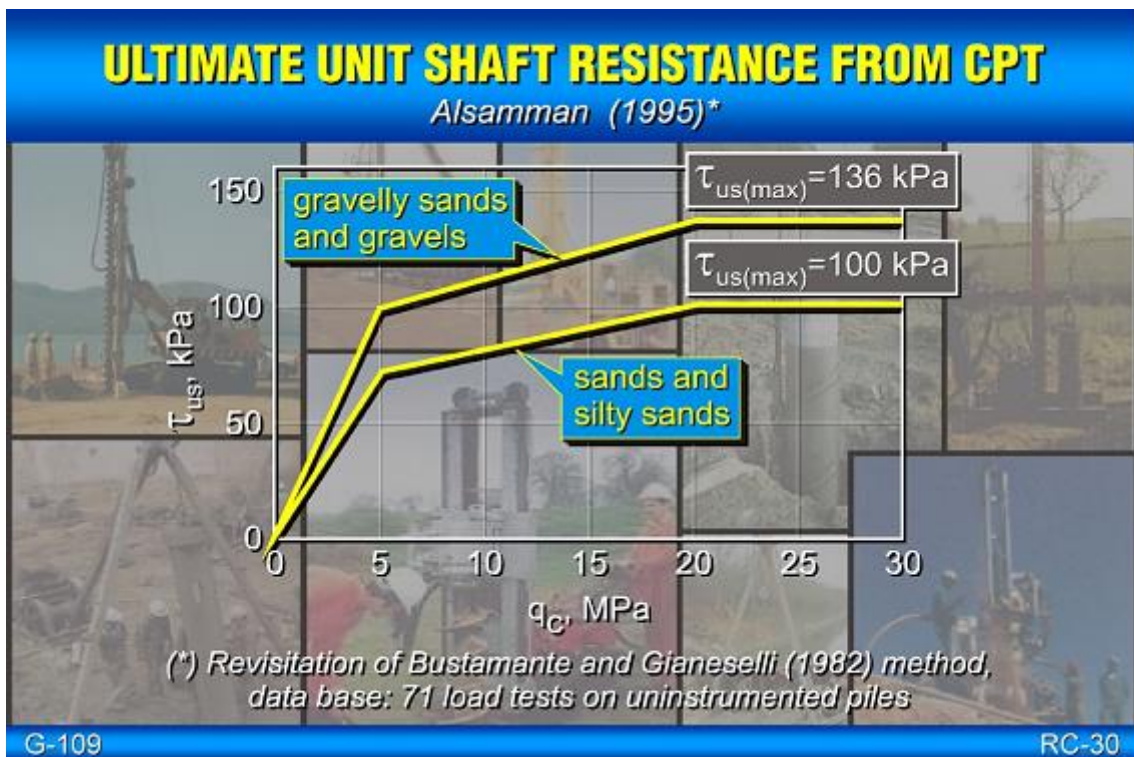


Figure 16. α values (Alsamman, 1995)

Base resistance

The base resistance Q_b is equal to:

$$Q_b = q_b \pi D^2 / 4$$

Where q_b is equal to $q_{c,0.05}$ (i.e. a critical value corresponding to a relative pile displacement $s/D = 0.05$).

$q_{c,0.05}$ is evaluated using the $q_{c,0.05}/q_c$ vs D relationship shown in Figure 17, where q_c is an average value of q_c within depth : $L-1.5D < z < L+1.5D$.

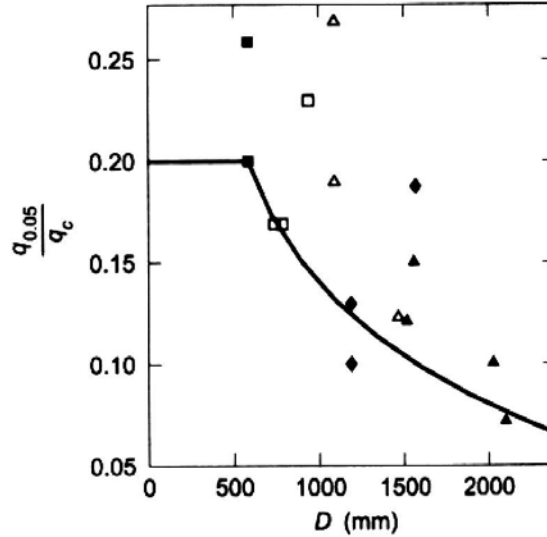


Figure 17. $q_{c,0.05}/q_c$ vs D relationship (Jamiolkowski et al., 1988)

4.2.3 Load-Settlement curve for the single pile

The load-settlement curve of the single pile is evaluated according to the analytical method proposed by Randolph and Wroth (1978). The pile is assumed to be rigid.

The shaft stiffness K_s (in kN/m) is considered equal to:

$$K_s = \frac{Q_s}{w} = \frac{2\pi L G_{av}}{\zeta}$$

Where Q_s is the load carried by the pile shaft, w is the pile settlement (equal for all the pile length, the pile is assumed to be rigid), G_{av} is the average shear modulus along the pile shaft and L is the pile length and ζ is equal to:

$$\zeta = \ln \left[2.5(1 - \nu) \frac{L}{R} \right]$$

The base stiffness is:

$$K_b = \frac{Q_b}{w} = \frac{4 R G_b}{1 - \nu}$$

Where Q_b is the load carried by the pile base, R is the pile radius G_b is the shear modulus at the pile tip and ν is the Poisson ratio.

The load-settlement curve is assumed to be a bi-linear curve. The first line (from 0 and up to the fully mobilization of the shaft resistance, having as coordinates (w_A, Q_A)) is expressed as:

$$Q_{tot} = (K_s + K_b)w$$

The second line, from the end of the first line and up to the fully mobilization of the pile base resistance (and so up to the available pile axial capacity) is expressed by:

$$Q_{tot} = Q_A + K_b(w - w_A)$$

4.2.4 Input data to perform the pile analyses (Driven and Bored Piles)

It is firstly required that you load the CPT test data and perform the interpretation as described in section 2. Then move in the “Driven Piles” or “Bored Piles” Tab.

The following input data are required:

- *Pile diameter*: specify here the external pile diameter in [m];
- *Inner diameter (only in the Driven Piles Tab)*: specify here the inner pile diameter only if the steel-pipes is open-ended in [m];
- *Pile Length*: specify here the total pile length in [m];
- *Starting depth*: specify here a depth value in case you want to remove a shallower soil layer [m].

Then press the “Verify Input” button to load the input data and finally the “Calculate Pile Capacity and Settlement” button perform the analysis. Press the “Plot Pile Capacity and Settlement” button to display the results (see Figure 18).

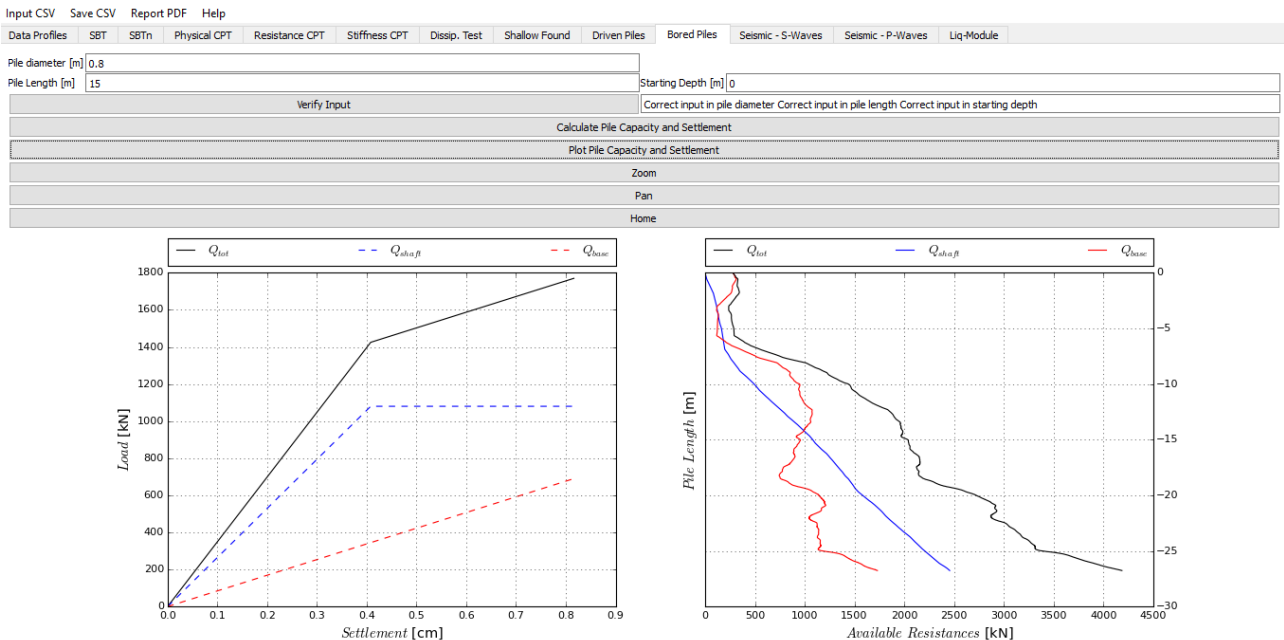


Figure 18. “Pile Foundation” Tab

4.2.5 Output of the Driven Piles and Bored Piles modules

The results of computations are saved as CSV files in a user-defined folder, using from the main bar *Save CSV* → *Save Driven Piles* or *Save Bored Piles*.

The saved file and its content and structure is reported in the following:

- ***filename_Driven_piles.csv*** – such a file consists of 4 columns:
 - *column 1*: z, depth [m];
 - *column 2*: available shaft resistance [kN];
 - *column 3*: available base resistance [kN];
 - *column 4*: available total resistance [kN].

- ***filename_Driven_piles_Load_Settlement.csv*** – such a file consists of 4 columns:
 - *column 1*: settlement [cm];
 - *column 2*: load carried by the shaft [kN];
 - *column 3*: load carried by the base [kN];
 - *column 4*: total load carried by the pile [kN].

- ***filename_Bored_piles.csv*** – such a file consists of 4 columns:
 - *column 1*: z, depth [m];
 - *column 2*: available shaft resistance [kN];
 - *column 3*: available base resistance [kN];
 - *column 4*: available total resistance [kN].

- ***filename_Bored_piles_Load_Settlement.csv*** – such a file consists of 4 columns:
 - *column 1*: settlement [cm];
 - *column 2*: load carried by the shaft [kN];
 - *column 3*: load carried by the base [kN];
 - *column 4*: total load carried by the pile [kN].

4.3 Settlements of shallow foundations on granular soils

The “settlement of shallow foundations” module computes the settlement using the Schmertamm method (1970, 1978a). This is strictly valid in case in of granular soils. The settlement is evaluated according to the following relationship:

$$\delta = C_1 \Delta P \sum_{i=1}^n \frac{\Delta Z_i}{E_{si}} I_{zi}$$

Where:

- C_1 = correction factor to account for strain relief from excavated soil = $1 - \frac{\sigma'_{cd}}{2\Delta P}$;
- σ'_{cd} = effective overburden pressure at the bottom of the footing;
- ΔP = the net applied footing pressure;

- E_{si} = one-dimensional elastic modulus of soil layer i ;
- Δz_i = thickness of the soil layer i ;
- I_{zi} = influence factor at the center of soil layer i .

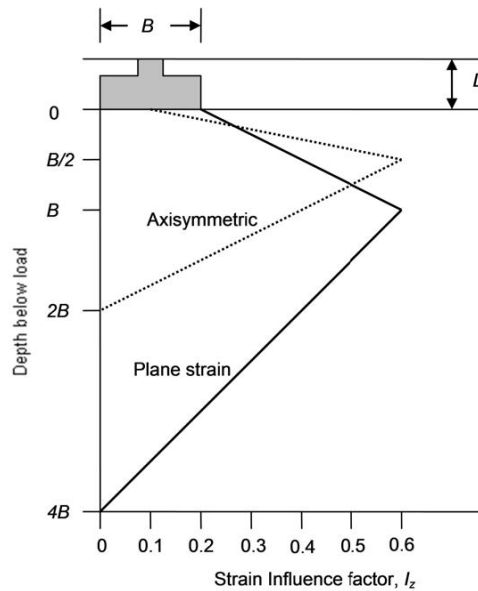


Figure 19. Strain Influence factor vs Depth (Schmertmann, 1978a)

Schmertmann (1978a) suggests evaluating the peak value (I_{zp}) of the influence factor I_z using the following expression:

$$I_{zp} = 0.5 + 0.1 \left(\frac{\Delta P}{\sigma'_{op}} \right)$$

Where σ'_{op} is the effective overburden pressure at the depth (z_p) at which I_{zp} occurs. In case of axisymmetric load condition (i.e. circular or square footing) the depth z_p is equal to $B/2$ (see Figure 19), in case of plane-strain load condition this depth is equal to B (see Figure 19).

The E_{si} (one-dimensional elastic modulus of each soil layer i) values are equal to $2.5q_c$ and $3.5q_c$ in case of axisymmetric and plane-strain load condition, respectively (Schmertmann, 1978a).

4.3.1 Input data to perform the settlement analysis for shallow foundations

It is firstly required that you load the CPT test data and perform the interpretation as described in section 2. Then move in the “Shallow Foundation Tab”.

The following input data are required:

- *Pressure*: specify here the total pressure applied over the foundation area in [kPa];
- *Foundation depth*: specify here the foundation depth if it is embedded in [m];
- *Load type*: insert 1 if the load is axisymmetric, insert 2 in the plane-strain loading condition;
- *Width*: specify here the foundation width in [m].

Finally press the “Calculate settlement” button to load the input data and perform the analysis. Press the “Plot Settlement” button to display the Depth – Cumulative settlement curve (Figure 20).

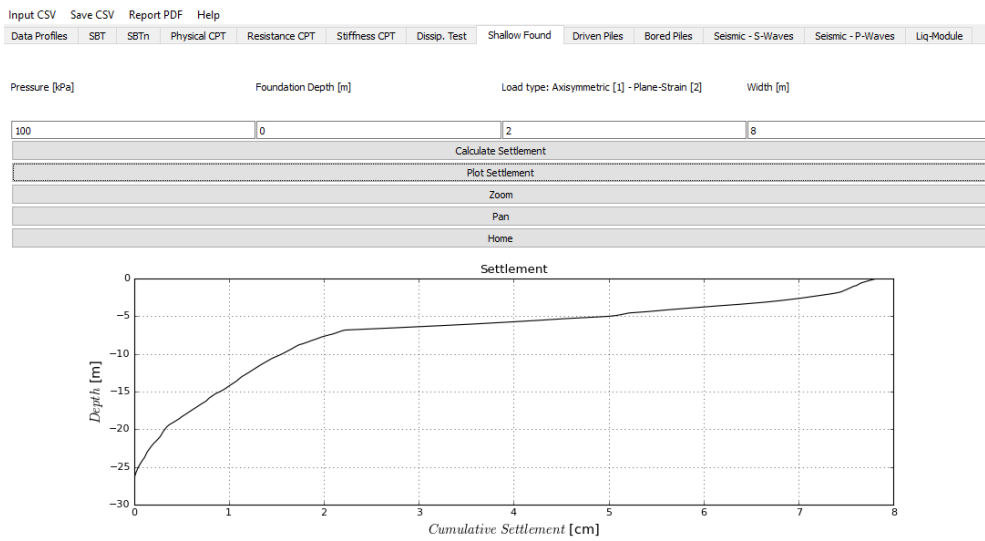


Figure 20. “Shallow Foundation” Tab

4.3.2 Output of the Shallow Foundation module

The results of computations are saved as CSV files in a user-defined folder, using from the main bar *Save CSV* → *Save Shallow Found*.

The saved file and its content and structure is reported in the following:

- *filename_Shallow_foundation.csv* – such a file consists of 2 columns:
 - *column 1*: z, depth [m]
 - *column 2*: Cumulative settlements [m]

5 SPECIAL ISSUES

5.1 Small Strain Damping Ratio from Seismic Measurements

The spectral slope method is used to determine the small strain damping ratio from seismic measurements. In particular only S wave signals are used. The success of the method mainly depends on the following experimental aspects:

- a single hit for generating the two signals;
- use of accelerometers, instead of geophones, with an increased repetitiveness of signal amplitude measurement.

The method is explained in the Annexes. The practical aspects of the use of such method are explained in the present section. The program generates a plot of the Napierian logarithm of the spectral ratio vs. frequency.

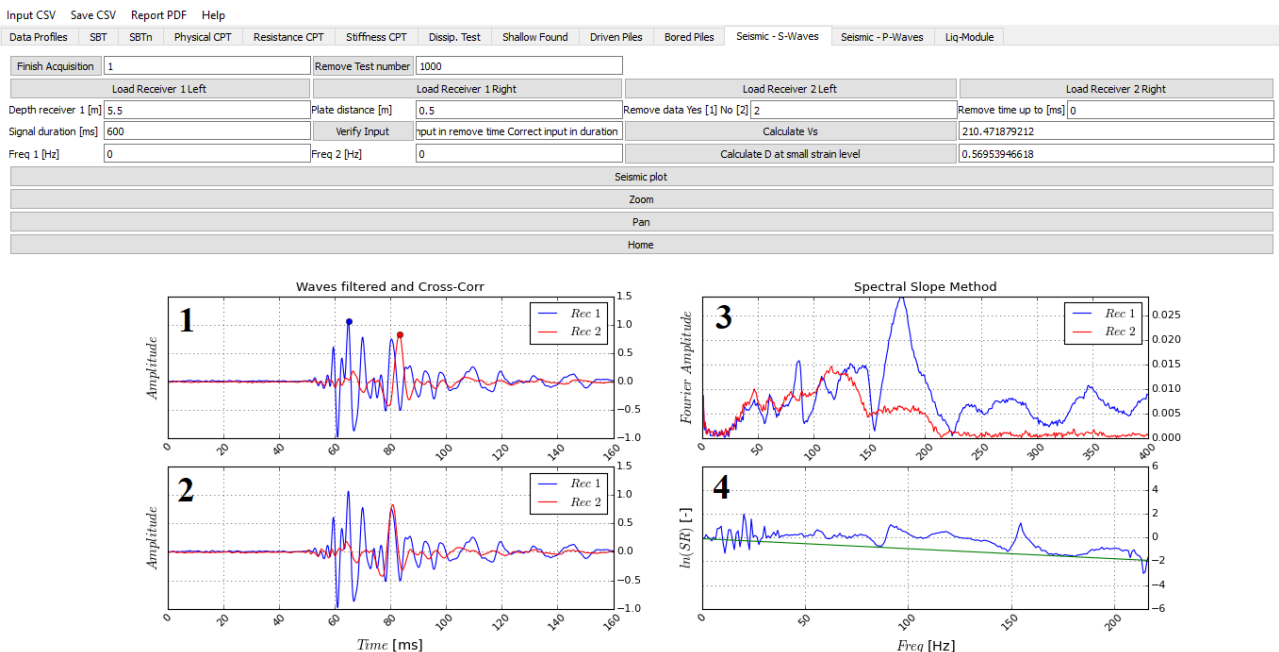


Figure 21. Damping computed using the Spectral Slope Method

The frequency interval is from zero to 120% of the frequency corresponding to the peak of the Fourier Spectrum. Two waveforms are analyzed, therefore two Fourier spectra are computed and two different frequencies are observed as far as the maxima of the spectra are concerned. In order to generate the plot of the Napierian logarithm of the spectral ratio vs. frequency, the higher between these two frequencies is selected. The user can zoom this plot and select a different frequency interval. It is suggested to consider a frequency interval in between 80-120% of the natural frequency. This is estimated, in a first approximation, by means of the following equation:

$$f_n = \frac{V_s}{4H}$$

Where: V_s = propagation velocity of shear waves at the considered depth; H = thickness of the considered layer. We suggest considering H equal to the testing depth.

5.2 Unusual soils

The available soil classification charts or SBT classification systems refer to different databases and mainly consider “conventional soil” i.e. saturated clays/silts/sands or their mixtures. These databases

do not include partially saturated soils or compacted soils or underconsolidated soils (i.e. dredged sediments or poorly compacted earthworks). In any case the applicability of the proposed empirical approaches in a different context becomes questionable.

On the Authors experience, the available classification systems (CPTu) did not give a correct SBT identification in many cases and in particular in the case of loose/very loose silt mixtures.

On the other hand, for soil deposits above the water table, the measured parameters may be affected by two different phenomena:

- partial saturation (i.e. partial drainage);
- soil suction

These two aspects are particularly relevant in the case of fine grained soils or intermediate soils (silt mixtures)

Two different methodologies are proposed for a more accurate CPT interpretation. The first methodology refers to a better estimate of the effective stress state.

For homogeneous (clay) layers above the water table a typical trend of I_c , such as that shown in Figure 22 is observed.

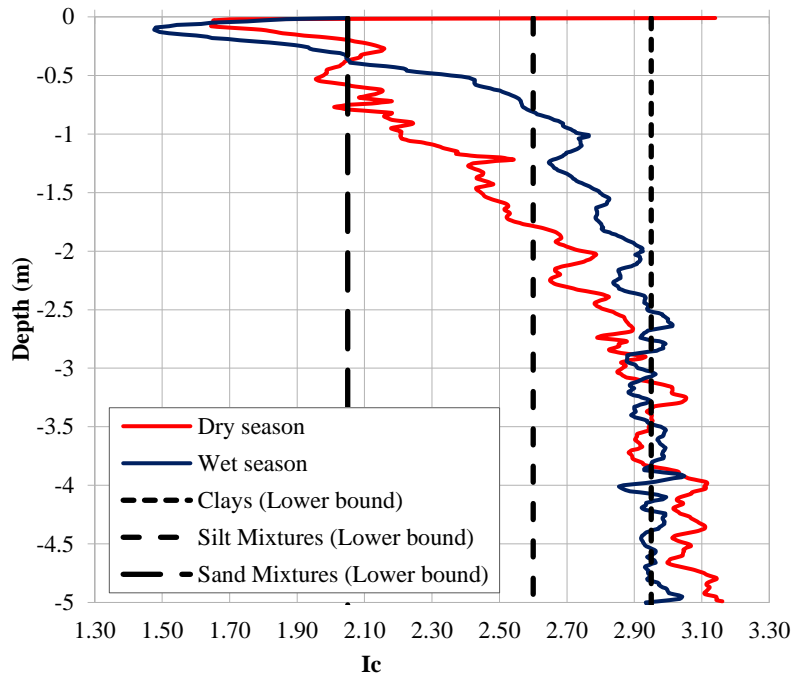


Figure 22. CPTu results – Broni (PV - Italy)

The proposed methodology increases the computed values of σ'_{v0} in order to obtain a reduction of the normalized tip resistance, Q_{tn} , and consequently, an increase of the Soil Classification Index I_c (Robertson, 1990; Robertson and Wride, 1998), according to the equations reported below:

$$I_c = \sqrt{(3.47 - \log Q_{tn})^2 + (\log F + 1.22)^2} \quad (10)$$

$$Q_{tn} = \left(\frac{q_t - \sigma_{v0}}{\sigma_{atm}} \right) \left(\frac{\sigma_{atm}}{\sigma'_{v0}} \right)^n \quad n = 0.381 \cdot I_c + 0.05 \cdot \left(\frac{\sigma'_{v0}}{\sigma_{atm}} \right) - 0.15 \quad (11)$$

$$F = \frac{f_s}{q_t - \sigma_{v0}} \cdot 100 \quad (12)$$

In such a way the I_c index is increased until becomes equal to the target value (i.e. the I_c index value below the water table).

The second methodology is purely empirical and consists in a calibration of the I_c values as inferred from CPTu results against the evidences obtained from direct logging (boreholes). ΔI_c values are user defined. The Annex A3 shows an example of both methodologies.

5.2.1 Input data to estimate the soil effective stress state of shallow layers using a target I_c (1st method)

In order to apply the method to estimate the soil effective stress state of shallow layers by means of a target Classification Index (I_c), firstly, you have to load the CPT test raw data as described in section 2, then you have to move in the “SBTn” Tab and fill the following fields:

1. I_c target: insert here the user defined I_c value;
2. Correction up to depth: insert here the depth (starting from the ground surface) of the shallow soil layer where you want to have an estimate of the soil effective stress state (in meter).

Press the “Apply Method [1]” button (Figure 23) and then move back to the first Tab (“Data Profiles” Tab) and update the plot where are displayed the soil effective and total stresses (Figure 24).

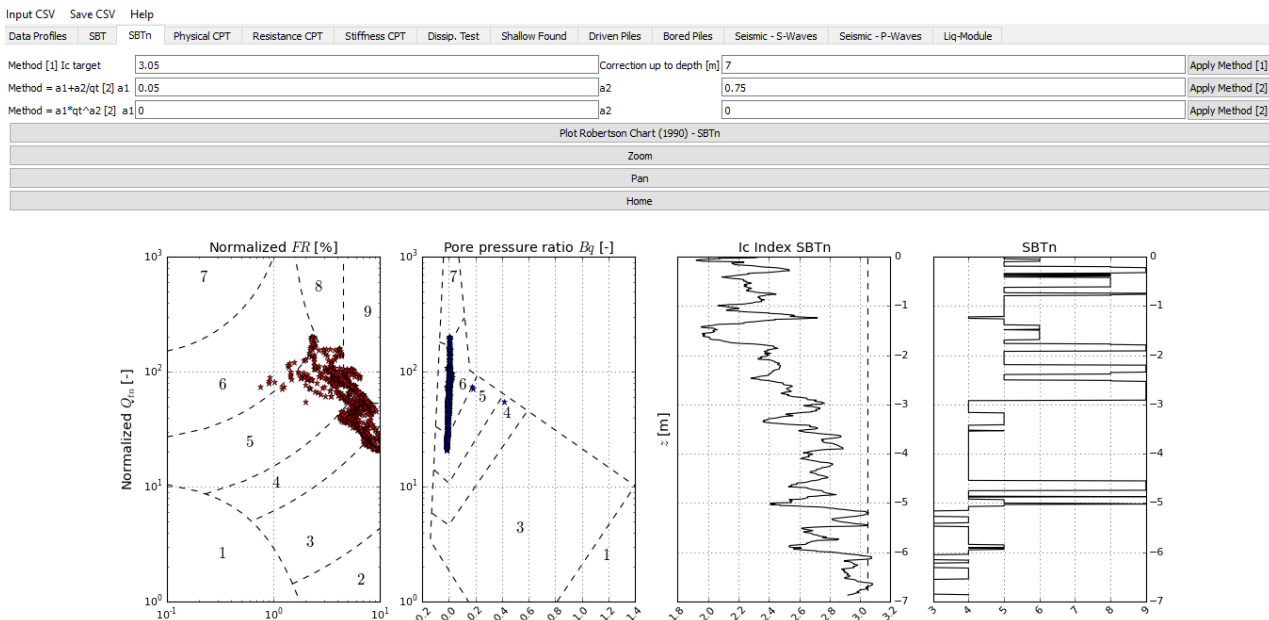


Figure 23. “SBTn” Tab. Application of Method 1 (I_c target)

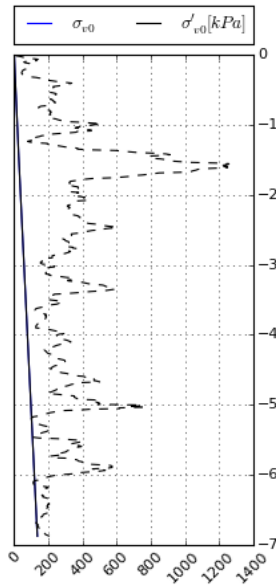


Figure 24. Method 1 results. Estimated soil effective stresses

5.2.2 Output (1st method)

The result of this computation can be saved as CSV file in a user-defined folder, using from the main bar *Save CSV* → *Save CPTu results*.

The estimated soil effective stresses are saved in the column 18 of the output file. Please note that this data column is saved by default in the “filename_CPTu_data.csv” file even if you haven’t used this method, in this case the last column is exactly the copy of the column 8, containing the effective geostatic vertical stress values. This method only gives a possible estimate of suction and consequently of OCR. All the other parameters and classification are not modified.

5.2.3 Input data to apply an I_c correction using an available $\Delta I_c(q_t)$ function (2nd method)

In order to apply this method, firstly, you have to load the CPT test raw data as described in section 2, then you have to move in the “SBTn” Tab and fill the following two fields:

1. Coefficient a_1
2. Coefficient a_2

The values of a_1 and a_2 are necessary to apply a correction (ΔI_c) to all the I_c values evaluated starting from the CPT test raw data. These parameters should be user defined. They can be obtained, for a given site, after calibration of CPT data against borehole information as explained in Annex 3.

$$I_{c,corrected} = -\Delta I_c + I_c$$

Where ΔI_c can be expressed as a function of q_t according to one of the following equations. The type of equation is selected by user:

$$\Delta I_c = a_1 + \frac{a_2}{q_t}$$

$$\Delta I_c = a_1 q_t^{a_2}$$

Press the “Apply Method [2]” button and update the plots in the “SBTn”, “Physical CPT”, “Resistance CPT”, “Stiffness CPT” Tabs using the “Plot...” buttons of each Tab. Modification of I_c index by the user implies a re-interpretation of the test both in term of SBT and of soil parameters.

5.2.4 Output (2nd method)

The results can be saved as CSV file in a user-defined folder, using from the main bar: *Save CSV* → *Save CPTu results*.

5.3 Liquefaction potential from CPTm

In case the results of CPTm are available, we suggest using these data for predicting liquefaction risk after appropriate correction.

In particular, the measured sleeve friction is corrected according to the following equations:

$$f_s(CPTu) = [0.0797 f_s(CPTm)]^{2.504} \quad \text{if } f_s(CPTm) < 65 \text{ kPa}$$

$$f_s(CPTu) = f_s(CPTm) \quad \text{if } f_s(CPTm) \geq 65 \text{ kPa}$$

The I_c (Robertson, 1990; Robertson and Wride, 1998) index is also corrected according to the following equations:

$$\Delta I_c = -0.296 \ln(q_c) + 0.8568$$

$$I_c(\text{corrected}) = I_c(\text{Robertson and Wride, 1998}) - \Delta I_c$$

As explained in Annex 4, the correction was obtained by comparing soil classes of the Schemertmann (1978) approach to those inferred by using the Robertson (1990) SBTn. Mainly the use of Robertson (1990) for interpreting CPTm leads to an underestimate of soil granulometry. The proposed correction applies only when the Robertson (1990) classification underestimate that of Schmertmann (1978b). Details of the method and its rationale are given in the Annexes. As for CPTm, the program only gives the possibility of estimating liquefaction risk. Interpretation of CPTm for soil profile and parameter is not included.

5.3.1 Computation of FS_L from CPTm (Juang et al., 2006)

CSR is computed according to the following equation:

$$CSR = 0.65 \frac{\sigma_v}{\sigma'_v} \frac{a_{max}}{g} r_d$$

Where: σ_v , σ'_v total and effective vertical geostatic stresses; a_{\max} = peak ground acceleration. In principle should be inferred from seismic response analysis in terms of effective stresses. In practice can be inferred from SRA (seismic response analysis) in terms of total stresses or from the simplified procedures prescribed by technical codes. Italian Building Code recommends assuming $a_{\max} = S_S S_T a_{\max,R}$ where $a_{\max,R}$ = peak ground acceleration for a given site and a given return period (Type A soil). S_S and S_T = stratigraphic and topographic amplification factors respectively, which depend on soil type and topography. In absence of specific SRA, type D soil should be considered. Moreover:

$$r_d = \exp[\alpha(z) + \beta(z) M]$$

This shear stress reduction factor accounts for soil flexibility.

$$\alpha(z) = -1.012 - 1.126 \sin\left(\frac{z}{11.73} + 5.133\right)$$

$$\beta(z) = 0.106 + 0.118 \sin\left(\frac{z}{11.28} + 5.142\right)$$

M = Magnitude.

The soil's cyclic strength (CRR) depends on number of cycles of a given amplitude. In other words, it depends on earthquake duration, i.e. earthquake Magnitude. This is accounted for by the MSF (magnitude scale factor). Moreover, an increase of the mean normal stress inhibits the dilatancy. This aspect, relevant for very high stresses, is accounted for by the K_σ factor.

$$K_\sigma = 1 - C_\sigma \ln\left(\frac{\sigma'_v}{p_{atm}}\right) \leq 1.1$$

$$C_\sigma = \frac{1}{37.3 - 8.27(q_{c1N})^{0.264}} \leq 0.3$$

Where:

$$q_{c1N} = C_N \frac{q_c}{p_{atm}} \quad C_N = \left(\frac{p_{atm}}{\sigma'_v}\right)^m \leq 1.7 \quad m = 1.338 - 0.249 q_{c1N}$$

Moreover:

$$MSF = -0.058 + 6.9 \exp(-M/4) \leq 1.8$$

Therefore, the computation of K_σ involves an iterative procedure.

In the approach proposed by Juang et al. (2006) the soil classification index (I_c) is a variant of the soil behavior type index defined by Roberston (1990) and after by Robertson and Wride (1998).

$$I_c(\text{Juang et al., 2006}) = \{[3.47 - \log_{10} q_{c1N}]^2 + [1.22 + \log F]^2\}^{0.5}$$

$$F = \left(\frac{f_s}{q_c - \sigma_{v0}}\right) 100 \quad \text{Note: here } f_s \text{ is the corrected value (see section 5.3)}$$

Fine content (FC) is accounted based on the previously defined soil classification index (I_c) and on the definition of $q_{c1N,m}$, which is the “stress-normalized cone tip resistance q_{c1N} adjusted for the effect of fines on liquefaction”, as follows:

$$q_{c1N,m} = K q_{c1N}$$

The adjustment factor K is part of the regression model (Juang et al., 2006) and is expressed as:

$$K = 1 \quad \text{for} \quad I_c < 1.64$$

$$K = 1 + 80.06(I_c - 1.64)(q_{c1N})^{-1.2194} \quad \text{for} \quad 1.64 \leq I_c \leq 2.38$$

$$K = 1 + 59.24(q_{c1N})^{-1.2194} \quad \text{for} \quad I_c > 2.38$$

The above I_c is that computed according to the procedure proposed by Juang et al., 2006. According to published empirical equations (Lunne et al., 1997; Baez et al., 2000), $I_c = 1.64$ corresponds approximately to a fines content (FC) of 5%, and $I_c=2.38$ corresponds approximately to $FC=35\%$. Thus, the three classes of liquefaction boundary curves are consistent with the commonly defined classes of boundary curves, namely, $FC<5\%$, $5\% \leq FC \leq 35\%$ and $FC>35\%$ (Seed et al., 1985; Andrus and Stokoe, 2000).

The cut-off I_c parameter can be user defined. The default value is 2.6.

The cyclic resistance ratio is computed as follows:

$$CRR = \exp \left[-2.9439 + 0.000309(q_{c1N,m})^{1.8} \right]$$

The safety factor is then computed as follows:

$$FS_L = MSF K_\sigma \frac{CRR}{CSR}$$

The final output consists of:

- a profile of the safety factor against liquefaction and an estimate of LPI, as shown in Figure 15 in section 4.1.1.
- an output file as follows:
 - **filename_mech_liq_output.csv** – such a file consists of 17 columns:
 - *column 1*: z, depth [m]
 - *column 2*: q_c , tip resistance [MPa]
 - *column 3*: f_s , sleeve friction [kPa]
 - *column 4*: corrected f_s , corrected sleeve friction [kPa]
 - *column 5*: Total geostatic vertical stress [kPa]
 - *column 6*: Effective geostatic vertical stress [kPa]
 - *column 7*: Q , normalized tip resistance [-]
 - *column 8*: I_c (Roberston, 1990), classification index
 - *column 9*: corrected I_c , corrected classification index
 - *column 10*: equivalent SBTn class (using the Schmertmann Classification Chart)

- *column 11*: SBTn (Robertson, 1990)
- *column 12*: q_{c1N} (Juang et al., 2006)
- *column 13*: $q_{c1N,m}$ (Juang et al., 2006)
- *column 14*: $CRR_{7.5}$ (Juang et al., 2006)
- *column 15*: CSR (Juang et al., 2006)
- *column 16*: FS_L (Juang et al., 2006)
- *column 17*: cumulative LPI (Juang et al., 2006)

6 REFERENCE LIST

Alsamman, O. M. (1995). The use of CPT for calculating axial capacity of drilled shafts (Doctoral dissertation, University of Illinois at Urbana-Champaign).

Andrus, R. D., & Stokoe II, K. H. (2000). Liquefaction resistance of soils from shear-wave velocity. *Journal of Geotechnical and Geoenvironmental Engineering*, 126(11), 1015-1025.

Aubertin M., Mbonimpa M., Bussière B., and Chapuis R.P. (2003) “A physically-based model to predict the water retention curve from basic geotechnical properties”. *Canadian Geotechnical Journal*

Aubertin M., Ricard J.F., Charpuis R.P. (1998), “A predictive model for the water retention curve: application to tailings from hard-rock mines. *Canadian Geotechnical Journal*, 35, pp. 55-69 (with Erratum, 36, 401)

Baez, J. I., Martin, G. R., & Youd, T. L. (2000). Comparison of SPT-CPT liquefaction evaluations and CPT interpretations. In *Innovations and Applications in Geotechnical Site Characterization* (pp. 17-32).

Baldi, G., Bellotti, R., Ghionna, V. N., Jamiolkowski, M., & Lo Presti, D. C. F. (1989, August). Modulus of sands from CPTs and DMTs. In *Proc. 12th ICSMFE* (Vol. 1, pp. 165-170).

Boulanger, R. W., & Idriss, I. M. (2015). CPT-based liquefaction triggering procedure. *Journal of Geotechnical and Geoenvironmental Engineering*, 142(2), 04015065.

Chen B.S.-Y. and P.W. Mayne (1996) “Statistical Relationships Between Piezocone Measurements and Stress History of Clays,” *Canadian Geotechnical Journal*, Vol. 33, No. 3 pp. 488–498

Chen, B.S.-Y., P.W. Mayne (1996) “Profiling the Overconsolidation Ratio of Clays by Piezocone Tests”, Report No. GIT-CEEAGEO-94-1 to National Science Foundation by Geosystems Engineering Group, Georgia Institute of Technology, Atlanta, 1994, 280 pp. [Online]. Available:<http://www.ce.gatech.edu/~geosys/Faculty/Mayne/papers/index.html>.

Fahey, M., & Carter, J. P. (1993). A finite element study of the pressuremeter test in sand using a nonlinear elastic plastic model. *Canadian Geotechnical Journal*, 30(2), 348-362.

GEOLOGISMIKI (2009) – *CPeT-IT User's Manual v.1.3*. <http://www.geologismiki.gr/Documents/CPeT-IT/HTML/index.html>.

Geostru (2017) Static Probing, https://www.geostru.eu/wp-content/plugins/pdfcatalog2/cache/categories/full-it_217c86ab29.pdf

Iwasaki, T. (1978). A practical method for assessing soil liquefaction potential based on case studies at various sites in Japan. In Proc. Second Int. Conf. Microzonation Safer Construction Research Application, 1978 (Vol. 2, pp. 885-896).

Iwasaki, T., Tokida, K., Tatsuoka, F., Watanabe, S., Yasuda, S., & Sato, H. (1982, June). Microzonation for soil liquefaction potential using simplified methods. In Proceedings of the 3rd international conference on microzonation, Seattle (Vol. 3, pp. 1310-1330).

Jardine, R., Chow, F., Overy, R., & Standing, J. (2005). ICP design methods for driven piles in sands and clays (p. 112). London: Thomas Telford.

Jamiolkowski, M., Ghionna, V. N., Lancellotta, R., & Pasqualini, E. (1988). New applications of penetration tests in design practice. In Proceedings of the First International Symposium on Penetration Testing (ISOPT I).

Juang, C. H., Fang, S. Y., & Khor, E. H. (2006). First-order reliability method for probabilistic liquefaction triggering analysis using CPT. *Journal of Geotechnical and Geoenvironmental Engineering*, 132(3), 337-350.

Kovacs G. (1981) "Seepage Hydraulics" Elsevier Science Publishers, Amsterdam

Kulhawy, F.H., P.W. Mayne (1990) "Manual on Estimating Soil Properties for Foundation Design" Report EPRI EL-6800, Electric Power Research Institute, Palo Alto, Calif., 306 pp.

Lancellotta, R. (1983). Analisi di affidabilità in ingegneria geotecnica. Atti Istituto Scienza Costruzioni, No. 625, Politecnico di Torino.

Lo Presti, D., Giusti, I., Cosanti, B., Squeglia, N., & Pagani, E. (2016). Interpretation of CPTu in "unusual" soils. *Italian Geotechnical Journal*, 4/2016.

Lo Presti D., Jamiolkowski M., Pepe M. (2003) "Geotechnical characterization of the subsoil of Pisa Tower" Invited Lecture International Workshop on Characterization and Engineering Properties of natural soils", (National University of Singapore, Dec. 2003), Balkema, vol. II, pp. 909-946

Lunne T, Roberston PK, and Powell JJM (1997). Cone penetration testing, Blackie Academic & Professional, London.

Mayne, P.W. (2005) "Integrated Ground Behavior: In-Situ and Lab Tests," Deformation Characteristics of Geomaterials, Vol. 2 (Proc. Lyon, France), Taylor & Francis, London, United Kingdom, pp. 155-177

Mayne, P. W. (2006). The Second James K. Mitchell Lecture Undisturbed sand strength from seismic cone tests. *Geomechanics and Geoengineering: An International Journal*, 1(4), 239-257.

Mayne, P. W. (2006, November). In-situ test calibrations for evaluating soil parameters. In *Characterisation and Engineering Properties of Natural Soils—Proceedings of the Second International Workshop on Characterisation and Engineering Properties of Natural Soils*: Taylor & Francis (pp. 1601-1652).

Mayne, P. W. (2007). NCHRP Synthesis 368: Cone penetration testing. Transportation Research Board, Washington, DC, 118.

Mayne P.W., Campanella, R.G. (2005) “Versatile Site Characterization by Seismic Piezocone,” Proceedings, 16th International Conference on Soil Mechanics and Geotechnical Engineering, Vol. 2 (Osaka), Millpress, Rotterdam, The Netherlands, pp. 721–724

Mayne P.W., Kulhawy F.H. (1982) “K₀-OCR Relationships in soil” Journal of Geotechnical Engineering, Vol. 108 (GT6), 851-872

Mayne, P. W., Mitchell, J. K., Auxt, J. A., & Yilmaz, R. (1995). US national report on CPT. In Proceedings of the International Symposium on Cone Penetration Testing, CPT (Vol. 95, pp. 263-276).

Mayne, P. W., & Peuchen, J. (2012). Unit weight trends with cone resistance in soft to firm clays. Geotechnical and geophysical site characterization, 4, 903-910.

Pagani (2017) <http://www.pagani-geotechnical.com/it/>

Puci, I., & Lo Presti, D. C. F. (1998, September). Damping measurement of reconstituted granular soils in Calibration Chamber by means of seismic tests. In Proceedings of the 11th European Conference on Earthquake Engineering (pp. 6-11).

Randolph, M. F., & Wroth, C. P. (1978). Analysis of deformation of vertically loaded piles. Journal of Geotechnical and Geoenvironmental Engineering, 104(ASCE 14262).

Robertson, P.K. (1990) “Soil classification using the cone penetration test”; Canadian Geotechnical Journal, 27(1): 151–158

Robertson P.K. (2009a) “Interpretation of cone penetration tests – a unified approach” Canadian Geotechnical Journal, 46: 1337-1335

Robertson, P. K. (2009b). Evaluation of flow liquefaction and liquefied strength using the cone penetration test. Journal of Geotechnical and Geoenvironmental Engineering, 136(6), 842-853.

Robertson, P. K., & Cabal, K. L. (2012). Guide to Cone Penetration Testing, Greg Drilling & Testing. INC. Corporate Headquarters, Signal Hill, California

Robertson, P. K., Campanella, R. G., Gillespie, D., & Greig, J. (1986, June). Use of piezometer cone data. In Use of in situ tests in geotechnical engineering (pp. 1263-1280). ASCE.

Robertson P.K., Wride C.E. (1998), “Evaluating cyclic liquefaction potential using the cone penetration test” Canadian Geotechnical Journal 35, N. 3: 442-459

Schmertmann, J.H. (1970). Static cone to compute static settlement over sand. ASCE Journal of Soil Mechanics & Foundations Division, 96 (3), 1011-1043.

Schmertmann J.H. (1978b) “Guidelines for cone penetration test performance and design” US Dept. of Transportation, FHWA, R.78-209. Washington D.C.

Schmertmann, J.H., Hartmann, J.P. and Brown, P.R. (1978a). Improved strain influence factor diagrams, ASCE Journal of the Geotechnical Engineering Division, 104 (GT8), 1131-1135.

Seed, H.B., Tokimatsu, K., Harder, L. F., & Chung, R. M. (1985). Influence of SPT procedures in soil liquefaction resistance evaluations. *Journal of Geotechnical Engineering*, 111(12), 1425-1445.

Sully J.P., P.K. Robertson, R.G. Campanella, D.J. Woeller, (1999) "An approach to evaluation of filed CPTU dissipation data in overconsolidated fine-grained soils", Canadian Geotechnical Journal 36: 369-381

Teh, C. I., & Houlsby, G. T. (1991). Analytical study of the cone penetration test in clay. *Geotechnique*, 41(1), 17-34.

Youd, T. L., & Idriss, I. M. (2001). Liquefaction resistance of soils: summary report from the 1996 NCEER and 1998 NCEER/NSF workshops on evaluation of liquefaction resistance of soils. *Journal of geotechnical and geoenvironmental engineering*, 127(4), 297-313.

7 ANNEXES:

7.1 VERIFICATION OF EMPIRICAL EQUATIONS FOR OCR

In literature, many empirical or semi-empirical correlations are available for the estimation of the value of the pre-consolidation stress, and therefore the over consolidation ratio. In the present chapter, the following relationships have been taken into account:

for Intact Clays (SBTn classes: 1,2,3,4,9):

- Mayne et al., 1995: $\sigma'_p = 0.33 (q_t - \sigma_{v0})$
- Chen & Mayne, 1996: $\sigma'_p = 0.53 (u_2 - u_0)$
- Mayne, 2005: $\sigma'_p = 0.60 (q_t - u_2)$

for Sands (SBTn classes: 5, 6, 7, 8), Mayne (2005):

$$OCR = \left[\frac{0.192 \left(\frac{q_t}{\sigma_{atm}} \right)^{0.22}}{(1 - \sin \varphi') \left(\frac{\sigma'_{v0}}{\sigma_{atm}} \right)^{0.31}} \right]^{\left(\frac{1}{\sin \varphi' - 0.27} \right)}$$

for all intact materials (Mayne, 2007):

$$\sigma'_p = 0.101 \sigma_{atm}^{0.102} G_0^{0.478} (\sigma'_{v0})^{0.420} ;$$

Where G_0 is (Robertson P.K.,2009a):

$$G_0 = (q_t - \sigma_{v0}) \cdot 0.0188 \cdot 10^{0.55I_c + 1.68}$$

The CPTu tests (16) have been carried out in Pisa (Italy) in the “Porta a Mare” district. The subsoil of Pisa belongs to the alluvial (Holocene-Pleistocene) deposits of the Arno River. The first 60 m are characterised by the following profile (Lo Presti et al., 2003):

- Horizon A: upper variable deposits from 3 to 10 meters, consists of silt, clay and sand of various thickness. The main characteristic of this horizon is that the sediments have been deposit in an estuarine environment, in salty water
- Horizon B: clayey deposits from 10 to 40 m, subdivided in four sub-layers
 - High plasticity marine clay. It is a soft sensitive clay called Pancone clay
 - Intermediate clay and sand layers, similar to the deposit of Horizon A
 - Soft clay similar to Pancone
- Horizon C: lower sand deposits from 40 to 60 m, consists of eolian sands with inter-layers of silt and clay

The CPTu tests have been carried up to a depth of 35 meters. The subsoil is characterised by a first layer of sandy silt from 1 to 3 meters, a second layer of silty clay from 3 to 5 meters and a third layer of clay from 5 to 7 meters. Below this layer sand is present from 6.8 m to 7.8 meters (Grey sands).

As far as the first 3 m is concerned, the subsoil is characterised by a first layer of sandy silt and a second layer of silty clay lying upon the clay layers of Horizon A.

The following figures show the results related to the correlations adopted to interpret CPTu data obtained in Pisa from 16 tests. Figure 25 shows the typical effective stress and overconsolidation ratio trend in the Pisa area. In particular, the figure is related to the studies made on the subsoil of Pisa Tower (Lo Presti et al., 2003). Figure 26 and Figure 27 show the OCR profile obtained with the analysed correlations.

The correct overall OCR trend is reproduced from all the correlations taken into account, but the most suitable and stable correlation seems to be the Mayne (2007), applicable to all intact materials and depending on the estimation of the small-strain shear modulus G_0 .

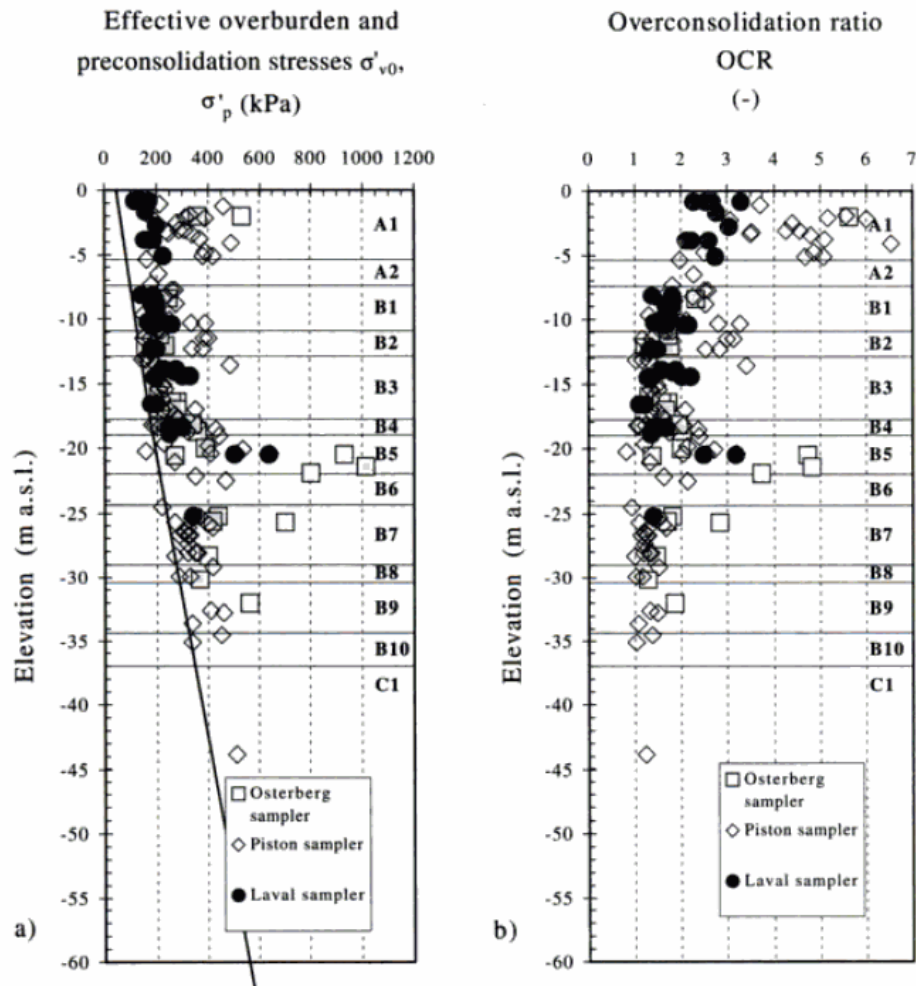


Figure 25: Effective stress and overconsolidation ratio profiles of the soils underlying the Pisa Tower (Lo Presti et al., 2003)

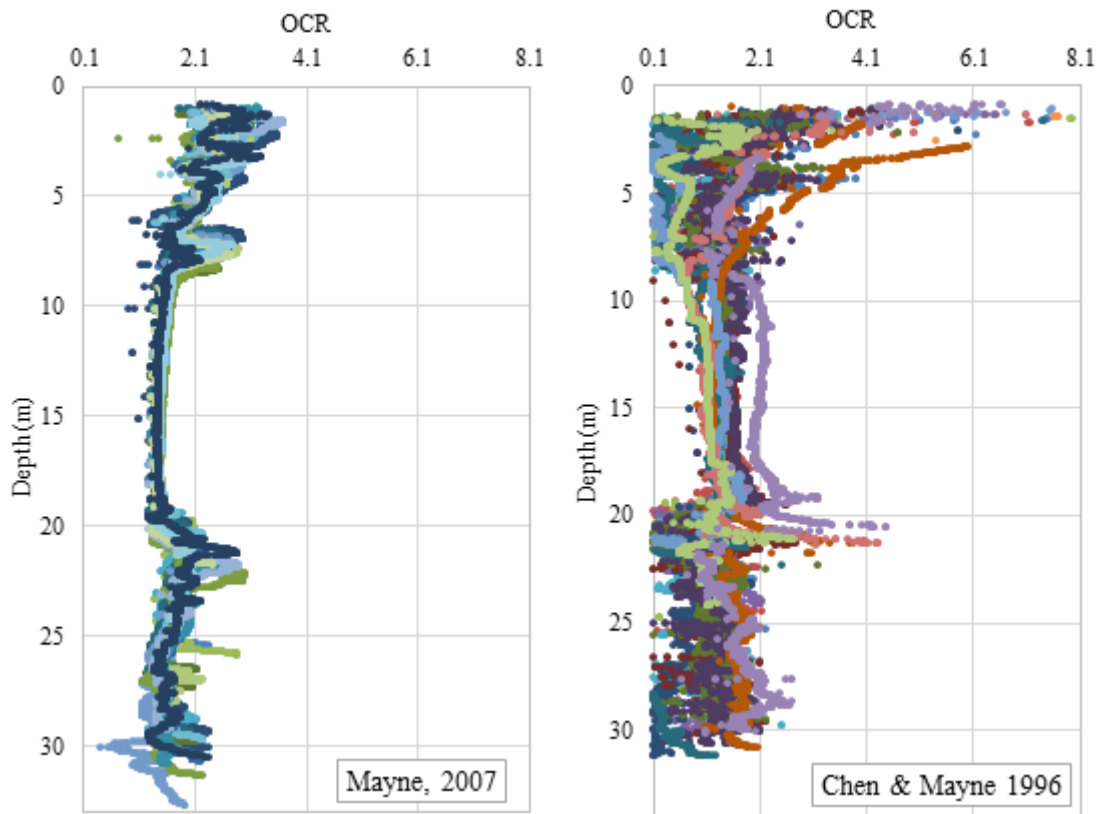


Figure 26: OCR valuation with Mayne (2007) and Chen & Mayne (1996) correlations.

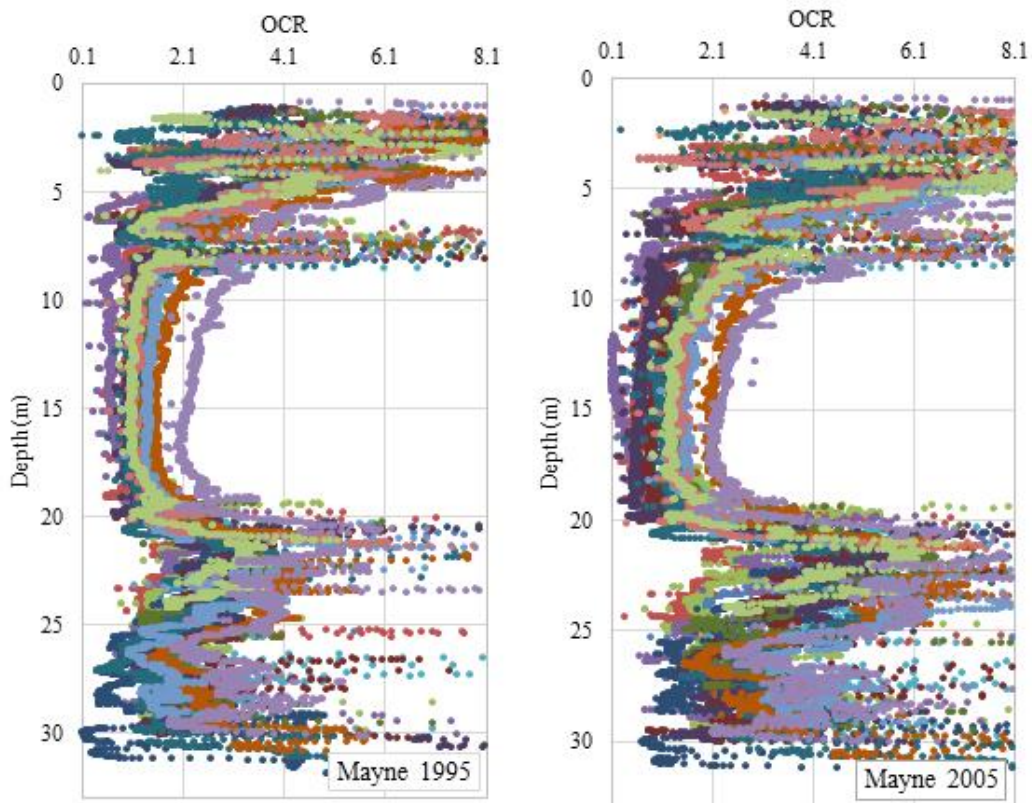


Figure 27: OCR valuation with Mayne (1995) and Mayne (2005) correlations.

7.2 *Lo Presti et al. (2017) – KL in 2017 ICCE – Use in practice of seismic tests*

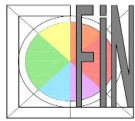
Lo Presti, D.; Stacul, S.; Giusti, I.; Meisina, C.; Persichillo, M. G.; Pagani, E.; Siviero, M.; Uruci, E. and Pagani, E. (2017) “*Use in practice of seismic tests according to Eurocodes*”. 2017 ICCE International Conference of Civil Engineering, Tirana.

7.3 *Lo Presti et al. (2016) - CPTu in unusual soil*

Lo Presti, D.; Giusti, I.; Cosanti, B.; Squeglia, N. and Pagani, E. (2016). “*Interpretation of CPTu in ‘unusual’ soils*”. Italian Geotechnical Journal, 4/2016.

7.4 *Meisina et al. (2017) in 2017 ICCE – Liquefaction risk analysis with mechanical CPT*

Meisina, C.; Persichillo, M. G.; Francesconi, M.; Creatini, M.; Uruci, E. and Lo Presti, D. (2017). “*Differences between mechanical and electrical cone penetration test in the liquefaction hazard assessment and soil profile reconstruction*”. 2017 ICCE International Conference of Civil Engineering, Tirana.



Use in practice of seismic tests according to Eurocodes

Diego Carlo Lo Presti¹, Stefano Stacul¹, Ilaria Giusti¹, Claudia Meisina², Maria Giuseppina Persichillo², Edoardo Pagani³, Massimiliano Siviero³, Ervis Uruci³, Ermanno Pagani³

¹*Department of Civil and Industrial Engineering, University of Pisa, Pisa, Italy*

²*Department of Earth and Environmental Sciences, University of Pavia, Pavia, Italy*

³*Pagani Geotechnical Equipment, Calendasco (PC) Italy*

Abstract

Seismic tests consist in the measurement of propagation velocity of body or surface waves into the subsoil or at the contact soil/air or soil/water. Surface waves are dispersive by nature and propagate along the contact surface of two media having very different properties. Surface waves velocities can be measured at ground surface or at the sea floor. Body wave velocities are measured in hole and therefore require a single or multiple holes. A cost effective way of conducting such a test is to push into the soil the receivers as in the case of Seismic CPT (SCPT) or Seismic DMT (SDMT). Measurements require a source, single or multiple receivers, trigger and data acquisition system. This KN paper gives some details about testing procedures and focuses on the practical use of seismic measurements in Civil Engineering. More specifically, the following applications are considered: assessment of seismic action at a given site, definition of impedance function for dynamic soil-structure interaction, in situ assessment of damping ratio. A comparative case that was conducted at the University of Pavia campus, is shown.

1

Keywords: *Seismic tests, seismic actions, Eurocode, impedance functions, damping ratio.*

1

2

1 INTRODUCTION

It is well known that the analysis of the complex dynamic soil-foundation-superstructure interaction can be simplified studying separately [1]:

1. the free-field response;
2. the kinematic interaction;
3. the inertial interaction.

The first step provides an estimate of the seismic motion variation during the propagation of the seismic waves from the bedrock to the ground surface, in terms of amplitude and frequency content, due to the presence of a weaker overlaying soil deposit. Such an analysis neglects the influence of both the foundation and the superstructure and only requires the wave velocity profile and the soil parameters (according to the selected constitutive model). The other two steps also require the foundation impedance functions.

It is worth noticing that free – field seismic response analyses are also used for seismic microzonation studies.

In any case, assessment of the soil volume which is relevant for the study problem and the velocity – wave profile within such a soil volume are fundamental. In the following, the measurement methods are shown as well as the parameters that can be obtained from the seismic measurements, in the light of Eurocode 8 prescriptions. The paper also shows a comparative study case of seismic measurements that were conducted in the campus of the University of Pavia, Italy.

2 METHODS FOR SEISMIC TESTS AND PARAMETER ASSESSMENT

Seismic tests are conventionally classified into borehole (invasive) and surface (non-invasive) methods. They are based on the propagation of body waves [compression (P) and/or shear (S)] and surface waves [Rayleigh (R)], which are associated to very small strain levels (i.e. less than 0.001 %) [2]. Assuming a linear elastic response, the following relationships allow to compute the small-strain deformation characteristics of the soil from the measured body wave phase velocities:

$$G_o = \rho V_s^2 \quad (1)$$

$$M_o = \rho V_p^2 \quad (2)$$

$$\nu = (V_p^2 - 2V_s^2) / 2(V_p^2 - V_s^2) \quad (3)$$

where: G_o, M_o = small strain shear and constrained modulus respectively; ρ = mass density; V_s, V_p = velocity of shear and compression waves respectively; ν = Poisson ratio.

The above relationships hold for elastic isotropic media. Moreover, in the case of saturated porous media the measured P wave velocity corresponds to the compression wave of the first kind [3-4] that is strongly influenced by the pore fluid. In this case the above equations are no longer valid and must be replaced with the corresponding ones of poroelasticity theory.

Seismic tests may also be used to determine the material damping ratio by measuring the spatial attenuation of body or surface waves:

$$D_o = \frac{\alpha V}{2\pi f} \quad (D_o < 10\%) \quad (4)$$

where D_o = small-strain material damping ratio; α, V = attenuation coefficient and velocity, respectively, of P, S or R waves and f = frequency.

Material damping measurements are difficult because they require accurate measurements of seismic wave amplitude and accurate accounting of the effects of geometric (radiation) attenuation [5].

Even at strains less than the linear threshold strain, soils have the capability not only of storing strain energy (elastic behaviour) but also of dissipating it over a finite period of time (viscous behaviour) [6]. This type of behaviour can accurately be modelled by the theory of linear viscoelasticity. An important result predicted by this theory is that soil stiffness and material damping are not two independent parameters, but they are coupled due to the phenomenon of material dispersion [7].

Lai and Rix (1998) [8], Lai et al. (2001) [9], Rix et al. (2001) [10] and Lai et al. (2002) [11] developed implies rigorous approaches for a simultaneous estimate of the velocity of propagation of seismic waves and material damping ratio.

2.1 Borehole Methods

The most widely used borehole methods in geotechnical engineering are Cross Hole (CH), Down Hole (DH), Suspension PS logging (PS) [12] tests. Strictly speaking, the Seismic Cone (SCPT) and Seismic Dilatometer (SDMT) tests are not borehole methods, but they are based on the same principle. Their popularity is due to the conceptual simplicity. The measurement of the travel time of P and/or S waves, travelling between a source and one or more receivers is determined from the first arrival of each type of wave. Current practice of borehole methods is covered by many comprehensive works [1; 13-17]. In the following, only some aspects of the borehole methods are briefly summarized. In particular, the focus is placed on emphasising the importance of respecting these testing procedures:

- good mechanical coupling between receiver, borehole casing (if used) and surrounding soil must be guaranteed. A distinct advantage of the SCPT and SDMT is that good coupling is virtually assured. With conventional cased and grouted boreholes, good coupling is less certain and, more importantly, is difficult to verify. The need for good coupling is particularly important for attenuation measurements, which require accurate amplitude data;
- a check of the borehole verticality with an inclinometer is also highly recommended in order to determine accurately the length of wave travel path in CH tests;
- it is important to generate repeatable waveforms with the desired polarity and directivity. This allows receivers to be oriented in such a way to optimise the measurement of a particular wave type, the use of reversal polarity to make the identification of wave arrivals easier, and measurements along different directions to infer structural and stress-induced anisotropy as explained below;
- in down-hole measurement, the use of two of receivers located at a fixed distance apart [18] can increase the accuracy and the resolution because the true interval method for data interpretation can be implemented;
- dedicated portable dynamic signal analysers and computer-based data acquisition systems allow more sophisticated data processing methods. Thanks to these enhancements, it is now possible to routinely use cross correlation (time domain) or cross power spectrum (frequency domain) techniques to estimate travel times instead of subjective identification of the first arrivals in the time histories. In addition, as multi-channel data acquisition systems become more common, the logical extension will be to use arrays of receivers and array-based signal processing (seismic tomography).

Generally, the shear wave velocity profiles inferred from various borehole tests are in good agreement (see the example in Figure 1). However, SCPTs generally provide values of the shear wave velocity slightly larger than those inferred from down-hole or cross-hole tests.

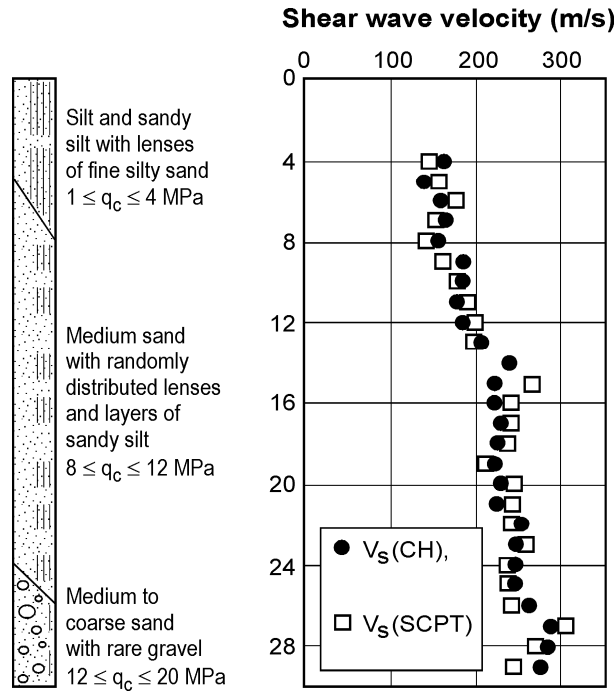


Figure 1 Shear wave velocity in Po river sand [19]

Some researchers stated that the differences between the velocities that were inferred from CH and DH tests could be attributed to soil heterogeneity and anisotropy. The following considerations explain why anisotropy cannot be responsible for these differences. In CH tests, S waves propagate in the horizontal direction with vertical particle motion (S_{hv}). This type of wave is generated by conventional mechanical source. Use of electromagnetic source (which is not usual) can generate waves that are polarized in the horizontal plane (S_{hh}). In DH tests, propagation of the S wave is sub vertical with horizontal particle motion (S_{vh}). In a continuous medium, the V_s^{vh} and V_s^{hv} shear wave velocities are the same and a unique value of the shear modulus ($G_{vh} \equiv G_{hv}$) is expected. Figure 2 shows that $V_s^{vh} = V_s^{hv}$ (i.e. $G_{vh} \equiv G_{hv}$) in the case of laboratory tests on reconstituted sample of Fujinomori clay [20]. Measurements of the propagation velocity S_{vh} and S_{hv} waves were performed by means of Bender Elements (BE). Similar results were obtained in the case of reconstituted sands by Stokoe et al. (1991)[21], Lo Presti & O' Neill (1991)[22] and Bellotti et al. (1996)[23]. Hence, different values of shear wave velocity from CH and DH tests are most likely due to soil heterogeneity, different volume of soil that was interested by the ray paths, as well as intrinsic scatter of experimental measurements [14].

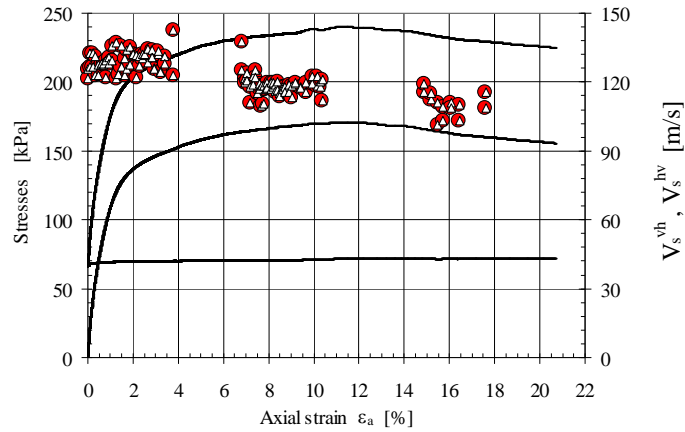


Figure 2 V_s^{vh} and V_s^{hv} measured with BE during drained CLTX test on Fujinomori clay

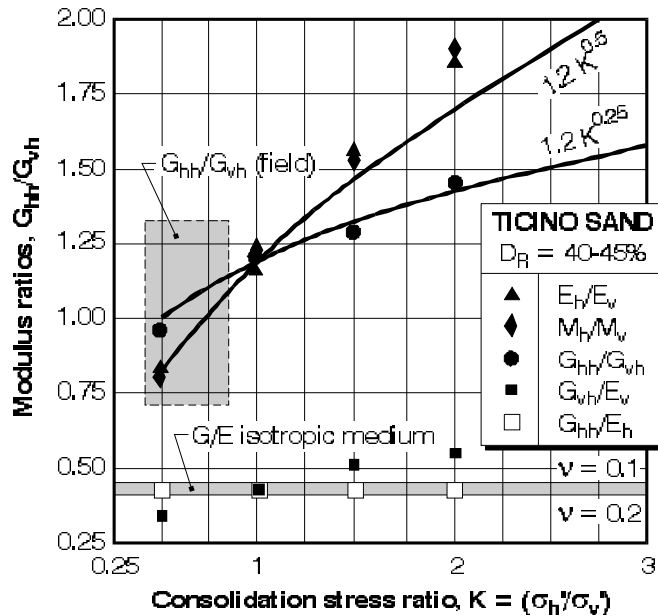


Figure 3 Small strain stiffness anisotropy: field versus laboratory data (modified after [23])

The assessment in situ of inherent and stress induced elastic anisotropy is possible by measuring the velocity of propagation of both S_{hv} and S_{hh} waves in CH tests [24-26]. S_{hh} waves propagate in the horizontal direction with particle motion polarized in the complementary horizontal direction. This additional information enables the evaluation of the G_{hh}/G_{vh} ratio, which is a function of inherent and stress-induced anisotropy. Figure 3 summarises some field and calibration chamber data. Figure 3 indicates that, for the considered granular soils, the inherent anisotropy (inferred at $K_c = 1$) causes a 20% to 25% increase in G_{hh} over G_{vh} . The influence of stress induced anisotropy is apparent for other values of K_c .

Efforts have been done to inferring the small-strain damping ratio, D_o from borehole tests. The current methods are based on measures of the spatial attenuation between two or more receivers. The most widely used methods include:

- a) *The spectral ratio method* [27][28] is based on the following assumptions which hold only in the far field: i) the amplitude of the body waves decreases in proportion to r^{-1} , where r is the distance from the source, due to geometric attenuation and ii) the soil-receiver transfer function can be considered identical for both receivers. Based on the above assumptions, the damping ratio can be computed by means of the following equation:

$$D(f) = \frac{\ln[A_1(f) \cdot r_1 / A_2(f) \cdot r_2]}{\Phi(f)} \quad (5)$$

where: r_1 and r_2 are the distances from the source of a pair of receivers, $A_1(f)$ and $A_2(f)$ are the amplitude spectra at the two receivers and $\Phi(f)$ is the phase difference between the two receivers.

- b) *The spectral slope method*, originally developed for downhole measurements [29] [30] differs from the spectral ratio method because it assumes that material damping is frequency independent and that it is not necessary to define the law for geometric attenuation. The attenuation constant, defined as the ratio of attenuation coefficient to frequency $k = \alpha / f$, represents the spectral slope, i.e. the slope of the spectral ratio vs. frequency curve:

$$k = \frac{-\Delta\{\ln[A_1(f) / A_2(f)]\}}{\Delta f (r_2 - r_1)} \quad (6)$$

therefore the material damping can be computed using the following expression:

$$D(f) = \frac{-\Delta\{\ln[A_1(f) / A_2(f)]\}}{\Delta f \cdot 2\pi \cdot \Delta t(f)} \quad (7)$$

Both methods require signal processing prior to interpretation to isolate direct arrivals and frequency ranges. They provide damping values in the bandpass range of the filter.

Khawaja (1993) [31] and Fuhrman (1993) [28] recommend performing crosshole tests with four boreholes, in order to obtain stable values of damping with the spectral ratio method. They suggested placing the source in the outer boreholes, in order to propagate waves in both forward and reverse directions, and the receivers in the two central boreholes. The spectral ratio method with combined directions provides stable values of damping and avoids the extreme case of negative damping values [32]. The main concerns with the application of these methods is the accuracy in measuring wave attenuation. Use of combined directions and of a maximum distance (source – receiver) of about 8 m should compensate the low repeatability of geophones in terms of amplitude. On the other hand the use of calibrated accelerometers should be preferable especially in the case of short distances between receivers. Campanella & Stewart (1990) [32] studied the applicability of the above methods to the downhole SCPT's. They found that the spectral slope method provides more realistic values of material damping. However, in downhole tests, wave amplitudes are also affected by reflection/transmission phenomena at the interfaces between layers and by ray path divergence: these phenomena make more complicate the interpretation of the particle motion amplitude.

Examples of damping measurements with the spectral ratio and spectral slope methods for reconstituted Ticino sand can be found in Puci & Lo Presti, (1998) [33]. The results are from seismic tests, performed with miniature geophones embedded in large-size calibration

chamber specimens. Figure 4 [33] compares the damping ratio values obtained in the case of reconstituted Ticino sand from laboratory tests (RCT) and those inferred from the spectral ratio and spectral slope methods applied to calibration chamber seismic tests. In this very controlled experiment, the seismic methods yield values of the material damping ratio that generally agree with laboratory values. Measured damping ratios are plotted vs. the corresponding consolidation stresses which have a great influence on the results.

Other approaches to measure the material damping ratio include the rise time method, based on the experimental evidence that a seismic wave signal broaden with distance because of material damping, and the waveform matching method. However, at the present time, none of the available borehole methods to measure material damping ratio appears to be robust enough for routine use in geotechnical engineering practice.

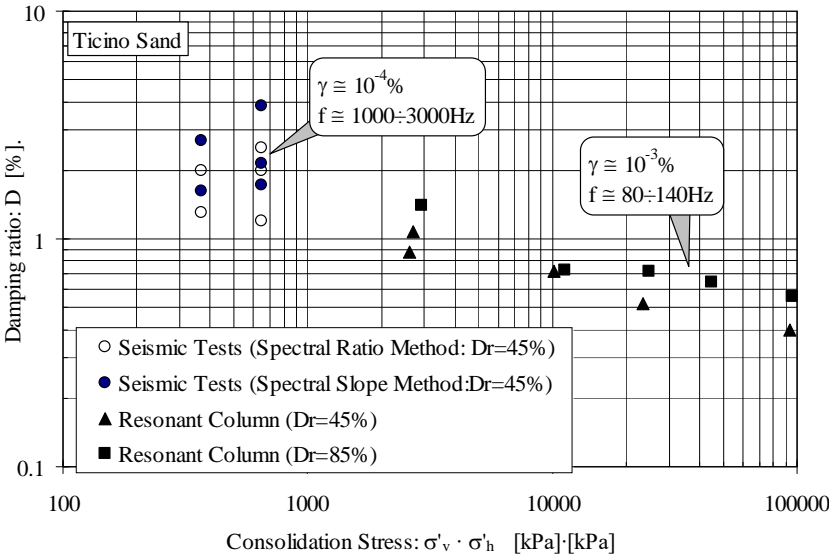


Figure 4 Damping ratio from laboratory and geophysical seismic tests on reconstituted sands [33].

2.2 Surface Methods

Surface methods are non-invasive field techniques that are executed from the ground surface of a soil deposit or from the sea floor, hence they do not require drilling of boreholes or insertion of probes. They include seismic refraction, high-resolution reflection and surface wave methods. Seismic refraction and reflection methods are not widely used for near-surface site characterisation, particularly for S-wave velocity profiling. This is partially due to the fact that there are situations (stiffer-over-softer layers; hidden layers) where the seismic refraction method cannot be reliably applied [34]. High-resolution reflection, on the other hand, does not suffer such limitations, however it requires very intensive data processing.

Advantages of surface methods are mainly related to their non-invasive nature. They are more economical and can be performed more rapidly than borehole methods. Furthermore, in sites like solid waste disposals and landfills, due to environmental concerns, surface methods can be the only choice for geotechnical investigations. Another peculiar aspect of surface methods is related to the volume of soil involved in the test, which is much larger than in borehole methods. As a result, surface methods are particularly useful if the average properties of a soil deposit are to be assessed as in the case of ground response analyses.

In the following, the discussion on surface methods will focus exclusively on Rayleigh wave methods mainly because of their relevance in near-surface site characterization.

It is well known that, in the case of an elastic isotropic medium, the shear wave and Rayleigh wave velocities are correlated as follows, depending on the Poisson ratio:

$$V_R = \frac{0.862 + 1.14\nu}{1 + \nu} V_s \quad (8)$$

Early surface wave methods employed laborious field procedures to measure the dispersion curve (i.e. a plot of Rayleigh phase velocity vs. frequency) and crude inversion techniques to obtain the S-wave profile from the experimental dispersion curve [35]. Stokoe and his co-workers (i.e. [36][37]) re-invented engineering surface wave testing by taking advantage of portable dynamic signal analysers, to efficiently measure the dispersion curve, and of the widespread availability of high-speed computers, to implement theoretically-based robust inversion algorithms. Actually, the Spectral Analysis of Surface Waves (SASW) method was replaced by the Multichannel Analysis of Surface Waves (MASW) which uses an array of geophones instead of only two. MASW method uses either impulsive sources such as hammers, steady-state sources like vertically oscillating hydraulic or electro-mechanical vibrators that sweep through a pre-selected range of frequencies, typically between 5 and 200 Hz [38], as well as passive source [39-41]. R-waves are detected by a geophone array. Usually 24 geophones with an inter - geophone distance X in between 1.5 and 5 m are used (Figure 5). The source can be external (Figure 5) or internal to the geophone array. Different impulse, with different frequency content, can be generated in order to sample different subsoil depths. The signals at the receivers are digitised and recorded by a dynamic signal analyser.

The use of a multi-station testing setup can introduce several advantages in surface wave testing. In this case, the motion generated by an impact source is detected simultaneously at several receiver locations and the corresponding signals are analysed as a whole (i.e. in both the time and space domains) using a double Fourier Transform. It can be shown [42] that the composite dispersion curve can be easily extracted from the location of the spectral maxima in the frequency-wavenumber domain in which the original data are transformed. Using this technique, the evaluation of the experimental dispersion curve becomes straightforward; furthermore, the procedure can be easily automated [43].

The experimental dispersion curve is used to obtain the shear wave velocity profile via a process called inversion. A theoretical dispersion curve is calculated for an assumed vertically heterogeneous layered soil profile using one of several available algorithms [44-49]. The theoretical dispersion curve is then compared with the corresponding experimental curve and the “distance” between the two curves is used as a basis of an iterative process consisting of updating the current soil profile until the match between the two curves is considered satisfactory. The soil profile may be updated manually by trial and error or using an automated minimisation scheme based on an unconstrained or constrained inversion algorithm [8]. When a satisfactory agreement between theoretical and experimental dispersion curves is attained (Figure 6a), the final shear wave velocity profile (Figure 6b) is taken as representative of the site conditions.

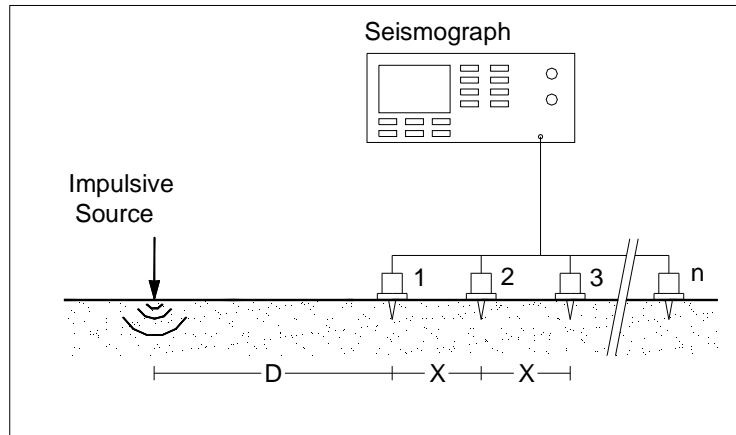


Figure 5 MASW configuration

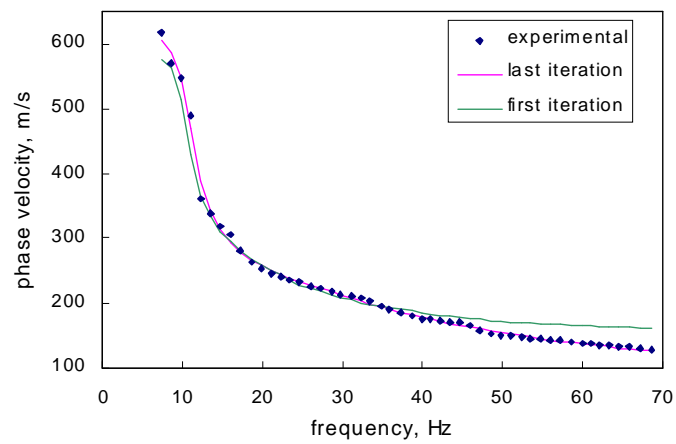


Figure 6a Theoretical and experimental dispersion curve

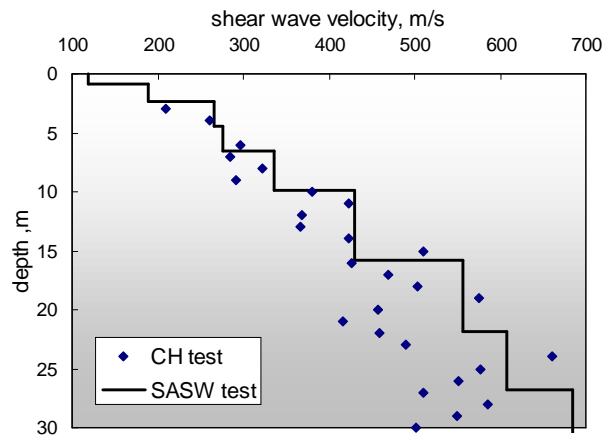


Figure 6b Shear wave velocity profile

For a successful application of MASW testing, it is recommended to observe the following guidelines:

- in choosing the relative spacing between source and receivers, attention should be placed to minimize near-field effects and spatial aliasing. In this context, the near-field is defined as a region close to the source where the magnitude of the body wave components of the wave field are of comparable magnitude to the surface

wave components. Efforts should be made to eliminate or minimize near-field effects unless they are explicitly accounted for during the inversion process [50][51]. In normally dispersive media, the body wave field is significant until D/λ exceeds about 0.5, hence the nearest receiver should be located at least one-half wavelength from the source:

$$D \geq \lambda / 2 \quad (9)$$

This recommendation is consistent with other studies of the influence of near-field effects, but more strict requirements are necessary for inversely dispersive stratigraphies [52][40]. It is also important to limit the distance between receivers to avoid spatial aliasing, a simple criterion is given by:

$$X \leq \lambda / 2 \quad (10)$$

- the length of the receiver array must be sufficiently large, if the stiffness profile at great depth has to be estimated. A rule of thumb is that the survey length must be as long as about 3 times the maximum depth of interest. This requirement may not be compatible with the space available at the site. Moreover, massive sources are needed to get good quality signals with long testing arrays, causing an increase of testing time and cost;
- it is important to account for multiple modes of surface wave propagation, especially in irregular, inversely dispersive soil profiles [53][40]. Currently several approaches are used to account for multiple modes. Individual, modal dispersion curves can be calculated and compared with the experimental dispersion curve during the inversion process. Unfortunately, the use of only two receivers in the traditional SASW method prohibits resolving individual modes in the experimental dispersion curve; only the effective velocity representing the combination of several modes can be determined. Also using a multi-station approach the individual modes cannot be separated if a relatively short receiver array is used, as required by engineering practice [54]. Thus, it must be assumed that the experimental curve represents an individual mode, usually the fundamental mode. This approach is satisfactory only in normally dispersive profiles. Another approach is to calculate the effective velocity directly and use it as the basis of the inversion. Lai and Rix (1998)[8] have developed an efficient procedure based on the normal mode solution to calculate the effective velocity as well as closed-form partial derivatives required for inversion. Finally, it is possible to numerically simulate the SASW test using Green's functions that calculate the complete wave field [50]. This approach is computationally expensive, in part because the partial derivatives must be calculated numerically, but it accurately models the actual field procedure used in SASW tests;
- for the inversion of the experimental dispersion curve, it is essential to use theoretically-based inversion algorithms. Prior to the widespread availability of high-speed computers, simple empirical inversion techniques were used. Furthermore, in recent years, there have been attempts to develop simple methods based on parametric studies and regression equations. These methods have limited usefulness and are likely to yield erroneous results. It is remarked that the rapidly increasing power of personal computers makes it possible to use theoretically-based inversion methods routinely;
- the non-linear inversion of the experimental dispersion curve is inherently ill-posed with the consequence that the solution (i.e. the S-wave profile) is not unique. This

problem can be overcome with the recourse of two strategies [8]. First, a priori information about the soil profile can be used to limit the range of possible solutions. Second, additional constraints such as smoothness and regularity (e.g. [55]) may be imposed on the solution.

3 ENGINEERING PARAMETERS

Soil parameters for Civil Engineering applications are mainly $(Vs)_{30}$ and impedance functions. The $(Vs)_{30}$ parameter was suggested by Ordaz and Arciniegas in 1992 [56] to account for stratigraphic amplification. Many Technical Codes, including Eurocodes adopt such a parameter to define the response spectrum (i.e. seismic action) at the soil – deposit outcrop, in a simplified way. Such an approach is applicable in the case of simplified stratigraphic profiles. Eurocode 8 part 1, defines two shapes of the response spectrum (low and moderate seismicity) at rock outcrop (reference spectra – class A). Moreover, Eurocode 8 defines four classes (B, C, D, E) in terms of simplified stratigraphic profiles and of $(Vs)_{30}$ range. Different shapes of the response spectra and different amplification factors (S) are prescribed for these classes of seismic subsoil. Eurocode 8 also adopts an importance factor but does not consider simplified approaches to account for topographic amplification.

The Italian Building Code [57] (NTC 2008) represents the Italian implementation of Eurocodes. Some peculiarities are worth noticing.

The response spectra are defined, for each prescribed exceedance probability within a reference period (i.e. for a given return period), starting from site-dependent parameters.

In particular, the reference period is inferred from the life-time and importance of the considered construction/structure, while the return period is obtained by the following equation:

$$T_R = -\frac{P_R}{\ln(1-p_L)} \quad (11)$$

Where P_R is the reference period and p_L is the exceedance probability.

Therefore, such a procedure implicitly incorporates an importance factor.

The site-dependent parameters are listed below and were obtained at the nodes of a square grid of 0.05° size, covering the whole Italian territory. The seismic hazard parameters were obtained by using a probabilistic approach:

- a_g = maximum free-field acceleration for a given return period and for a rigid reference site, with horizontal topographical surface;
- F_0 = maximum spectral amplification factor for a rigid reference site, with horizontal topographical surface (the minimum value for F_0 is 2.2);
- T_C^* = is used to determine the period above which the spectral velocity is constant.

The elastic response spectrum shape is then defined according to the following expressions:

$$S_e(T) = a_g \cdot S \cdot F_0 \left[\frac{T}{T_B} + \frac{1}{F_0} \left(1 - \frac{T}{T_B} \right) \right] \quad 0 \leq T < T_B \quad (12a)$$

$$S_e(T) = a_g \cdot S \cdot F_0 \quad T_B \leq T < T_C \quad (12b)$$

$$S_e(T) = a_g \cdot S \cdot F_0 \left(\frac{T_C}{T} \right) \quad T_C \leq T < T_D \quad (12c)$$

$$S_e(T) = a_g \cdot S \cdot F_0 \left(\frac{T_C T_D}{T^2} \right) \quad T_D \leq T \quad (12d)$$

Where S ($=S_S \times S_T$) is the result of the product among two coefficients that take into account for the subsoil site class (S_S coefficient – stratigraphic amplification) and for the topographic conditions (S_T coefficient – topographic amplification); T_C ($=T_C^* \times C_C$) is the corrected period at which the spectral acceleration initiates to decrease and above which the spectral velocity is constant. The corrected period is obtained as the product between T_C^* and the coefficient C_C (C_C depends on the subsoil site class), T_B ($=T_C/3$) is the period above which the spectral acceleration is constant and T_D ($=4.0 \times a_g + 1.6$) is the period above which the spectral displacement is constant.

The S_T coefficient can assume values of 1.0 – 1.2 – 1.4. The S_S coefficient is computed according to equations of the following type:

$$S_S = 1.4 - 0.4 \cdot F_0 \cdot a_g \leq 1.2 \quad (13)$$

(for class B subsoil. Different numerical coefficients and upper limit are prescribed for different soil classes).

The subsoil classes (Table 1) are identified on the basis of the a simplified profile and of the parameter V_{s30} , that is computed in the following way.

$$V_{s30} = \frac{30}{\sum \frac{h_i}{V_{s,i}}} \quad (14)$$

Where h_i and $V_{s,i}$ are respectively the thickness of the generic sub-layer i and the corresponding shear wave velocity.

Table. 1 Subsoil site classes according to the Italian Building Code (NTC 2008) [57]

Site Class	V_{s30} [m/s]
A	$V_{s30} \geq 800$
B	$360 \leq V_{s30} < 800$
C	$180 \leq V_{s30} < 360$
D	$V_{s30} < 180$
E	Subsoil of class C or D with thickness 5- 20 m, overlying class A bedrock

The simplified procedure is not applicable in the case of complex stratigraphic profiles or irregular topographic conditions.

In these cases, the response spectrum is inferred from seismic response analyses which require the knowledge of the shear wave velocity profile, as well as the dynamic characteristics of the subsoil (at least shear modulus and damping ratio). In addition an appropriate selection of accelerograms on rock outcrop is necessary (see as an example [58] and [59]).

The impedance is defined as the ratio between the harmonic excitation (force/moment) to the resulting displacement/rotation. As force and displacement are not in phase, the impedance is a complex expression depending on frequency. For a massless single degree of freedom system the impedance can be written in the following way:

$$K(\omega) = k + i \cdot c \cdot \omega \quad (15)$$

Where: ω = circular frequency; c = viscosity coefficient.

In practice the problem reduces to the definition of the real (static) part. More generally, a 6x6 impedance matrix should be defined in order to account for different types of motion (vertical translation, torsion, sliding/rocking).

The problem can be simplified in the following way:

- neglect the embedment i.e. the sidewall contact [60];
- neglect the so called trench effect [60];
- assume a circular foundation of equivalent perimeter and radius (R).

Therefore the vertical stiffness is given by the following equation:

$$k_v = \frac{4 \cdot G \cdot R}{(1 - \nu)} \quad (16)$$

Where: G = shear modulus; R = equivalent radius of the foundation; ν = Poisson ratio (assume 0.2).

The shear modulus can be inferred from the average shear wave velocity of the soil volume relevant for the considered problem. As for the non – linearity it could be possible to refer to Eurocode 8 part 5:

$$G_o = \rho \cdot V_s^2 \quad G / G_o = 0.8 - 0.5 - 0.35$$

when respectively $a_g = 0.1 - 0.2 - 0.3$ (17)

More accurate estimate of impedance can be obtained by referring to the Gazetas (1983) [60] recommendations. In any case an estimate of the static stiffness is necessary (i.e. of shear wave velocity from seismic in situ tests).

4 COMPARATIVE STUDY - CASE OF SEISMIC MEASUREMENTS

On February 2017 SCPT were conducted at the campus of the University of Pavia. At the same location Down – Hole test (DH) was performed inside a borehole. P and S wave measurements from these two types of tests were compared. Moreover SCPT measurements were used to obtain the small strain damping ratio.

According to the borehole stratigraphic log, the first 3 meters consist of man – made soil of various nature (very hard and coarse material). The natural deposit consists of a sequence of sands with different percentages of silt and gravel. Ground water table was located at 12.2 m depth from ground level.

SCPT were performed by means of a Pagani TG63 – 200 penetrometer. As for the first 3 meters, a preliminary dynamic penetration was carried out (a sort of pre-boring).

Two different types of source were used for SCPT:

- a sledgehammer of 10 kg with a special anvil (drop height of about 1.8 m)
- a manual hammer of 5 kg. This hammer was used to hit the aluminium blocks from right or left. The blocks were kept well in contact to the soil by the penetrometer - legs.

In principle, the first type of source mainly produced PV and SV waves while the second type of source mainly produced PV and SH waves. In any case, the generated wave field is usually quite complex.

The seismic module of SCPT was equipped with a pair of triaxial accelerometers. The relative distance between the accelerometers was 0.5 m. Therefore, two waveforms were recorded for each hit by the data acquisition system. Test interpretation was carried out by means of the cross-correlation method. In other words, the travel time between the two

accelerometers was computed from the time delay which maximised the cross – correlation function between the two recorded waveforms. Butterworth filters were applied only to the shear wave signals.



Figure 7 SCPT set-up at the University of Pavia campus. A) Pagani TG63 – 200 penetrometer; B) manual hammer of 5 kg hitting the aluminium blocks; C) sledgehammer.

A 3D geophone pack was used for DH test together with a manual hammer. First arrival time of P and S wave was obtained by manual pick-up on the dromochrome plot.

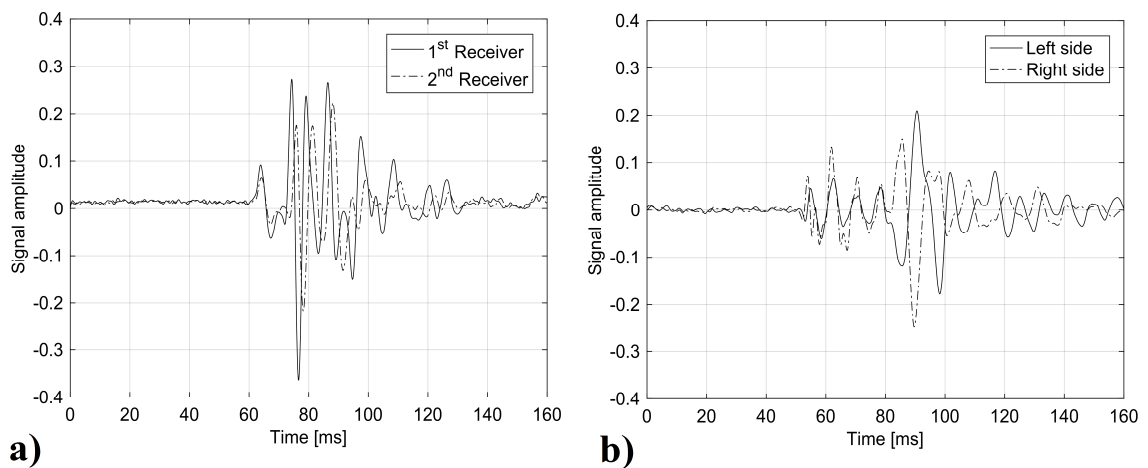


Figure 8 Waveform records (SCPT at Pavia site): a) sledge –hammer; b) manual hammer

Figure 8 shows typical examples of recorded waveforms (SCPT). Figure 8a shows the simultaneous measurements of the two accelerometers. In this case the sledge hammer was used as source. Figure 8b instead shows the waveform recorded by a single accelerometer when the manual hammer is used as source. In this case the polarity inversion of shear wave is shown.

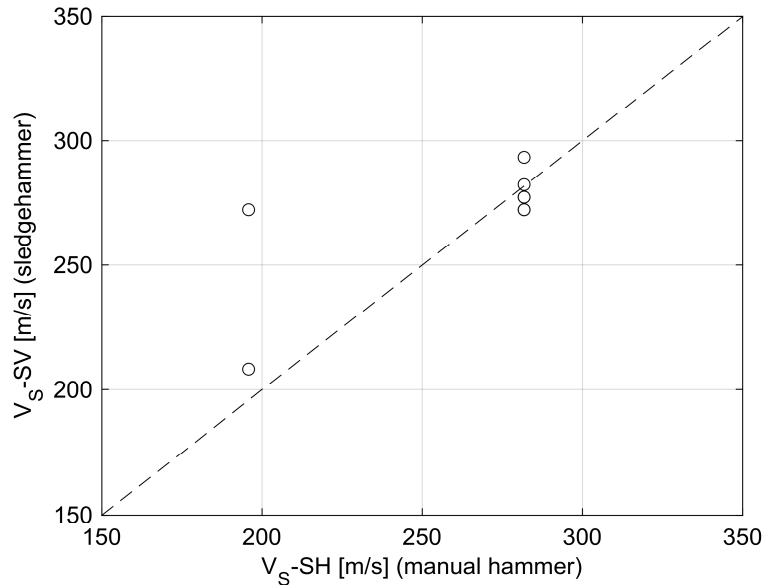


Figure 9 SV vs. SH

Figure 9 compares the shear wave velocities obtained, at the same depth, by using different sources (sledge hammer and manual hammer). The values are comparable and suggest that, for the considered case, the effects of anisotropy are negligible. Indeed it was postulated that by using the sledgehammer SV are generated, while the manual hammer mainly generates SH.

The measured S and P wave velocities are compared in Figure 10a. Figure 11 shows the dromocrome from DH and SCPT. The comparison has been done for depths in between 3 and 16 m. Indeed it was not possible to measure P wave at greater depths by SCPT because of the too low signal to noise ratio.

Figures 10 and 11 can be commented as follows:

- V_s from the two types of measurements are comparable;
- V_p are also comparable;
- V_p (from both SCPT and DH) increase for depth greater than 11 m (i.e. below the water table depth) and remains quite constant with values ranging in between 1700 – 1900 m/s. It could be argued that, at depth greater than 11 m, the P wave velocity of sound in water was measured.

The spectral slope method was used to determine the small strain damping ratio from SCPT. In particular only S wave signals were used. The success of the method mainly depended on the following experimental aspects:

- a single hit for generating the two signals;
- use of accelerometers, instead of geophones, with an increased repetitiveness of signal amplitude measurement.

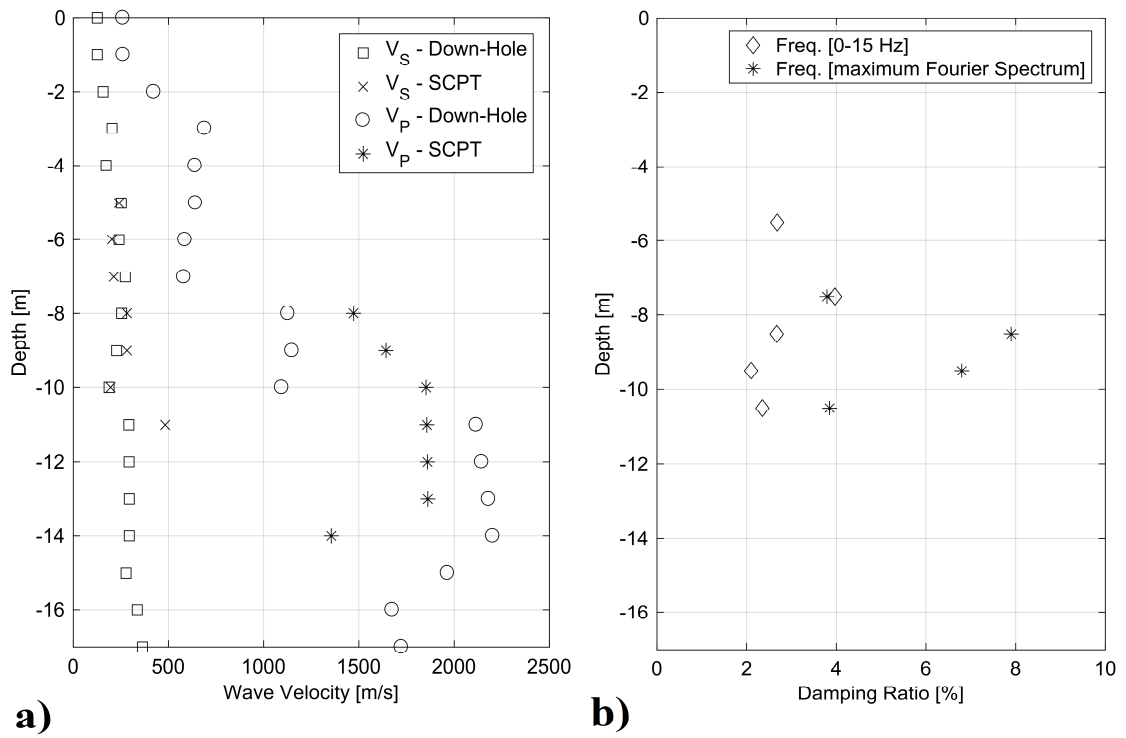


Figure 10 a) P and S wave velocities (SCPT ad Down-Hole data) and b) Damping ratios (SCPT data) at the University of Pavia campus

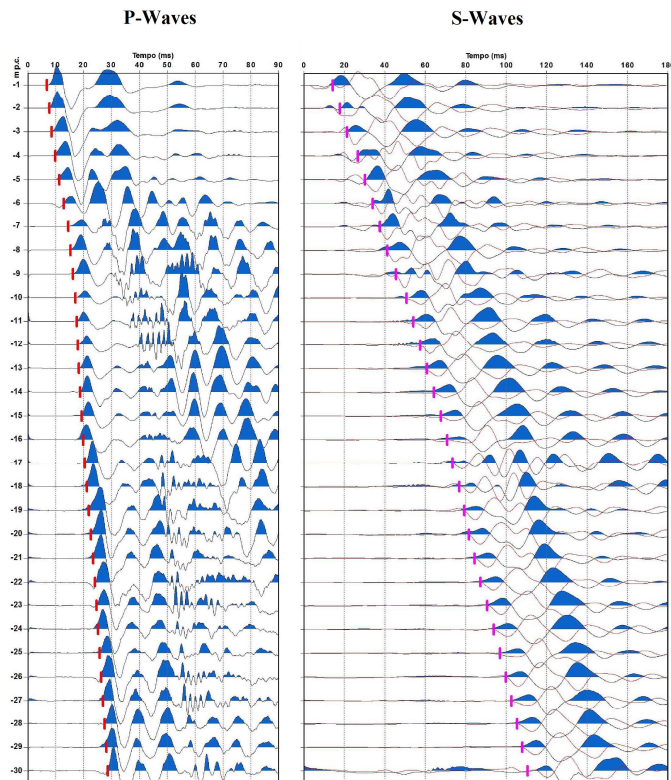


Figure 11a Dromocrome (DH)

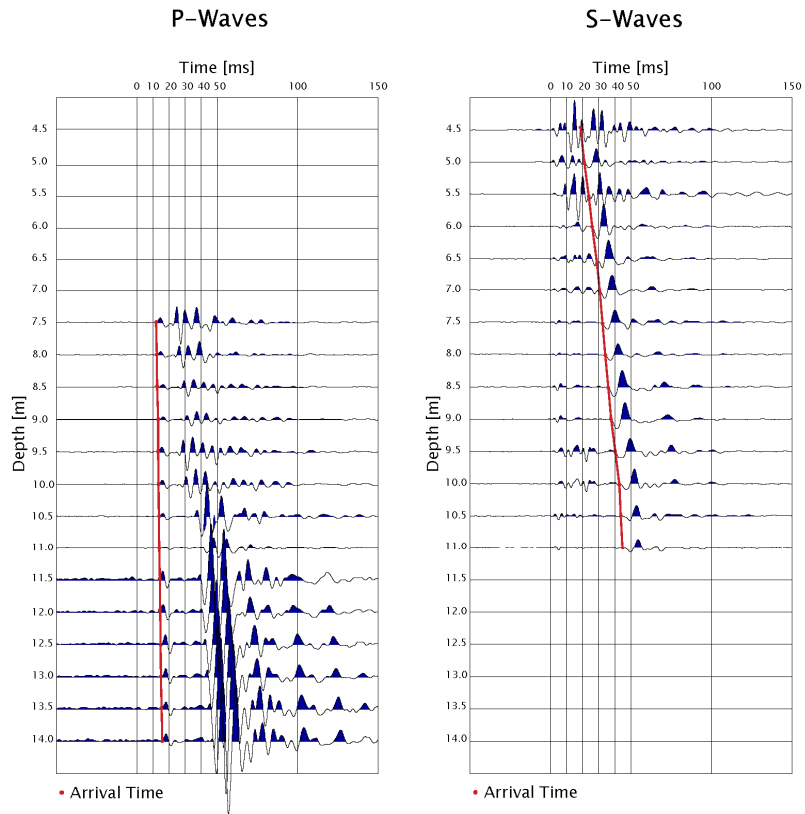


Figure 11b Dromocrome (SCPT)

Figures 12a to 12c show the Spectral Ratio (Napierian Logarithm scale) vs. the frequency for different frequency intervals. Data shown in Figures 12a to 12c refer to the measurements at 9.5 m depth.

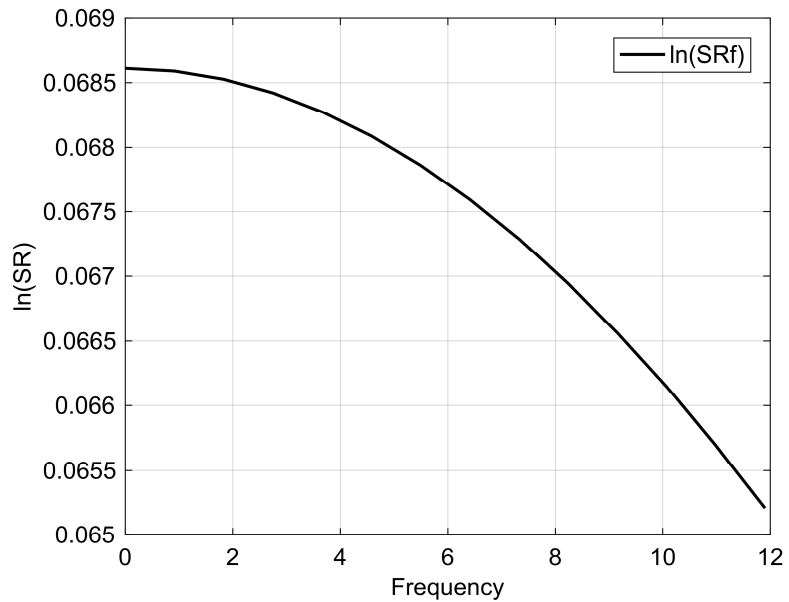


Figure 12a $\ln(\text{SR})$ vs. Frequency (natural frequency interval)

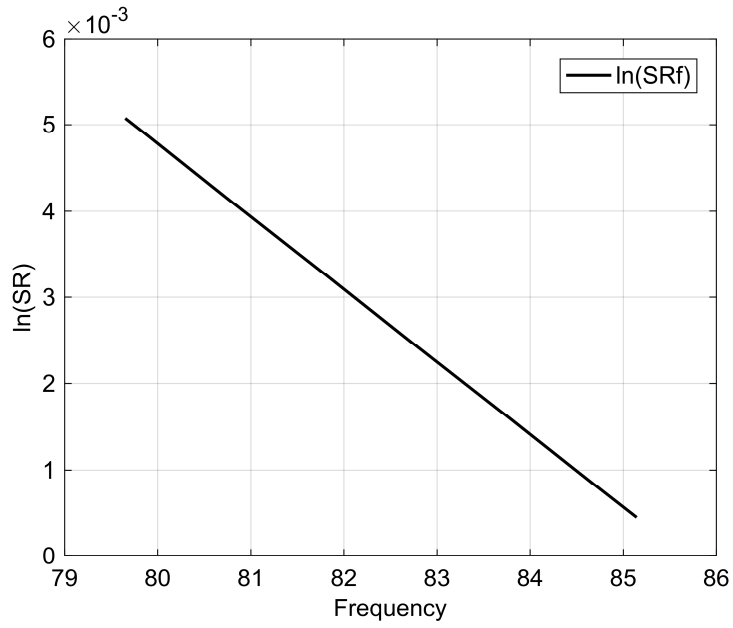


Figure 12b ln(SR) vs. frequency (frequency interval corresponding to the maximum Fourier Spectrum)

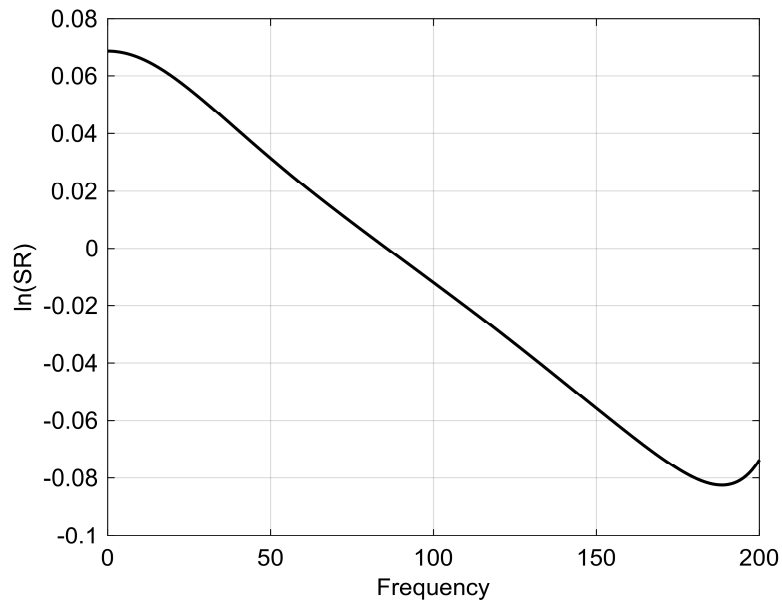


Figure 12c ln(SR) vs. frequency (full frequency range)

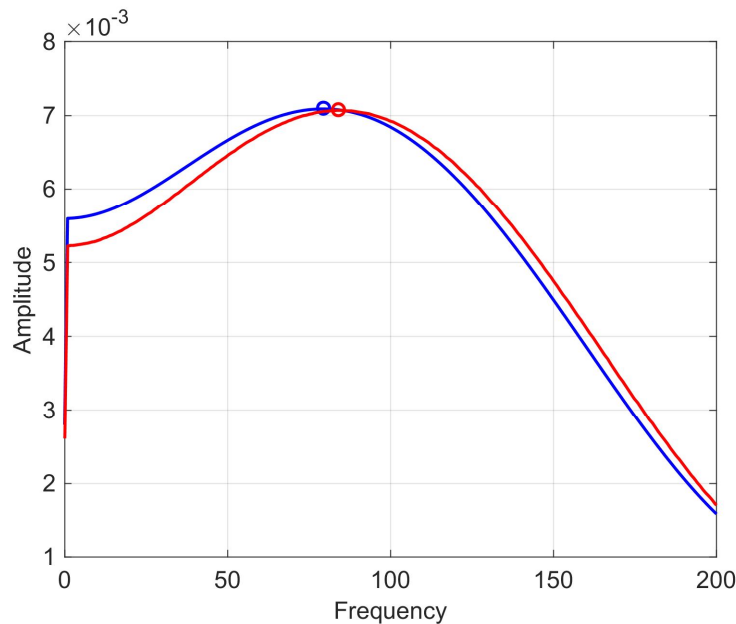


Figure 13 shows the Fourier spectra of the two waveforms.

A damping ratio of 2.1 % was obtained by considering a frequency interval in between 0 and 15 Hz. Such a frequency interval contains the natural frequency of the tested soil. Values of damping ratio ranging in between 2.1 and 4 % were obtained. Higher values of the damping ratio were obtained by considering the frequency interval containing the maximum of the response spectra. Under these conditions damping ratio values in between 1.3 and 7.9 % were obtained (see Figure 10b) for the two series of damping values with depth). These results suggest that damping ratio values increase with frequency (i.e. Maxwell type damping).

5 CONCLUDING REMARKS

The paper reviewed the capabilities of seismic tests in the light of Eurocodes. More specifically, the advantages and capabilities of in situ seismic piezocone tests (SCPT) were shown in general terms and with specific reference to a comparative experimental study case.

Experimental results suggest that a lower noise to signal ratio could be obtained by using geophones. Indeed, DH tests are carried out by using 3D geophones. Seismic module of piezocone could be equipped both with accelerometers and geophones. Obviously, in the case of the seismic piezocone small size instruments should be selected. The use of accelerometers gives the advantage of repetitive measurements of amplitude which, in turn, offers a better interpretation in terms of attenuation.

REFERENCES

- [1] Kramer, S.L. (1996) *Geotechnical Earthquake Engineering*, Prentice Hall, Inc., Upper Saddle River, New Jersey, 653 pp.
- [2] Woods R.D. 1978 Measurement of dynamic soil properties. *Earthquake Engineering and Soil Dynamics*, Pasadena CA. 1: 91-179.

- [3] Biot, M.A. (1956a) Theory of Propagation of Elastic Waves in a Fluid-Saturated Porous Solid.”, I. Lower Frequency Range, *J. Acoust. Soc. Am.*, 28: 168-178.
- [4] Biot, M.A. (1956b) Theory of Propagation of Elastic Waves in a Fluid-Saturated Porous Solid. II. Higher Frequency Range, *J. Acoust. Soc. Am.*, 28; 179-191.
- [5] Rix, G.J., Lai C.G., Spang A.W. Jr (2000) In situ measurement of damping ratio using surface waves, *J. Geotech. and Geoenviron. Eng.*, ASCE, 126: 472-480.
- [6] Ishihara, K. (1996) Soil Behaviour in Earthquake Geotechnics. Oxford Science Publications, Oxford, UK, pp. 350.
- [7] Aki K., Richards P.G. (1980) Quantitative seismology: theory and methods - 2 vol., Freeman, S. Francisco.
- [8] Lai, C. G. and Rix, G. J. (1998) Simultaneous inversion of Rayleigh phase velocity and attenuation for near-surface site characterization. Technical Report GIT-CEE/GEO-98-2, Georgia Institute of Technology.
- [9] Lai, C.G., Pallara O., Lo Presti, D.C.F., and Turco, E. (2001) Low-Strain Stiffness and Material Damping Ratio Coupling in Soils. Advanced Laboratory Stress-Strain Testing of Geomaterials. TC29 Summary Book. 15th ICSMGE, Istanbul, Turkey. August 27-31, 2001. Ed. Tatsuoka, F., Shibuya, S. and Kuwano.
- [10] Rix, G.J., Lai C.G., Foti S. (2001) Simultaneous measurement of surface wave dispersion and attenuation curves, accepted for publication *Geotech. Testing J.* 24(4): 350–358.
- [11] Lai C.G., Rix G.J., Foti S., Roma V. (2002) “Simultaneous Measurement and Inversion of Surface Wave Dispersion and Attenuation Curves”, *Soil Dynamics and Earthquake Engineering*, 22, 9-12: 923-930.
- [12] Nigbor R.L. & Imai T. (1994) The Suspension P-S Velocity Logging Method. Proc. XIII ICSMF New Delhi, India TC # 10, pp. 57-61.
- [13] Auld B. (1977) Cross-Hole and Down-Hole Vs by Mechanical Impulse. *Journal GED*, ASCE. 103 (GT12): 1381-1398.
- [14] Stokoe K.H. II & Hoar, R.J. (1978) Variable Affecting In Situ Seismic Measurements. Proc. of the Conference on Earthquake Engineering and Soil Dynamics, ASCE, Pasadena, CA.2: 919-939.
- [15] Woods, R.D. and Stokoe, K.H. II (1985) Shallow Seismic Exploration in Soil Dynamics. Richart Commemorative Lectures, ASCE. 120-156.
- [16] Woods, R.D. (1991) Field and Laboratory Determination of Soil Properties at Low and High Strains. Proc. of 2nd International Conference on Recent Advances in Geotechnical Earthquake Engineering and Soil Dynamics, St. Louis, Missouri, SOA1.
- [17] Woods, R.D. (1994) Borehole Methods in Shallow Seismic Exploration. Proc. of XIII ICSMF New Delhi, India TC # 10: 91-100.

- [18] Patel, N.S. (1981) Generation and Attenuation of Seismic Waves In Downhole Testing. M. Sc. Thesis GT81-1, Department of Civil Engineering, University of Texas at Austin.
- [19] Jamiolkowski M. and Lo Presti D. (1998) Geotechnical Characterization of Gravelly Deposits. 13th SEAGC, Taipei.
- [20] Lo Presti D., Pallara O., Jamiolkowski M., Cavallaro A. (1999) Anisotropy of small strain stiffness of undisturbed and reconstituted clays. Proc. IS Torino 99, Balkema, 1: 3-10.
- [21] Stokoe, K.H. II, Lee, J.N.K. & Lee, S.H.H. (1991) Characterization of Soil in Calibration Chambers with Seismic Waves. Proc. ISOCCT1, Postdam, NY
- [22] Lo Presti, D.C.F. & O'Neill, D.A. (1991) Laboratory Investigation of Small Strain Modulus Anisotropy in Sand. Proc. of ISOCCT1, Postdam, NY.
- [23] Bellotti R., Jamiolkowski M., Lo Presti D.C.F. & D.A. O'Neill (1996) Anisotropy of Small Strain Stiffness in Ticino Sand. *Geotechnique*. 46(1): 115-131.
- [24] Jamiolkowski M. & Lo Presti D.C.F. (1991) Anisotropy of Soil Stiffness at Small Strain. Panel Discussion to Session 1, 9th ARC on SMFE, Bangkok, Thailandia.
- [25] Mitchell, J.K., Lodge, A.L., Coutinho, R.Q., Kayen, R.E., Seed, R.B., Nishio, S. & Stokoe, K.H. II, (1994) In Situ Test Results from four Loma Prieta Earthquake Liquefaction Sites: SPT, CPT, DMT and Shear Wave Velocity. EERC Report No. UCB/EERC - 94/04.
- [26] Fioravante V., Jamiolkowski M., Lo Presti D.C.F., Manfredini G. & Pedroni S. (1998) Assessment of coefficient of earth pressure at rest from shear wave velocity measurements. *Géotechnique*, 48(4): 1-10.
- [27] Mok, Y.J. (1987) Analytical and Experimental Studies of Borehole Seismic Methods. Ph.D. Thesis, Univ. of Texas at Austin, Austin, TX.
- [28] Fuhriman, M.D. (1993) Cross-Hole Seismic Tests at two Northern California Sites Affected by the 1989 Loma Prieta Earthquake. M. Sc. Thesis, The University of Texas at Austin.
- [29] Redpath, B.B., Edwards, R.B., Hale, R.J. & Kintzer, F.C. (1982) Development of Field Techniques to Measure Damping Values for Near Surface Rocks and Soils. Prepared for NSF Grant No. PFR-7900192.
- [30] Redpath B.B. & Lee R.C. (1986) In-Situ Measurements of Shear-Wave Attenuation at a Strong-Motion Recording Site. Prepared for USGS Contract No. 14-08-001-21823.
- [31] Khawaja A.S. (1993) Damping Ratios from Compression and Shear Wave Measurements in the Large Scale Triaxial Chamber. M. Sc Thesis, The University of Texas at Austin.
- [32] Campanella, R.G. & W.P. Stewart (1990) Seismic Cone Analysis Using Digital Signal Processing for Dynamic Site Characterization. 43rd Canadian Geotechnical Engineering Conference, Quebec City.

- [33] Puci I & Lo Presti D.C.F. (1998) Damping Measurement of Reconstituted Granular Soils in Calibration Chamber by means of Seismic Tests. Submitted to the 11 European Conference on Earthquake Engineering.
- [34] Reynolds J.M. (1997) An introduction to applied and environmental geophysics. J. Wiley & sons, New York
- [35] Jones R.B. (1958) In-situ measurement of the dynamic properties of soil by vibration methods, *Geotechnique*, 8 (1): 1-21
- [36] Nazarian S. (1984) In situ determination of elastic moduli of soil deposits and pavement systems by Spectral-Analysis-of-Surface waves method, PhD Diss., Un. of Texas at Austin
- [37] Stokoe KH II, Mok Y.S., Lee N. & Lopez R. (1989) In Situ Seismic Methods. Recent Advances in Testing, Understanding and Applications. Proc. XIV CGT, Politecnico di Torino, Department of Structural Engineering.
- [38] Rix, G.J. (1988) Experimental Study of Factors affecting the Spectral Analysis of Surface Waves Method. Ph. D. Thesis. The University of Texas at Austin, 315 pp.
- [39] Horike M. (1985) Inversion of phase velocity of long-period microtremors to the S-wave-velocity structure down to the basement in urbanized areas”, *J. Phys. Earth*, 33: 59-96
- [40] Tokimatsu K. (1995) Geotechnical Site Characterisation using Surface Waves. Proc. IS Tokyo 1995, Balkema, 1333-1368
- [41] Zywicki D., Rix G.J. (1999) Frequency-wavenumber analysis of passive surface waves, Proc. Symp. on the Appl. of Geophysics to Environm. and Eng. Problems, Oakland, pp. 75-84
- [42] Tselentis G.A., Delis G. (1998) Rapid assessment of S-wave profiles from the inversion of multichannel surface wave dispersion data, *Annali di Geofisica*, 41: 1-15
- [43] Roma V., Hebel G., Rix G., Lai C.G.: (2002) Geotechnical soil characterization using fundamental and higher Rayleigh modes propagation in layered media , XII European Conference on Earthquake Engineering, London 9-13 Settembre 2002
- [44] Haskell N.A. (1953) The dispersion of surface waves on multilayered media, *Bullettin of the Seismological Society of America*, 43 (1): 17-34
- [45] Thomson W.T. (1950) Transmission of elastic waves through a stratified solid medium”, *J. Applied Physics*, 21 (1): 89-93
- [46] Kausel E., Roesset J.M. (1981) Stiffness matrices for layered soils, *Bullettin of the Seismological Society of America*, 71 (6): 1743-1761
- [47] Chen X. (1993) A systematic and efficient method of computing normal modes for multilayered half-space, *Geophys. J. Int.*, 115: 391-409

- [48] Hisada Y. (1994) An efficient method for computing Green's functions for a layered half-space with sources and receivers at close depths, *Bulletin of the Seismological Society of America*, 84 (5): 1456-1472
- [49] Hisada Y. (1995) An efficient method for computing Green's functions for a layered half-space with sources and receivers at close depths (part 2), *Bulletin of the Seismological Society of America*, 85 (4): 1080-1093
- [50] Roësset, J.M., Chang, D.W., Stokoe, K.H. II, (1991) Comparison of 2-D and 3-D Models for Analysis of Surface Wave Tests, 5th International Conference on Soil Dynamics and Earthquake Engineering, Karlsruhe, Germany, pp. 111-126.
- [51] Ganji, V., Gucunski, N., and Nazarian, S., (1998) Automated Inversion Procedure for Spectral Analysis of Surface Waves, *Journal of Geotechnical and Geoenvironmental Engineering*, 124(8): 757-770.
- [52] Sánchez-Salineró I. (1987) "Analytical investigation of seismic methods used for engineering applications", PhD Diss., Un. of Texas at Austin
- [53] Gucunski N., Woods R.D. (1991) Use of Rayleigh modes in interpretation of SASW test, Proc. 2th int. Conf. Recent Advances in Geot. Earthq. Eng. and Soil Dyn.-S.Louis, pp. 1399-1408
- [54] Foti S., Lancellotta R., Sambuelli L., Socco L.V. (2000) Notes on fk analysis of surface waves *Annali di Geofisica*, 43(6): 1199-1210
- [55] Constable S.C., Parker R.L., Constable C.G. (1987) Occam's inversion: a practical algorithm for generating smooth models from electromagnetic sounding data, *Geophysics*, 32 (3): 289-300
- [56] Dobry R. & Iai S. (2000) Recent Developments in Understanding of Earthquake Site Response and Associated Seismic Code Implementation. *Geoen 2000*, Melbourne, 19-24 November 2000. Vol. 1 (Invited Papers): 186-219.
- [57] Norme Tecniche per le Costruzioni, NTC (2008). Italian Building Code. *DM, 14*, 2008.
- [58] Lo Presti, D. C., Lai, C. G., & Puci, I. (2006). ONDA: Computer code for nonlinear seismic response analyses of soil deposits. *Journal of geotechnical and geoenvironmental engineering*, 132(2): 223-236.
- [59] Lo Presti D.C.F., Stacul S. (2017) - ONDA (One-dimensional Non-linear Dynamic Analysis): ONDA 1.4 User's Manual Version 1.4. DOI: 10.13140/RG.2.2.32409.83043
- [60] Gazetas, G. (1983). Analysis of machine foundation vibrations: State-of-the-art, *Soil Dynamics and Earthquake Engrg.*, 3(1): 2-42.

Interpretation of CPTu in “unusual” soils

Diego Lo Presti,* Ilaria Giusti,** Barbara Cosanti,*** Nunziante Squeglia,**** Ermanno Pagani*****

Summary

The paper deals with the interpretation of CPTu in unusual soils, such as shallow clayey layers above the water table and loose, intermediate - permeability soils (loose silt mixtures).

The paper shows an approach that could be used for the first type of soil to infer the effective vertical stress from CPTu measurements and in particular from the I_c index. The approach has been checked on a very limited amount of experimental evidence. Moreover, an empirical correction of the I_c index is provided in order to obtain a more realistic soil profiling of loose silt mixtures. The foundation soils of the Serchio River levee system and some dredged sediments, which had been stored in the Port of Livorno, have been considered for the second type of soil.

1. Introduction

Cone penetration tests (CPTs) are mainly used for an indirect evaluation of soil profiles, as well as for the assessment of mechanical/hydraulic soil parameters with depth, the assessment of liquefaction susceptibility and the direct assessment of the Ultimate Limit State (ULS) and Serviceability Limit State (SLS) of shallow/deep foundations. A cost – effective investigation campaign should consider both CPTs (and/or other in situ tests) and boreholes. For obvious reasons, the reference soil profile should be inferred by means of direct investigation tools (*i.e.* boreholes), while CPTs, after an appropriate calibration, should be used for confirmation purposes, especially for large investigation areas. However, CPT interpretation always requires a preliminary “Soil Behavior Type (SBT)” identification.

Soil profiling using mechanical CPT (CPTm), electrical CPT (CPTe) or piezocone (CPTu) can be performed by means of empirical (or semi – empirical) approaches [BEGEMANN, 1965; SCHMERTMANN, 1978; SEARLE, 1979; DOUGLAS and OLSEN, 1981; ROBERTSON *et al.*, 1986; ROBERTSON, 1990; JEFFERIES and DAVIES, 1993; ESLAMI and FELLENIUS, 1997]. These approaches refer to different databases and mainly consider “conventional soil” *i.e.* saturated clays/silts/sands or their mixtures. These databases consider “well – educated” soils, but not unusual soils such as: a) soil layers above the water table with relevant suction effects, b) partially saturated soils (partial drainage conditions), c) compacted soils (earth-

works), d) very loose silt mixtures with intermediate permeability, d) underconsolidated soils, etc. In any case, the applicability of the currently available empirical approaches in a different context becomes questionable.

In the Authors experience, the available classification systems (CPTu) have not led to a correct SBT identification of the loose silt mixtures that they have encountered in different contexts. More specifically, very loose silt mixtures have been found within the chaotic dredged sediments stored in the artificial basin of the Port of Livorno and in the case of loose silt mixtures of the Serchio River levee – system and its foundation soil [COSANTI *et al.*, 2012]. The poorly compacted silt mixtures of the Serchio River levee – system and the loose silt mixtures of the foundation soil of these levees are often classified as clay or even organic clay. A similar systematic type of miss – classification was also observed in the case of dredged sediments of the Livorno Port artificial basin. The term miss – classification here refers to SBT classes and not to the grain size distribution and Atterberg Limits.

Soil layers above the water table may be partially saturated. In this situation, the cone penetration occurs under a partial drainage condition. While the effect of saturation degree appears quite negligible for sands [SCHMERTMANN, 1976; BELLOTTI *et al.*, 1988; JAMIOLKOWSKI *et al.*, 2001], it may become very relevant for fine – grained soils. JAMIOLKOWSKI *et al.* [2001] analyzed CPTu test results in a Calibration Chamber on dry or fully saturated, reconstituted sand samples. They found that the tip resistance of fully saturated samples is slightly lower than that of dry samples (at the same relative density and boundary stresses) for fine to medium sands.

However, even when soil layers are fully saturated by capillarity, the in situ stress state is controlled

* D. Lo Presti (Associate professor - University of Pisa, DESTeC)

** I. Giusti (Doctoral student - University of Pisa DESTeC)

*** B. Cosanti (Post - Doc. Researcher - University of Pisa DESTeC)

**** N. Squeglia (Researcher, University of Pisa DESTeC)

***** E. Pagani (Holder Pagani Geotechnical Equipment - PC)

by suction, which is usually not known. The possible effects of suction on soil profiling, in the case of fine-grained soil deposits, can lead to another type of miss – classification, that is, overconsolidated clays (because of suction) are sometimes erroneously identified as sands. This is also a consequence of the fact that, for practical reasons, only the pore pressure behind the tip (U2) is measured.

This paper proposes two different approaches that could be used to overcome some of the above mentioned problems and to obtain a better interpretation for some “unusual” soils. Two different methodologies are here proposed for a more accurate CPT interpretation. The first methodology results in a better estimate of the effective stress state in soil layers above the water table (suction estimate). To this end, the modified KOVACS model (MK) has been used in the first step. Details of the model can be found in the original work by KOVACS [1981] and in the subsequent paper by AUBERTIN *et al.* [2003]. This method offers the possibility of estimating the soil suction from simple physical soil parameters (*i.e.* from soil classification). In the second step, the I_c index has been used to obtain a more realistic estimate of the in situ effective stresses. Such a methodology has been applied to re - interpret the CPTu carried out in two different sites. The second methodology is purely empirical, and consists of a calibration of the I_c values [ROBERTSON, 1990; JEFFERIES and DAVIES, 1993], as inferred from CPTu results, with evidence obtained from direct logging (boreholes) in the case of very loose silt mixtures. This methodology has been applied to the foundation soil of the Serchio River levee system and to some dredged sediments that had previously been stored in the artificial basin of the Livorno Port.

2. Evidence of some profiles of unusual soils

Figure 1a shows the I_c values with depth of three CPTu carried out along the Serchio River Levees. The tests were extended down to about 30 m and included the River embankment, for the first 4 m, and the foundation soils. Two aspects can be observed:

- the I_c values in the upper meters indicate the presence of sand and sand mixtures;
- the I_c values, at depths of 10, 20 and 30 meters, indicate the presence of organic clays;

In both cases, the indications obtained from the CPTu interpretation appear to contrast the borehole evidence. In the first case, the miss – classification may be a consequence of partial saturation and in particular due to the fact that suction was not taken into account. The second type of miss – classification is a consequence of the inability of the currently available approaches to correctly identify very loose silt mixtures.

The I_c values from two CPTus, which were carried out at the same location (Broni) in different periods, are shown in figure 1b [MEISINA, 1996]. The deposit is homogeneous and on the basis of laboratory testing on undisturbed samples retrieved from the first three meters was mainly classified as CL to CH. The water table was found at a depth of 3.5 m during the wet season (June 2001) and at a depth of 5 m during the dry season (September 2001). The two CPTus were carried out at the same location (the distance between the two CPTus and boreholes was about 0.5 m) in June and September 2001. Figure 1c (MEISINA, 1996) shows the location of the boreholes, CPTus and a number of wells. In spite of the homogeneity of the deposit, it can be observed that the tip resistance (q_c) is influenced to a great extent by the water table depth (suction) so that q_c increases from 1 – 2 MPa to 3 – 4 MPa in the vadose zone above the water table (Fig. 2). It is worth noticing that such an increase is higher during the dry season. The effect of suction on the I_c values and SBTn classes (ROBERTSON, 1990) is shown in the subsequent figures 10 to 13. As far as the I_c index is concerned, the values decrease from about 3 at the water table depth to about 2.0 at a depth of 50 cm. In terms of SBTn classes, silts and sand mixtures become predominant instead of OC stiff clay (SBTn class 9).

3. The MK model

More information about the model can be found in the works by KOVACS [1981] and AUBERTIN *et al.* [2003]. The MK model has been used to evaluate the matrix suction (ψ_r) at the residual water content and the equivalent capillary height above the water table (h_{co}) from simple soil parameters [AUBERTIN *et al.*, 1998; MBONIMPA *et al.*, 2000; 2002]. For granular soils $h_{co,G}$ (the suffix “G” stands for granular soils) can be considered equivalent to the height of the capillary fringe, and can be evaluated using the following expression:

$$h_{co,G} = \frac{b}{eD_{10}} \quad (1)$$

$$b [\text{cm}^2] = \frac{0.75}{1.17 \cdot \log(C_u) + 1} \quad (2)$$

where: e = void ratio and $C_u = \frac{D_{60}}{D_{10}}$ is the coefficient

of uniformity. KOVACS [1981] defined the following parameter (equivalent particle diameter), embedded in equations (1) and (2), for heterogeneous material:

$$D_H = [1 + 1.17 \cdot \log(C_u)] \cdot D_{10} \quad (3)$$

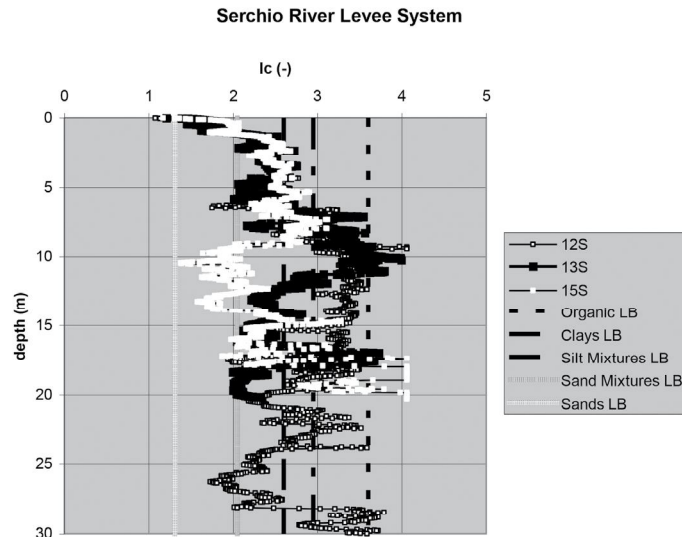


Fig. 1a – CPTu results - the Serchio River embankments and foundation soil (CPTu 12S, 13S, 16S) – LB = Lower Bound.
 Fig. 1a – Risultati prove CPTu relative agli argini del fiume Serchio e del terreno di fondazione (CPTu 12S, 13S, 16S) – LB = Limite Inferiore.

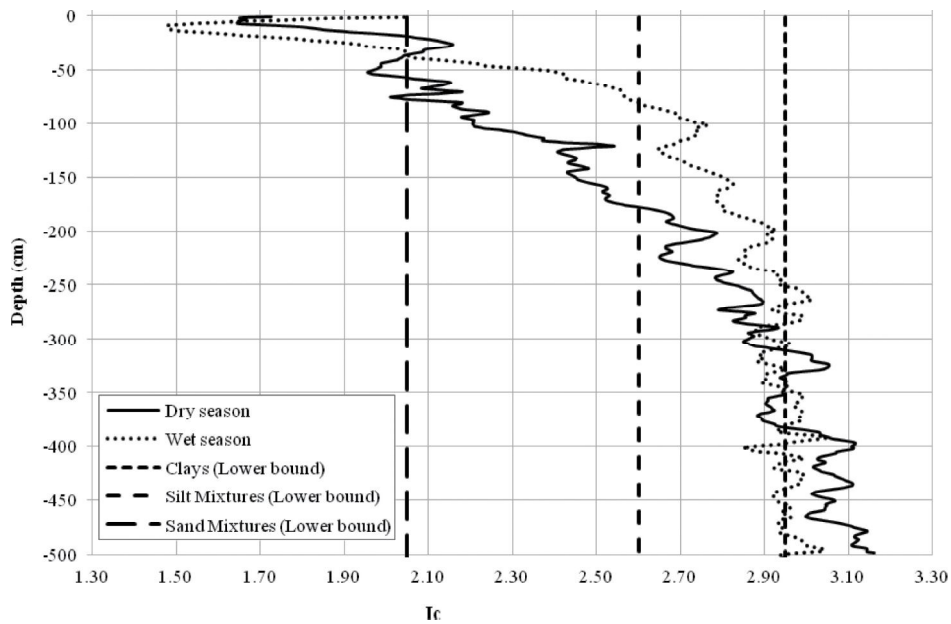


Fig. 1b – CPTu results - Broni (PV – Italy).
 Fig. 1b – Risultati prove CPTu - Broni (PV – Italy).

For fine grained (plastic, cohesive) materials (the suffix P stands for plastic soils), the following expression is more appropriate:

$$h_{co,P} = \frac{\xi}{e} w_L^{1.45} \quad (4)$$

where: w_L is the liquid limit and ξ (cm) $\approx 0.15\rho_s$ (Kg/m³) (ρ_s = solid density)

The MK model uses h_{co} as a reference value to define the relationship between the degree of saturation and the matric - suction ψ . The suction at residual water content is defined as follows:

$$\psi_r = \frac{0.42}{(\epsilon D_H)^{1.26}} \quad (5)$$

For granular materials:

$$\psi_r = 0.86 \cdot h_{co,G}^{1.2} \quad (6)$$

For clayey soils:

$$\psi_r = 0.86 \left(\frac{\xi}{e} \right)^{1.2} w_L^{1.74} \quad (7)$$

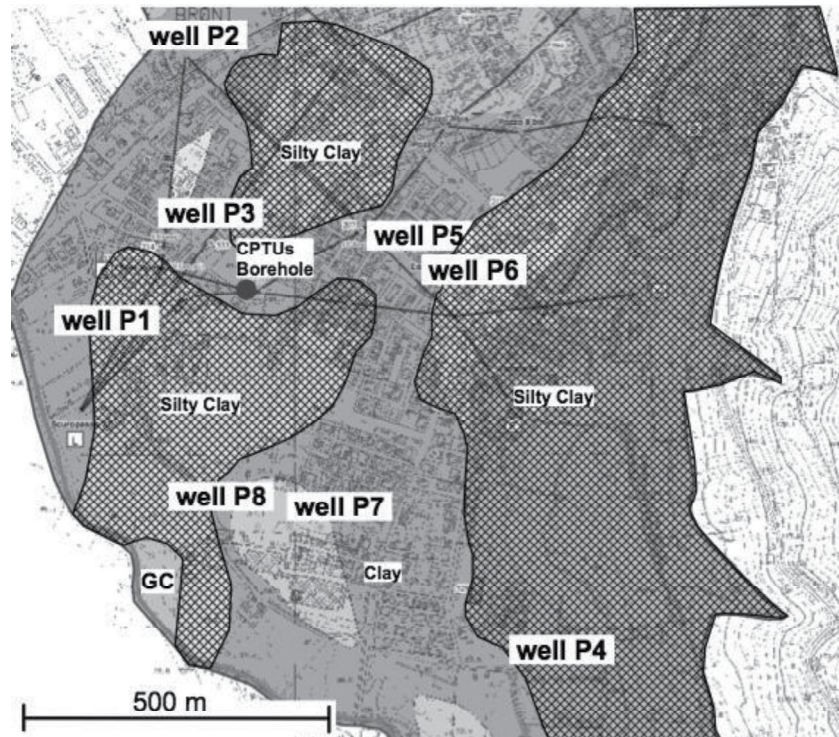


Fig. 1c – Broni area – Geological map, test and well (P1 to P7) locations.

Fig. 1c – Area di Broni – Carta Geologica, ubicazione delle prove e dei pozzi (P1 - P7).

In order to take in to account the influence of suction on the interpretation of the test results, a negative pore water pressure was computed above the water table according to the following equations:

$$u = -\gamma_w h \quad (\text{for } 0 < h < h_{co}) \quad (8)$$

$$u = -\gamma_w h_{co} \quad (\text{for } h > h_{co}) \quad (9)$$

h = height above the water table. The adopted hypotheses obviously represent an oversimplification and may still underestimate the effective stresses.

4. Reinterpretation of CPTu at Broni

Broni is in the North of Italy in the Po River area near Pavia. From a geological point of view, it is characterized by alluvial deposits that have been generated by the Po River and its tributaries. Over the years, geotechnical investigations, including geotechnical soundings and CPTu tests conducted at various depths of between 20m and 30m [MEISINA, 1996; LO PRESTI *et al.*, 2009], have been carried out by the University of Pavia. Moreover, data from 8 wells are available [MEISINA, 1996]. These wells are located in the residential area of Broni, and were used to monitor the water table depth from July 2002 to July 2003 (Tab.I). Well P3 (Fig. 1c) is the closest one to the CPTus and borehole.

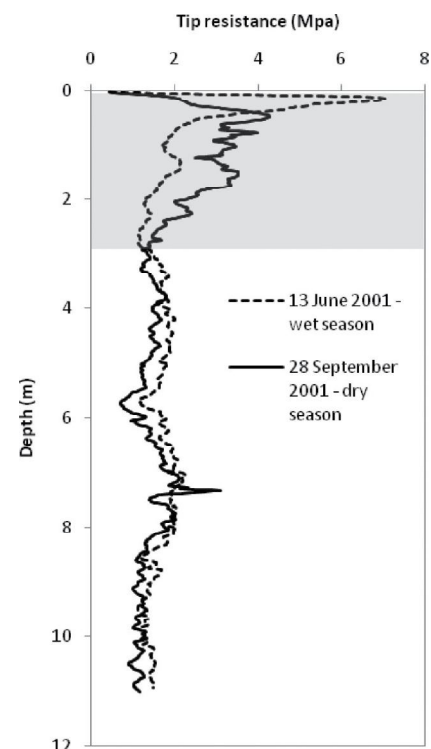


Fig. 2 – CPTu1 and CPTu2 (Broni). The highlighted layer shows the zone of influence of seasonal changes of the water table.

Fig. 2 – Prove CPTu1 and CPTu2 (Broni). Lo strato evidenziato individua la zona interessata dalla variazione stagionale della profondità di falda.

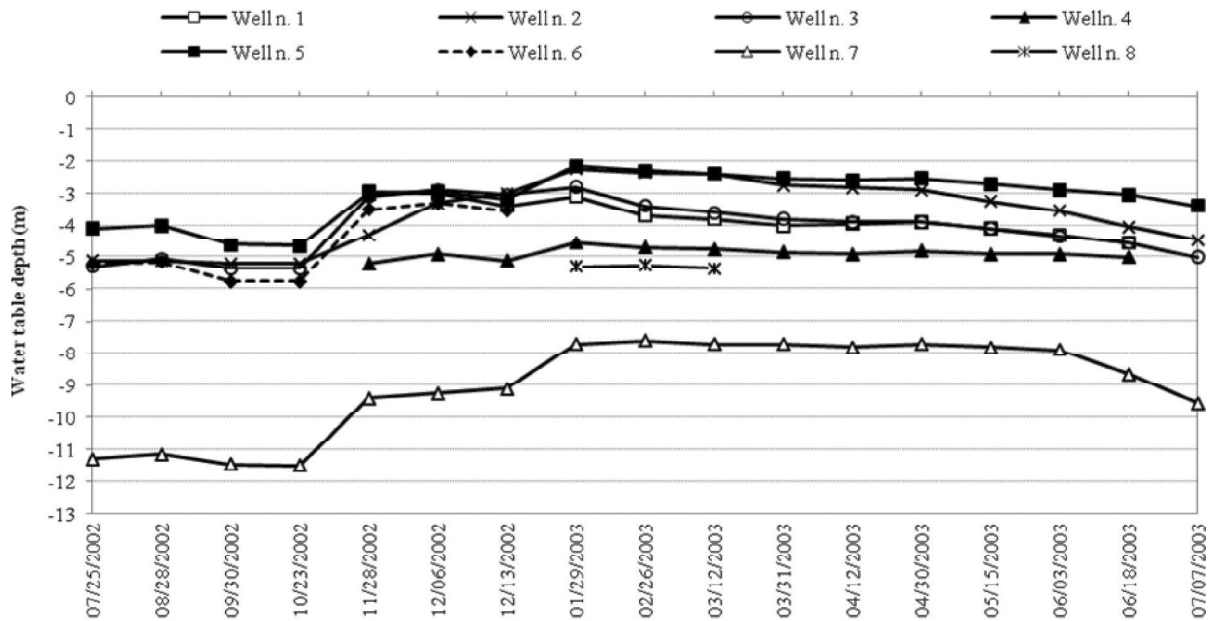


Fig. 3 – Water table depth during the observation period, residential area of Broni [MEISINA, 1996].

Fig. 3 – Soggiacenza della falda monitorata nel periodo di osservazione, area residenziale di Broni [MEISINA, 1996].

Almost all the wells reach a depth of between 5.4 and 12 meters and their levels are therefore controlled by the superficial aquifer, while well P7, with a depth of 18.5, meters is believed to reach the principal and deeper aquifer

It is possible to observe from figure 3 and figure 4 that the water level follows the pluviometric levels and reaches a maximum in January. The pluviometric range for the superficial aquifer is about 2-2.5 m, while it reaches 3.8 meters for the deeper aquifer. The observed trend of the water table depth with time, over the whole area, confirms the correctness of the measured values that have been considered to interpret CPTU1 and CPTU2.

4.1. Cone Penetration tests

The results of the two CPTu tests (the same as those in figures 1b and 2) are shown in figure 5 and figure 6. The possible effects of suction on the q_c and I_c values have already been mentioned. The layer in which it is possible to observe differences between tip resistances related to a different suction is highlighted in figure 2. It is not possible to ascertain beyond reasonable doubt the reasons for the differences in q_c for the first 0.5 m. However, it is possible to hypothesize local texture heterogeneities (man – made soil).

As far as the pore water pressure measurements are concerned, an almost nil value of U2 can be ob-

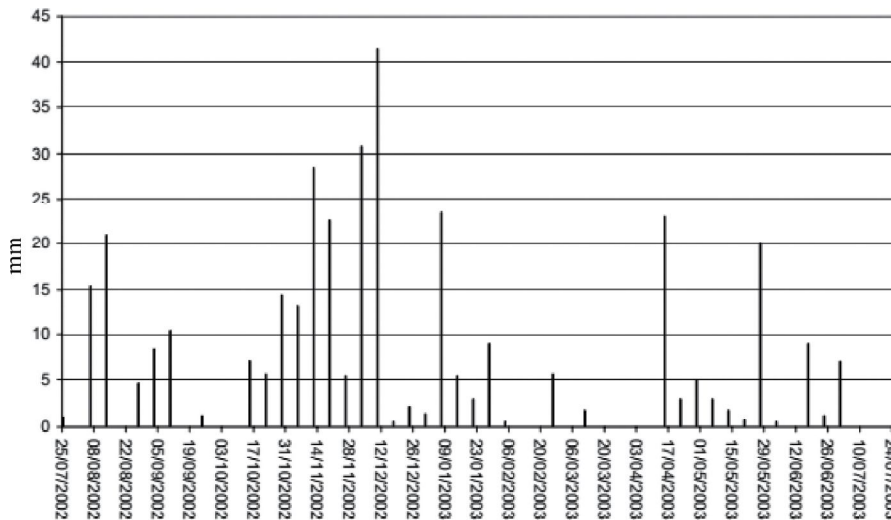


Fig. 4 – Pluviometric levels at Cigognola station (Pavia) – MEISINA [1996].

Fig. 4 – Intensità di pioggia rilevata alla stazione di Cigognola (Pavia) – MEISINA [1996].



Tab. I – Water Table Depth from July 2002 to July 2003, residential area of Broni. NA = Not Available (i.e. Dry Well).

Tab. I – Soggiacenza della falda dal luglio 2002 al luglio 2003, area residenziale di Broni. NA = Non disponibile (Pozzo asciutti).

Date	Well n. 1	Well n. 2	Well n. 3	Well n. 4	Well n. 5	Well n. 6	Well n. 7	Well n. 8
7/25/2002	NA	-5,1	-5,3	NA	-4,1	-5,2	-11,3	NA
8/28/2002	NA	-5,1	-5,05	NA	-4	-5,15	-11,15	NA
9/30/2002	NA	-5,2	-5,35	NA	-4,6	-5,75	-11,45	NA
10/23/2002	NA	-5,2	-5,35	NA	-4,65	-5,75	-11,5	NA
11/28/2002	-2,95	-4,3	-3,1	-5,2	-3	-3,5	-9,4	NA
12/06/2002	-3	-3,3	-2,9	-4,9	-2,95	-3,3	-9,25	NA
12/13/2002	-3,4	-3	-3,05	-5,1	-3,2	-3,55	-9,1	NA
1/29/2003	-3,1	-2,25	-2,8	-4,55	-2,15	NA	-7,7	-5,3
2/26/2003	-3,7	-2,35	-3,4	-4,7	-2,3	NA	-7,6	-5,25
03/12/2003	-3,8	-2,4	-3,6	-4,75	-2,4	NA	-7,7	-5,34
3/31/2003	-4	-2,75	-3,8	-4,85	-2,55	NA	-7,7	NA
04/12/2003	-3,95	-2,82	-3,9	-4,9	-2,6	NA	-7,8	NA
4/30/2003	-3,9	-2,9	-3,9	-4,8	-2,55	NA	-7,7	NA
5/15/2003	-4,1	-3,25	-4,1	-4,9	-2,7	NA	-7,8	NA
06/03/2003	-4,3	-3,55	-4,35	-4,9	-2,9	NA	-7,9	NA
6/18/2003	-4,55	-4,05	-4,55	-5	-3,05	NA	-8,65	NA
07/07/2003	NA	-4,45	-5	NA	-3,4	NA	-9,55	NA

W_l e W_p = Limite Liquido e Limite Plastico; W = contenuto d'acqua naturale; S = grado di saturazione; e_o = Indice dei vuoti; h_{co} = Altezza di risalita capillare da prove di laboratorio; σ_g = pressione di rigonfiamento da prove di laboratorio.

served until a depth of about 2 m for CPTu1, and the dynamic pore water pressure then increases with depth, until lower values than 25 kPa are reached. These measurements cannot be considered satisfactory because they indicate an initial de-saturation of the filter and subsequent sluggish measurements.

On the other hand, the dynamic pore water pressure assumes negative values at depths of between zero and -2.5 meters during the CPTu2 test, after which it increases with depth. The high pore water pressure value observed at -0.5 meters could be explained by considering the extreme stiffness of the shallower

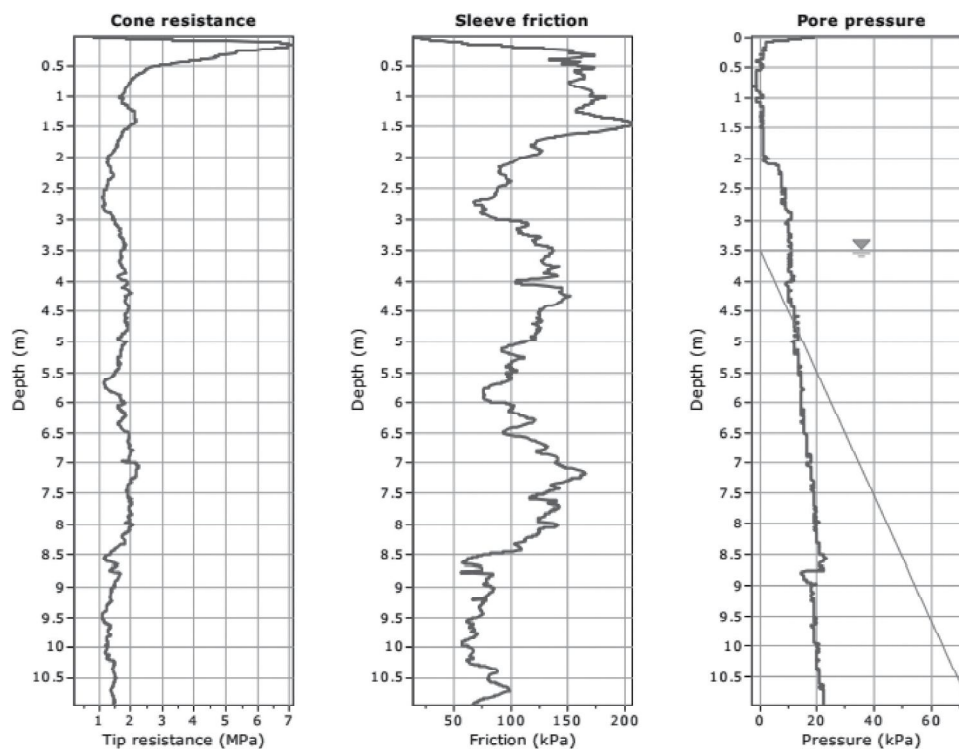


Fig. 5 – CPTu1 conducted during the humid season (Broni).

Fig. 5 – Prova CPTu1 eseguita nel corso della stagione umida (Broni).

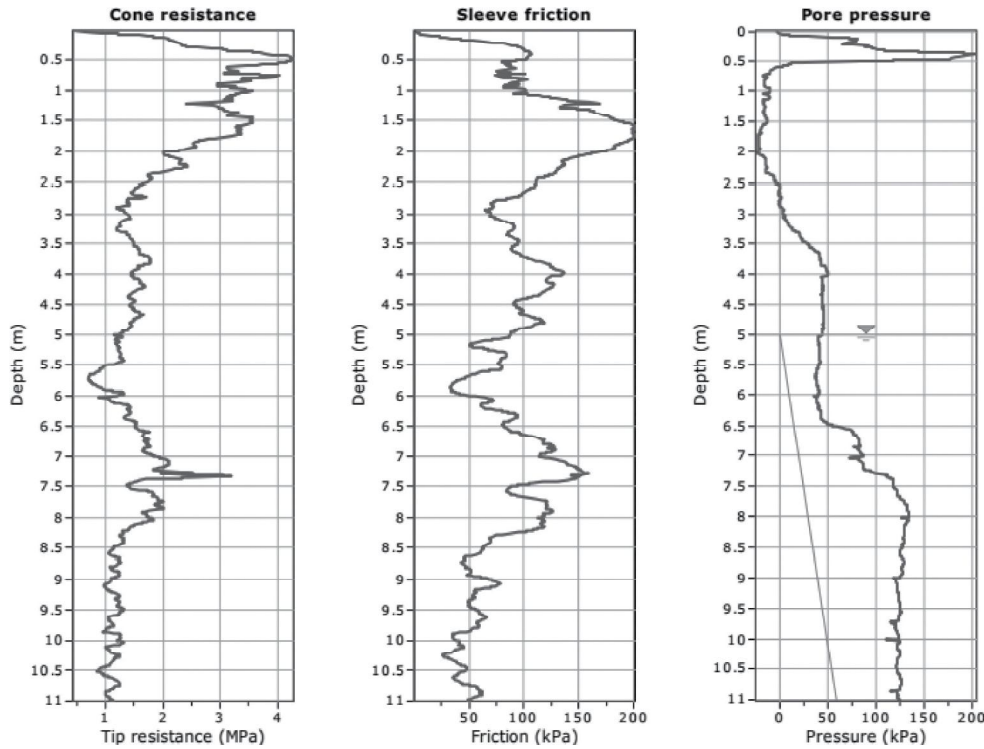


Fig. 6 – CPTu2 conducted during the dry season (Broni).
 Fig. 6 – Prova CPTu2 eseguita nel corso della stagione asciutta (Broni).

layer (man – made soil) and the consequent compressibility of the tip (including the filter). In the same way, as for CPTu1, this could be the cause of filter de – saturation.

The unsatisfactory measurement of U2 during the CPTu1 test does not influence the proposed method which pertains to the reinterpretation of the first 3 m using the total tip resistance and friction ratio. In fact the differences between the measured and total tip resistance for CPTu2 are negligible.

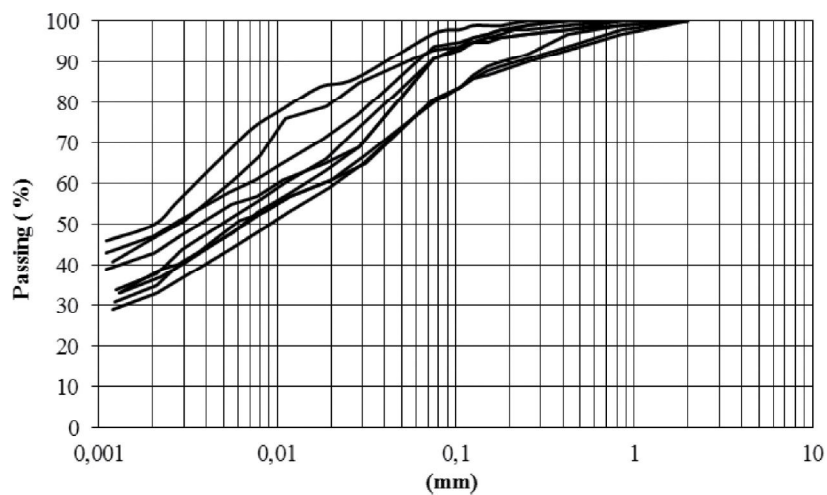
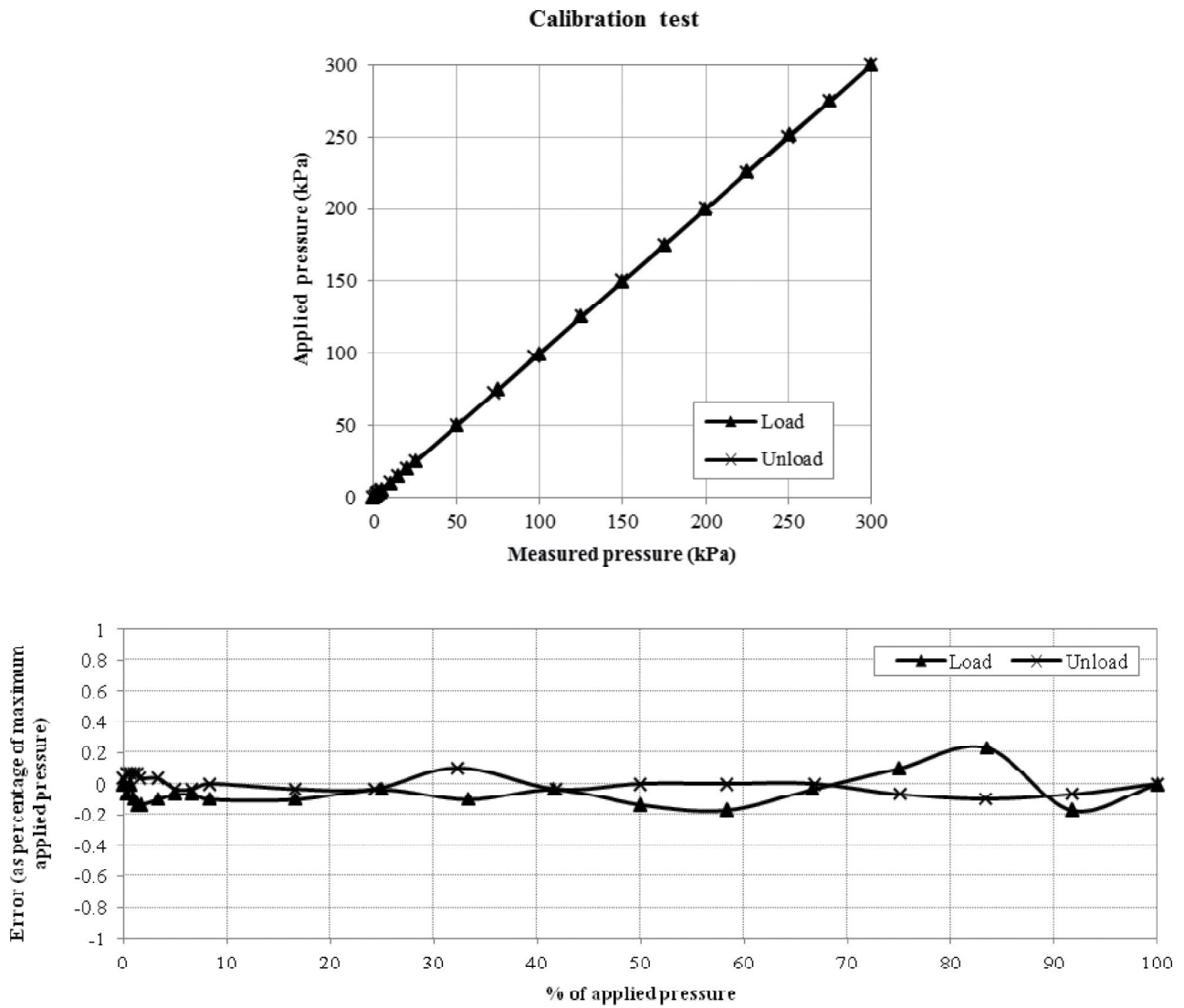
The pore water pressure was measured using silicone grease (very fluid, NLGI 00) as the slot filter satu-

ration fluid. The use of grease as a saturation fluid was first proposed by ELMGREN [1995] and LARSSON [1995], and various comparisons have testified its reliability. In addition, a calibration procedure was performed at Pagani Geotechnical Equipment (PC – Italy). Figure 7 shows the piezocone calibration test which was conducted in a specially devised calibration chamber: the upper diagram shows the relationship between the applied loads and readings during loading and unloading, while the lower diagram shows the calculated error, expressed as a percentage of the maximum applied pressure, during both the loading and unload-

Tab. II – Soil classification (Broni – first three meters) [MEISINA 1996].
 Tab. II – Classificazione del terreno (Broni – primi tre metri) [MEISINA 1996].

Sample	Depth (cm)	W _l (%)	W _p (%)	W (%)	gd (kN/m ³)	S (%)	e ₀	h _{co} (m)	σ _g (kPa)
B1	87	61	26	29.30	14,5	91,00	0,862	2,8	20
B2	130	59	28	27.90	15,1	96,00	0,788	2,7	15
B3	170	51	24	27.90	15,1	92,00	0,788	3,0	25
B4	200	49	19	27.00	15,4	96,00	0,753	2,6	15
B5	215	51	23	29.80	15,5	93,00	0,742	2,5	23
B6	230	44	25	30.00	14,7	97,00	0,837	2,6	8
B7	250	39	26	28.00	14,7	92,00	0,837	2,3	0
B8	263	41	22	26.00	15,5	95,00	0,741	2,5	13
B9	300	60	24	28.80	15,3	97,00	0,765	2,7	10

W_l and W_p = Liquid and plastic limit respectively; W = natural water content; S = Saturation degree; e₀ = Void ratio; h_{co} = Capillary rise from lab tests; σ_g = Swelling pressure from lab tests.



Tab. III – SBTn Classes [ROBERTSON, 1990].

Tab. III – Classi SBTn [ROBERTSON, 1990].

Soil classification (SBTn)	Zone number (Robertson SBT 1990)	SBT Index values
Organic soils: peats	2	$I_{Lc} > 3.60$
Clays: silty clay to clay	3	$2.95 < I_{Lc} < 3.60$
Silt Mixtures: clayey silt to silty clay	4	$2.60 < I_{Lc} < 2.95$
Sand Mixtures: silty sand to sandy silt	5	$2.05 < I_{Lc} < 2.60$
Sands: clean sand to silty sand	6	$1.31 < I_{Lc} < 2.05$
Gravelly sand to dense sand	7	$I_{Lc} < 1.31$

ing processes. It is possible to observe that there is a very good agreement between the measurements and applied pressures, with the absence of a threshold value, below which the transducer inside the cone would not be able to measure changes in the external pressure. Moreover, no relevant hysteresis loop can be observed. In conclusion, the slot filter saturation with grease instead of silicon oil can be considered acceptable. The use of grease is very popular in common practice, especially because the saturation procedure is much easier with grease than with oil and because the occurrence of de – saturation is more unlikely. Unfortunately, de – saturation occurred during test CP-Tu1 in spite of the use of grease.

The clayey nature of the deposit under consideration, and in particular of its shallower portion (first 3 meters), is shown in figures 8 and 9 and in table II. It is interesting to note that some measurements

of the negative pore pressure in the laboratory, conducted by means of the filter paper method, indicated values of about 2.6 – 3.0 m [MEISINA, 1996]. These values are about half those inferred by means of the M-K model. However, it is important to recall that the soil samples were not retrieved at the same time the CPTu test was conducted.

4.2. Interpretation of CPTu

The effective vertical geostatic stresses have been re-evaluated according to the method explained in the previous section. The pore water pressure was assumed to be linear from the water table to the capillary height, h_{co} calculated with the MK model, and then constant to the surface level. For the study case, the h_{co} values are higher than the water table depth,

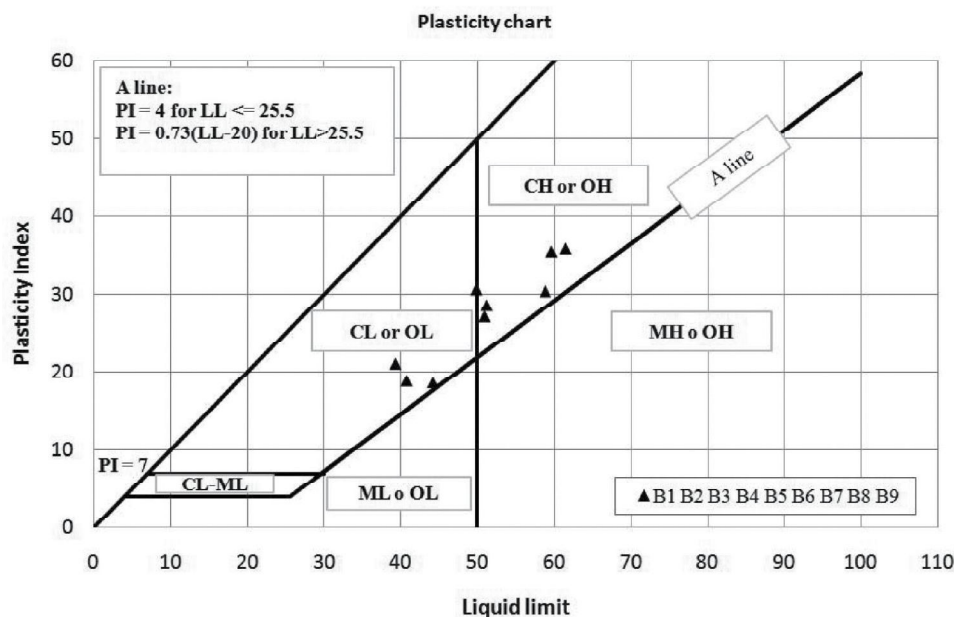


Fig. 9 – Casagrande classification chart [MEISINA, 1996].

Fig. 9 – Carta di classificazione di Casagrande [MEISINA, 1996].

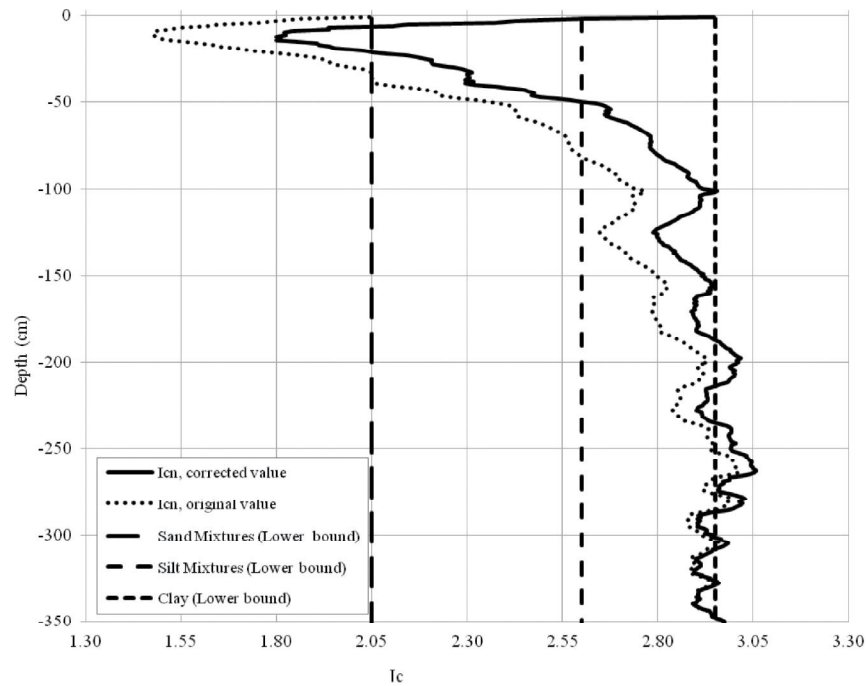


Fig. 10 – Variation of I_c values for CPTu1 (wet season).

Fig. 10 – *Variazione dei valori di I_c CPTu1 (stagione umida).*

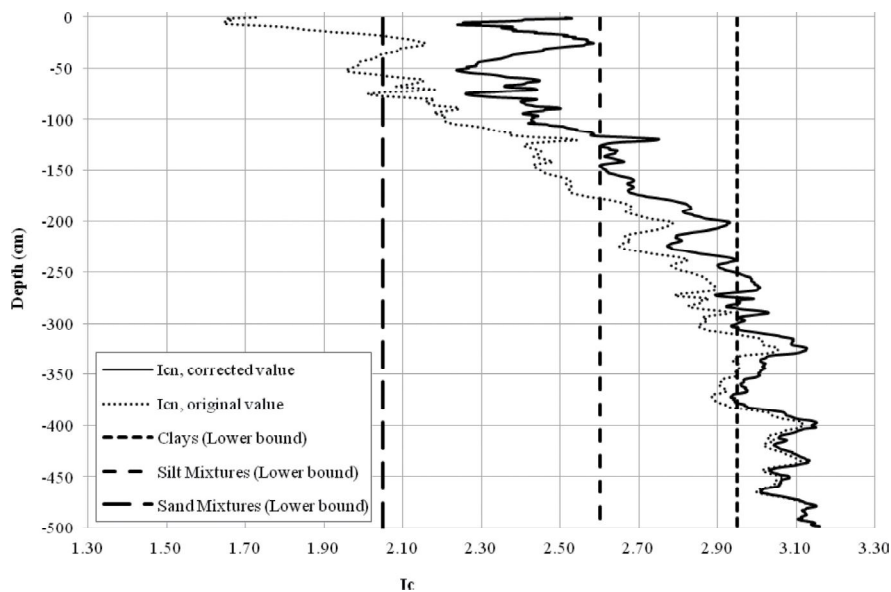


Fig. 11 – Variation of I_c values for CPTu2 (dry season).

Fig. 11 – *Variazione dei valori di I_c CPTu2 (stagione asciutta).*

and the pore water pressure was therefore assumed to linearly vary until the ground level. In practice, it was assumed that all the shallower portions of the subsoil were saturated by capillarity. This is in contrast with the saturation degree that was inferred from laboratory tests, as will be discussed in more detail later on.

It has been assumed that the h_{co} values are equal to Ψ_r as obtained from equation (7).

The increased values of σ'_{vo} led to a reduction in the normalized tip resistance, Q , and consequently, an increase in the Soil Classification Index I_c [ROBERTSON, 1990; ROBERTSON and WRIDE, 1998], on the basis of the equations reported below and the indications summarized in table III:

$$I_c = \sqrt{(3.47 - \log Q_m)^2 + (\log(F) + 1.22)^2} \quad (10)$$

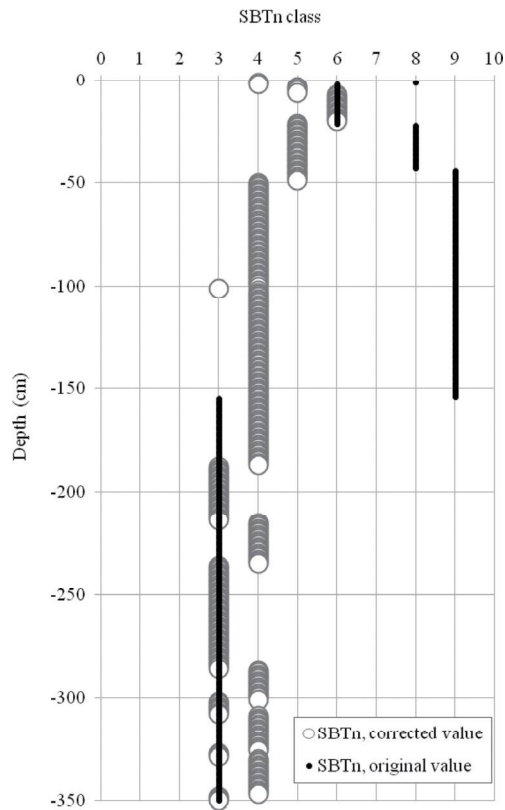


Fig. 12 – SBTn classes before and after correction for CPTu1 (humid season).

Fig. 12 – Classi SBTn prima e dopo la correzione CPTu1 (stagione umida).

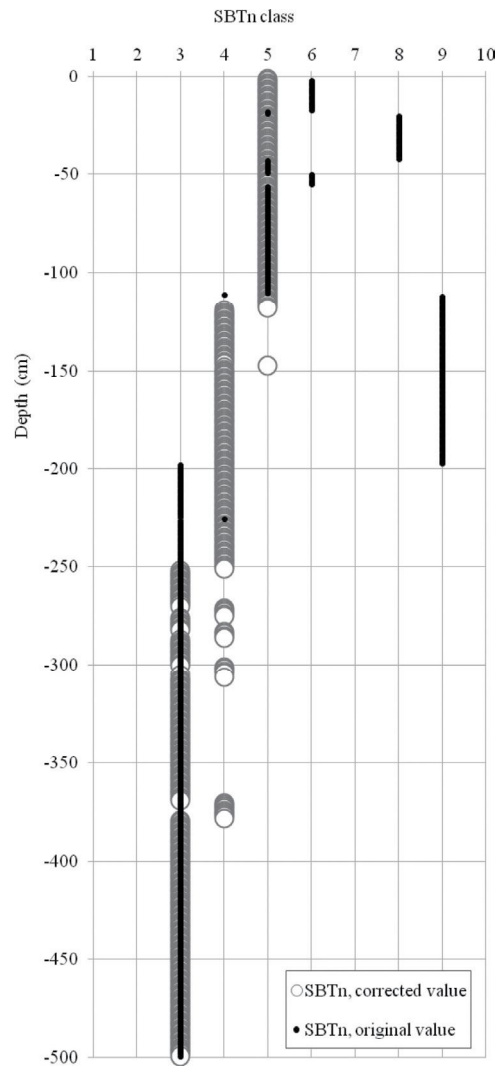


Fig. 13 – SBTn classes before and after correction for CPTu2 (dry season).

Fig. 13 – Classi SBTn prima e dopo la correzione CPTu2 (stagione asciutta).

$$Q_{tn} = \left(\frac{q_t - \sigma_{vo}}{\sigma_{atm}} \right) \left(\frac{\sigma_{atm}}{\sigma'_{vo}} \right)^n \quad (11)$$

$$F = \frac{f_s}{q_t - \sigma_{vo}} 100 \quad (12)$$

$$n = 0.381 \cdot I_c + 0.05 \left(\frac{\sigma'_{vo}}{\sigma_{atm}} \right) - 0.15 \quad (13)$$

The influence of the proposed correction on I_c is shown in figure 10 and figure 11. Such a correction moves the I_c parameter toward the target value of 3.0 (*i.e.* the I_c value that the homogeneous clay - deposit exhibits below the water table). In other words, after the correction, the target value of $I_c = 3.0$ is reached below the depth of 1.0 m for CPTu1 and below the depth of 2.0 m for CPTu2.

The effect of the correction on SBTn is shown in figures 12 and 13. The correction, in practice, produces an increase in SBTn classes 3 to 4 (clay to clayey silt) and completely cancels SBTn class 9 (*i.e.* very stiff fine grained soil). In other words, after the correction the SBT classification system seems to become a "Soil Type" classification. In fact the upper 5 m of the deposit is identified as fine-grained soil (SBTn classes 3 to 4), while the information on the

presence of "very stiff" fine-grained soils (SBTn class 9) disappears. This information is now incorporated in the much higher values of the vertical effective stress. Therefore, it could be possible to use the proposed correction to estimate the effective in situ stress for soil layers above the water table. Figure 14 shows the vertical effective stress value for the Broni case that produces a constant I_c , which is equal to that obtained below the water table. The two different curves, shown in figure 14, have been obtained from the two considered CPTus at Broni [BUSONI, 2016; MARCONCINI, 2016]. The curves coincide with those obtained through the use of the M-K model for greater depths than 1.0 and 2.0 meters for CPTu1 and CPTu2, respectively. The thus obtained vertical effective stress could be interpreted as the result of a preconsolidation pressure induced by desiccation of the shallower layers.

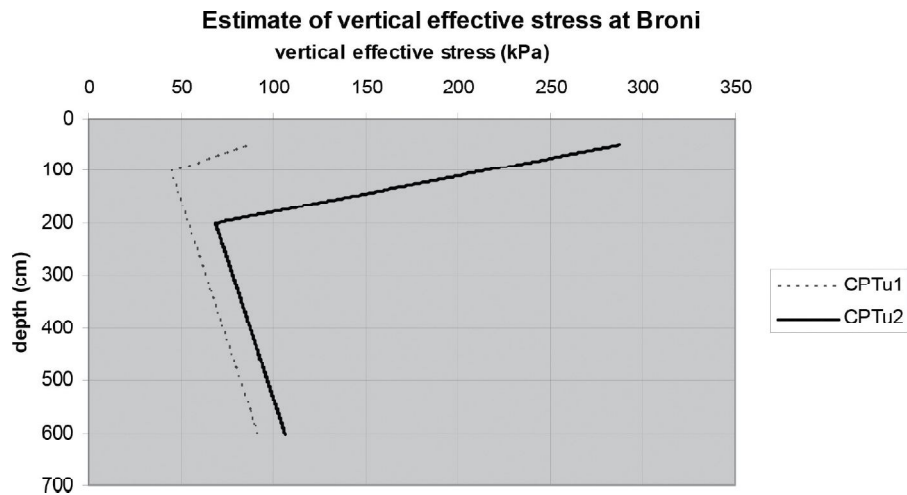


Fig. 14 – Assessment of in situ vertical stress from CPTu1 and CPTu2 (Broni).

Fig. 14 – Determinazione della tensione verticale efficace dalle prove CPTu1 and CPTu2 (Broni).

Unfortunately, this hypothesis could not be assessed for the Broni data because no laboratory tests on undisturbed samples were available. Therefore, the working hypothesis was checked by considering additional data [BARSANTI, 2016]. These data were obtained from Porcari (Lucca – Tuscany) and refer to a CPTu carried out in a partially saturated fine-grained layer (above the water table) and an oedometer test on an undisturbed sample

that had been retrieved at the same location as the CPTu test from a depth of 2.0-2.3 m (Figs. 15 and 16). It can be observed that the I_c value increases with depth moving toward the target value of about 2.55, which is reached below the water table, even though in a scattered way. However, when the I_c value at a depth of 2.0 – 2.3 m (about 2.05) and the I_c target are considered, the application of the proposed method leads to an estimate of the suction

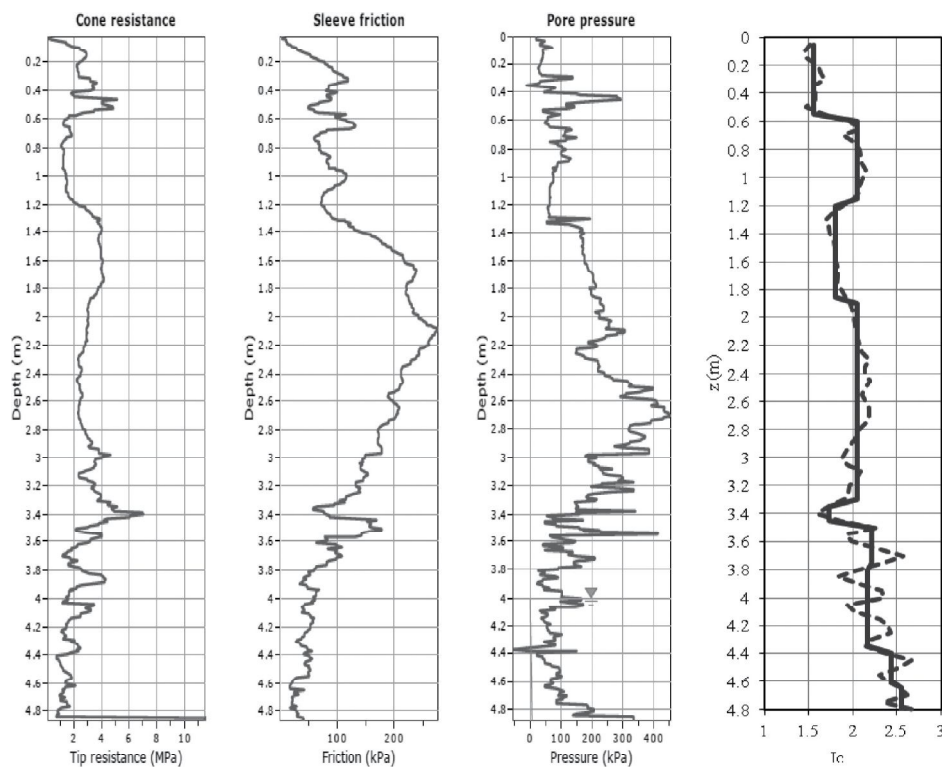


Fig. 15 – CPTu and I_c index (Porcari – Lucca).

Fig. 15 – CPTu e indice I_c (Porcari – Lucca).

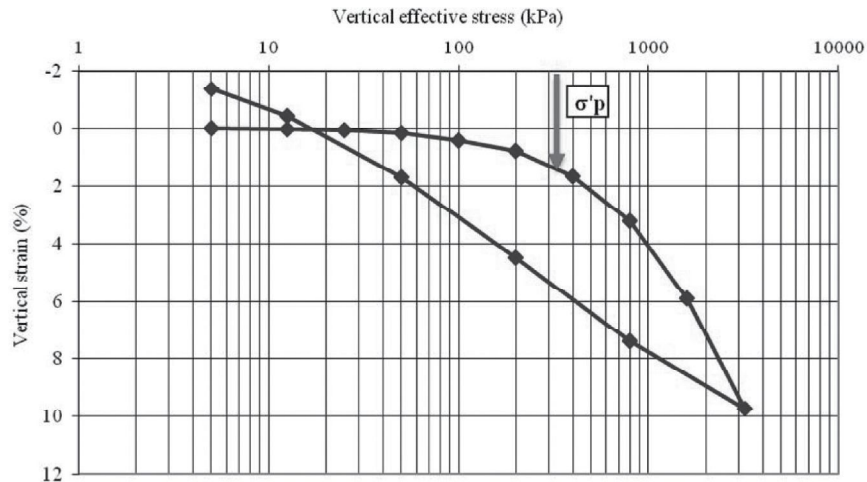


Fig. 16 – Oedometer test (Porcari Lucca).

Fig. 16 – Prova edometrica (Porcari Lucca).

of about 297 kPa. The interpretation of the oedometer test is shown in figure 16, and leads to an estimate of the preconsolidation pressure of about 320 kPa. Even though a single result cannot be considered sufficient to validate the working hypothesis, the analyzed data suggest that the proposed approach merits further investigation. The fundamental finding of this study is that the currently available classification systems have been found to be inadequate for those cases in which the effective stress state is controlled by suction. The proposed approach seems to offer the possibility of inferring the effective in situ stress state and of estimating the preconsolidation pressure. It is also worth noting the possible differences between the oedometer preconsolidation pressure and suction. The two values could only coincide when $K_0 = 1$, which is not unrealistic for highly mechanically overconsolidated soils.

5. Specific - empirical calibration of I_c vs. borehole evidence

As already mentioned this methodology is purely empirical and consists of a specific calibration of the I_c values [ROBERTSON, 1990; JEFFERIES and DAVIES, 1993], as inferred from CPTu results with evidence obtained from direct logging (boreholes). The proposed calibration is based on the following:

- the comparison was only made between the boreholes and CPTus, which were located very close to each other (maximum 1.0 m apart);
- the comparison was only made for those portions of the borehole where the grain size curve was available;
- the grain size curve was obtained and described according to AGI (1997);

- the I_c index from the CPTu was inferred by means of the CPeT-IT software [GEOLOGISMIKI, 2007];
- the I_c index from the grain size curve was established according to the indications reported in tables IV and V.

For those readers who are not familiar with the AGI (Italian Geotechnical Society) classification it is worth recalling the following rules:

- the name given to the soil is that of the main fraction;
- the expression “silt with clay” (as an example) means that there is a clay fraction of between 25 and 50%;
- the expression “clayey silt” (as an example) means that there is a clay fraction of between 10 and 25%;
- a fraction of less than 5% is not considered

Fractions of between 5 and 10% are shown in brackets in tables IV and V. An example is given to help understand how a correspondence between I_c and the granulometric curve has been defined. A “silt with clay” soil corresponds to SBTn class 4 with $2.60 < I_c < 2.95$. A more precise value of the index is assumed proportional to the percentage of clay fraction (from 25 to 50%).

It is worth recalling that the CPTu – based soil classification mainly refers to the soil behavior type (SBT), while the proposed borehole – based soil classification refers to the grain size distribution. However, one of the most relevant parameters, in the case of levees and dredged sediments as well, is the permeability which mainly depends on the grain size and degree of compaction [TATSUOKA, 2015].

Tables IV and V show the soil classification (according to AGI, 1997) and the I_c index that were selected for the various soil classes. In addition, the tables show the I_c index inferred from CPTu, the SBTn

Tab. IV – Serchio River data – I_c and classification from both CPTu and borehole – data interpretation.Tab. IV – Dati relative al Fiume Serchio – I_c e classificazione ottenuta dall'interpretazione di prove CPTu e sondaggi.

Borehole #	Soil classification from borehole (AGI 1997)	I_c from borehole	I_c from CPTu	ΔI_c	SBTn	Soil classification from CPTu
1	Clayey and sandy silt	2.60	2.79	0.19	4	Sand Mixtures
	Silty sand	2.10	2.05	-0.05	6	Sand
	Silty sand	2.10	2.49	0.39	5	Sand Mixtures
	Sand, gravel and fine gravel	1.30	1.72	0.42	6	Sand
	Silty sand	2.10	2.19	0.09	5	Sand Mixtures
2	Fine sand with silt	2.40	3.14	0.74	3	Clays
	Silty sand	2.10	2.20	0.10	5	Sand Mixtures
3	Clayey and sandy silt	2.60	1.63	-0.97	6	Sand
	Clayey and sandy silt	2.60	3.36	0.76	3	Clays
	Silty sand (5<clay<10%)	2.50	3.27	0.77	3	Clays
	Silty sand	2.10	2.85	0.75	4	Silt Mixtures
4	Silty sand	2.10	2.15	0.05	5	Sand Mixtures
	Sand, gravel and fine gravel	1.30	1.86	0.56	6	Sand
	Sand	1.70	1.93	0.23	6	Sand
	Clayey and sandy silt	2.60	3.70	1.10	2	Clay-Organic Soil
5	Sand with silt	2.50	2.74	0.24	4	Silt Mixtures
	Silt with clay	2.80	2.05	-0.75	6	Sand
	Silty sand	2.10	1.93	-0.17	6	Sand
	Sand	1.60	2.29	0.69	5	Sand Mixtures
	Silt with clay/clay with silt	3.00	3.23	0.23	3	Clays
6	Sand with silt/silt with sand	2.50	3.23	0.73	3	Clays
	Silt with clay	2.90	3.34	0.44	3	Clays
	Silty sand	2.10	3.18	1.08	3	Clays
	Clayey and sandy silt	2.60	2.99	0.39	3	Clays
	Silty sand	2.10	3.27	1.17	3	Clays
7	Silty sand	2.10	1.94	-0.16	6	Sand
	Medium silty sand	1.90	1.58	-0.32	6	Sand
	Sand, gravel and fine gravel	1.30	1.82	0.52	6	Sand
	Coarse sand (5<clay<10%)	2.00	2.06	0.06	5	Sand Mixtures
	Clayey and sandy silt	2.60	2.09	-0.51	5	Sand Mixtures
	Medium sand (5<clay<10%)	2.10	2.26	0.16	5	Sand Mixtures
	Silty sand	2.10	2.14	0.04	5	Sand Mixtures
8	Silty sand (5<clay<10%)	2.50	2.50	0.00	5	Sand Mixtures
	Silty sand	2.10	2.86	0.76	4	Silt Mixtures
	Clayey silt	2.80	3.06	0.26	3	Clays
	Sand (5<silt<10%)	2.00	3.18	1.18	3	Clays
9	Sand with silt	2.35	2.32	-0.03	5	Sand Mixtures
	Medium sand with gravel	1.40	1.73	0.33	6	Sand
	Sand (5<silt<10%)	2.00	2.95	0.95	3	Silt Mixtures
	Clayey and sandy silt	2.60	3.43	0.83	3	Sand Mixtures
	Silty sand	2.10	3.34	1.24	3	Clays
	Clayey and sandy silt	2.60	2.24	-0.36	5	Sand Mixtures
	Silty sand	2.10	2.16	0.06	5	Sand Mixtures
10	Silty sand (5<clay<10%)	2.50	3.16	0.66	3	Clays
	Silt with sand (5<clay<10%)	2.65	3.34	0.69	3	Clays
	Silty sand (5<clay<10%)	2.50	2.75	0.25	4	Silt Mixtures
	Silty sand	2.10	3.28	1.18	3	Clays
	Clayey silt	2.80	3.48	0.68	3	Clays
	Peat	3.60	3.48	-0.12	3	Clays
	Clayey silt	2.80	3.59	0.79	3	Clays
	Clayey and sandy silt	2.60	3.59	0.99	3	Clays
	Sand with silt/silt with sand	2.50	2.39	-0.11	5	Sand Mixtures
	Silty sand	2.10	2.75	0.65	4	Silt Mixtures
	Clayey silt with sand	2.55	3.73	1.18	2	Clay-Organic Soil
11	Medium to coarse sand	1.40	2.29	0.89	5	Sand Mixtures
	Clayey silt	2.80	3.64	0.84	2	Clay-Organic Soil
	Silty sand	2.10	2.79	0.69	4	Silt Mixtures
	Clayey silt	2.80	4.28	1.48	2	Clay-Organic Soil
	Medium sand (5<silt<10%)	2.00	2.73	0.73	4	Silt Mixtures
12	Medium to coarse sand	1.40	2.02	0.62	6	Sand
	Peat	3.60	4.80	1.20	2	Clay-Organic Soil
	Silt with clay	2.90	3.62	0.72	2	Clay-Organic Soil
	Clayey silty sand	2.50	3.77	1.27	2	Clay-Organic Soil
	Silt with clay	2.80	3.88	1.08	2	Clay-Organic Soil
	Silty sand	2.10	1.65	-0.45	6	Sand
	Medium to coarse sand	1.40	1.66	0.26	6	Sand Mixtures

Tab. V – Port of Livorno data – I_c and classification from both CPTu and borehole – data interpretation.

Tab. V – Dati relative al Port of Livorno – I_c e classificazione ottenuta dall'interpretazione di prove CPTu e sondaggi.

Borehole #	Soil classification from borehole (AGI 1997)	I_c from borehole	I_c from CPTu	ΔI_c	SBTn	Soil classification from CPTu
SC3	Silt with sand (5<clay<10%)	2.05	3.28	1.25	3	Clays to silty clay
	Silt with clay (5<sand<10%)	2.70	3.05	0.27	3	Clays to silty clay
SC4	Silt with clay	2.75	2.92	0.13	3	Clays to silty clay
SC7	Silt with clay (5<sand<10%)	2.10	2.30	0.17	5	Sand mixture
	Silt with clay (5<sand<10%) (5<gravel<10%)	2.65	3.10	0.40	3	Clays to silty clay
SC8	Sand with silt (5<clay<10%)	1.95	2.20	0.27	5	Sand mixtures
SC14	Sandy silt with clay (5<gravel<10%)	2.10	2.36	0.22	5	Sand Mixtures
	Sandy silt with clay (5<gravel<10%)t	2.10	3.96	1.82	2	Orhanic soils
	Clayey sand with silt	1.95	2.96	0.96	3	Clays to silty clay
	Clayey sand with silt	1.95	3.12	1.30	3	Clays to silty clay
	Silt with clay (5<sand<10%)	2.10	3.36	1.27	3	Clays to silty clay
	Silt with clay (5<sand<10%)	2.10	3.64	1.55	2	Organic soils

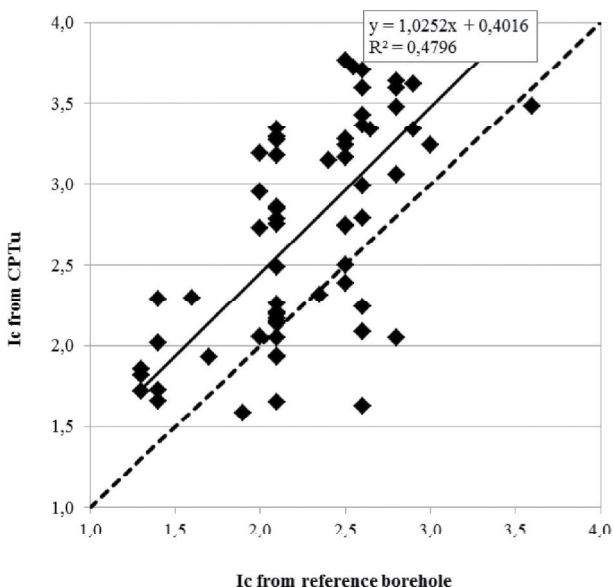


Fig. 17 – I_c values from boreholes and CPTu tests for soil layers below the water table (Serchio River area).

Fig. 17 – Valori di I_c da sondaggi e prove CPTu per strati di terreno al di sotto della falda (Serchio River area).

class number and the corresponding description. In practice, each row in tables IV and V shows the soil classification [AGI, 1997], as obtained for a homogeneous portion of borehole, and the “arbitrary” I_c value that was associated to that soil description. The term “arbitrary” I_c value refers to the fact that such an index was introduced to define an SBT and not a soil type. Both the I_c and SBTn values inferred from the corresponding CPTu at the same depth are reported in the same row. Tables IV and V only consider the soil portion below the water table. The comparison was

limited to those portions of boreholes below the water table. The proposed method is intended for a user – defined correction of the classification chart.

5.1. The database of the Serchio river levee system and Livorno port

After the Serchio River flood in December 2009 in the Pisa and Lucca Districts (Italy), a huge geotechnical characterization survey was conducted in order to study the safety conditions of the embankment system and the causes that had led to its failure [COSANTI *et al.*, 2014]: boreholes, Lefranc tests, the installation of piezometers for each borehole, piezocone tests (CPTu tests), 2D Electric Resistivity Tomography (ERT) and continuous sampling (4m deep). Among these, 149 CPTu tests were conducted in the Pisa area, at various depths of between 20 and 30 meters. Of these 149 CPTu tests only 12 have been used in the present work. In fact, the above stated conditions were only met for these 12 CPTus

In recent years, there has been a great proliferation of artificial basins for the storage of dredged sediments as a result of port developments, in both Italy and the rest of the world. There is now a great deal of interest in using the same storage basins for a range of urban infrastructure projects and this requires an accurate assessment of the stratigraphy and the state of consolidation of the dredged sediments. The main goal of geotechnical engineering is to assist planning authorities with the re-use of designated dredged fill storage areas for future infrastructure projects. An excellent example is that of the Port of Livorno, where the designated 40 hectare storage basin has been filled with dredged sediments (a total vol-

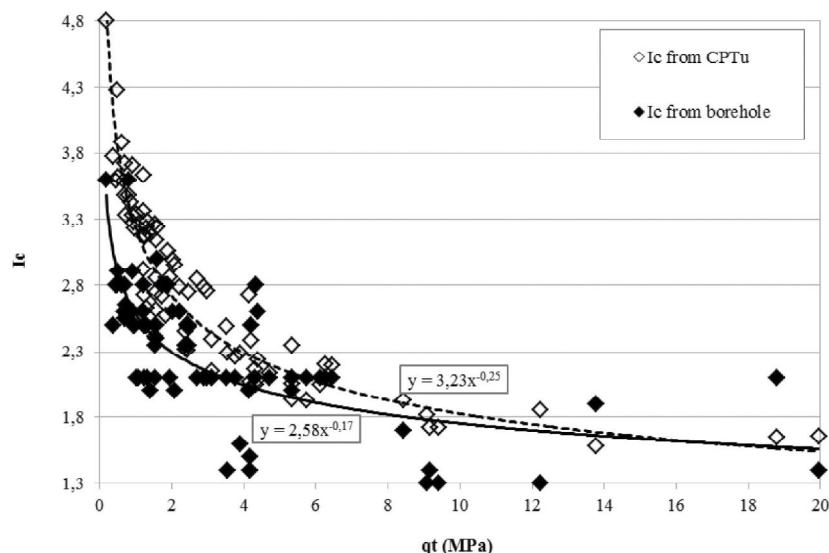


Fig. 18 – Dependency with q_t of I_c values inferred from both CPTu and boreholes (Serchio river area).
 Fig. 18 – Dipendenza di q_t dai valori di I_c ricavati da prove CPTu e dai sondaggi (Area del Fiume Serchio).

ume of 1.7M m^3) since 2000. The Port of Livorno Authority has therefore carried out a huge geotechnical (and environmental) investigation campaign consisting of: a) 22 boreholes (for a total of 196.5 m); b) 18 undisturbed samples; c) 34 remoulded samples; d) 11 Lefranc (variable head) permeability tests; e) the installation and reading of 4 piezometers (open pipe); f) 26 CPTus (for a total of 153 m); g) 6 DMT (for a total of 29 m); h) laboratory tests on 50 different samples. A comparison has only been made considering 12 CPTus, and only for those portions of subsoil for which the grain size curve was available.

5.2. Empirical I_c correction

The diagram in figure 17 displays the values of I_c obtained from the CPTu tests (Serchio River area) and from the corresponding boreholes for soil layers below the water table. The differences between the two values are particularly evident for SBTn classes 3, 4 and 5, in which I_c varies between 1.90 and 3.22. In particular, it is possible to observe an almost systematic bias between the two series of values. The dependence of the Soil Classification Index, I_c on the total tip resistance, q_t , is shown in figure 18 (Serchio River area). Figure 18 shows the I_c values obtained from both the CPTu and from borehole data interpretation. The values obtained from the CPTus are generally higher, while those inferred from boreholes are lower (Tab. IV). As the total tip resistance increases, the differences between the two series become negligible, and, from a practical point of view, not very relevant.

The difference between the two I_c series (ΔI_c) is plotted vs. the total tip resistance in figure 19 (Ser-

chio River and Port of Livorno areas). The best fit of such data is given by the following equation [RO-SIGNOLI, 2014; FULCINITI, 2016].

$$\Delta I_c = 0.05 + \frac{0.75}{q_t} \quad (14)$$

q_t (MPa)

The $\Delta I_c(q_t)$ function was used to correct the CPTu interpretation (Serchio river data). The new results, after the correction, are shown in figure 20. It is possible to observe that the dispersion of the corrected data is much lower than that of the original values. Moreover, the I_c values are arranged better around the 45° angle line, thus leading to a much better correspondence between the SBTn classes identified from the CPTu tests and those inferred from the boreholes (based on grain size).

The proposed correction is only applicable to the considered soils and the analyzed database. The proposed correction in fact depends on the tip resistance, and becomes particularly relevant for resistances below 1 MPa. On the other hand, the ROBERTSON [1990] classification – system has been applied successfully to obtain the soil stratigraphy of soft deposits with tip resistances of less than 1 MPa.

The Robertson [1990] classification-system has been applied successfully by the Authors, without any correction, for the interpretation of tests in the Arno River area (near the city of Pisa). These sediments mainly consist of [LO PRESTI *et al.*, 2002]:

- recent (Holocene) fluvio – lacustrine and silting deposits (sometimes with organic soil). These sediments are heterogeneous and mainly consist of silty-clayey soil, often containing archaeological remains;

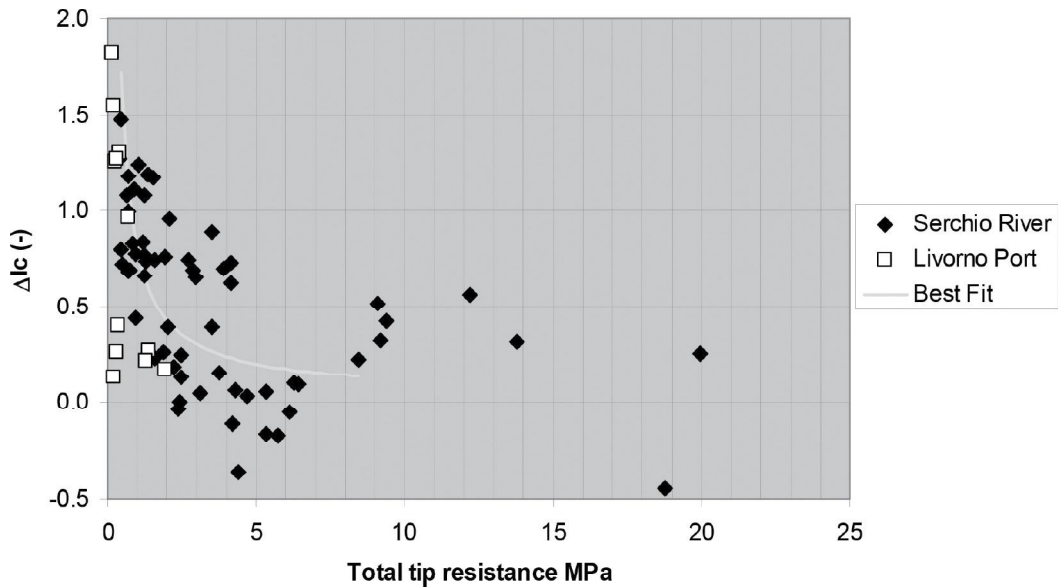


Fig. 19 – The difference between the two I_c series (ΔI_c) vs. the total tip resistance.
 Fig. 19 – Differenze tra le due serie di I_c (ΔI_c) in funzione della resistenza alla punta totale.

– (Holocene) soft marine clay deposits
 Therefore, an attempt has been made to distinguish the silt mixtures of the Serchio River ($q_t < 1$ MPa) from the soft marine clay or organic clay and silt of the Pisa valley ($q_t < 1$ MPa).

To this aim, a large database of CPTu tests, performed within the city of Pisa, has been used [COSCO and SPADARO, 2014; ZACCAGNINO, 2014; SCARDIGLI, 2014; PONZANELLI, 2014]. Penetration resistance and sleeve friction (only when $q_t < 1$ MPa) were considered. Boreholes and laboratory testing were also performed but, unfortunately, this information was not available to the Authors. Therefore, the nature of the tested soils (*i.e.* clay and organic clay) has only been assumed on the basis of geological evidence.

Figures 21a and 21b show the classification of the Serchio River sediments and that of the Pisa valley sediments according to ROBERTSON [1990]. Figure 21 does not point out too many differences between the two types of soil. On the other hand, clear differences can be observed when figures 22a and 22b are compared. These figures show the frequency distribution of the friction ratio for the considered database. It is evident that while most of the R_f values for the Serchio River sediments are equal or less than 4% (only 15% of the data has $R_f > 4\%$), about 50 to 60 % of the Pisa valley sediments exhibit an $R_f > 4\%$. It is worth recalling that the Serchio River sediments are mainly silts with intermediate permeability as inferred from boreholes and laboratory testing. The presence of clayey silts for the considered database is limited to only a very few cases that can be identified. On the other hand, the clayey nature of the Pisa valley sediments has only been hypothesized. At the same time, it is not possible to ex-

clude the presence of other silty layers in the database concerning the Pisa valley sediments.

In the absence of more detailed information, it is not possible to draw more precise conclusions, but simply reconfirm the very old and well - known criterion which indicates an $R_f > 4\%$ for very soft and organic clays.

6. Conclusions

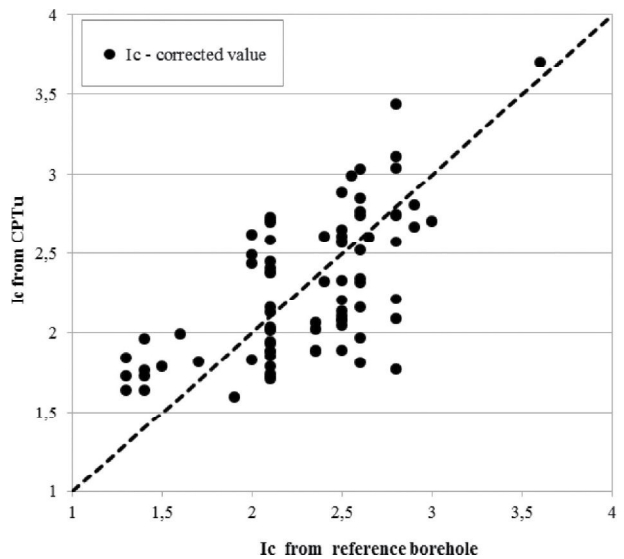


Fig. 20 – Comparison of I_c indexes from CPTu and boreholes after the proposed correction (Serchio river area).
 Fig. 20 – Confronto dei valori dell'indice I_c da prove CPTu e sondaggi dopo la correzione proposta (Area del Fiume Serchio).

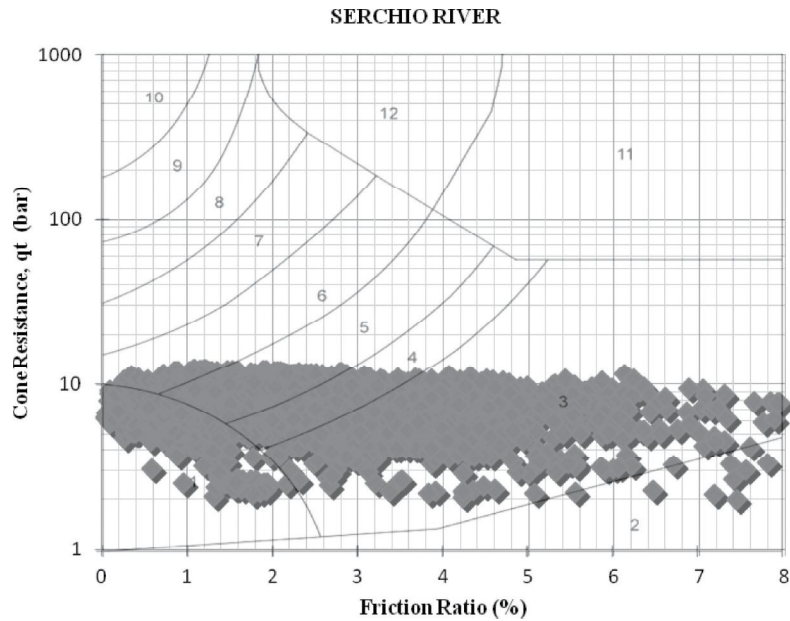


Fig. 21a – SBTn Serchio River.
Fig. 21a – SBTn (Fiume Serchio).

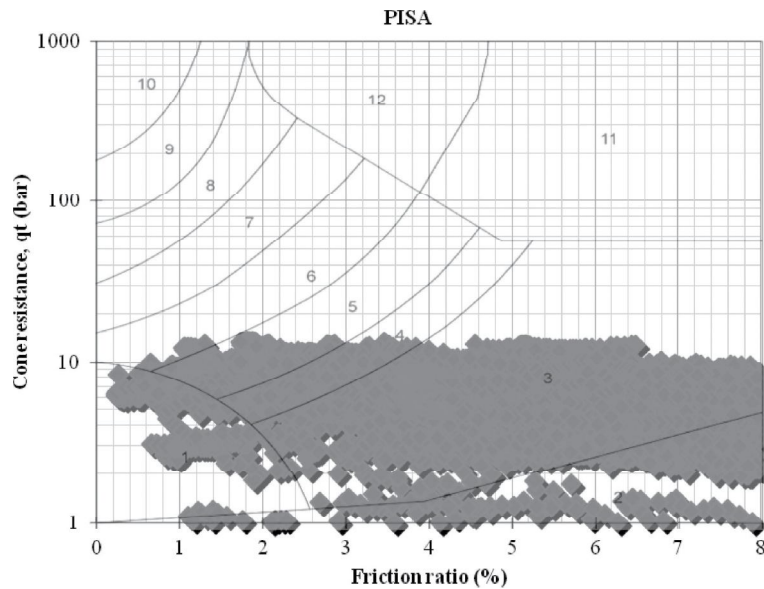


Fig. 21b – SBTn Pisa clayey sediments.
Fig. 21b – SBTn (Sedimenti argillosi – Pisa).

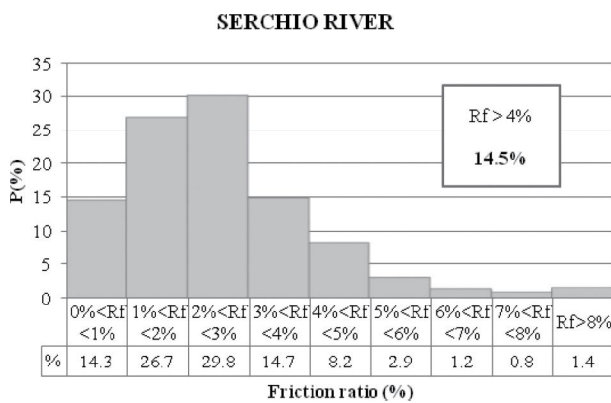


Fig. 22a – Rf distribution of Serchio River Levees.
Fig. 22a – Distribuzione di Rf (Rilevati dal Fiume Serchio).

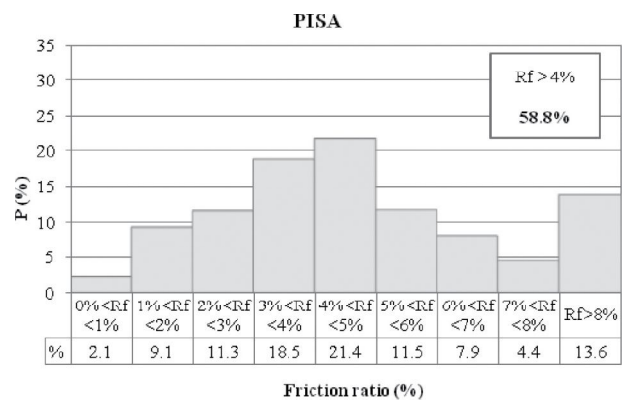


Fig. 22b – Rf distribution of the Pisa clayey sediments.
Fig. 22b – Distribuzione di Rf (Sedimenti argillosi – Pisa).

The shown data allow the following conclusions to be drawn:

- the use of the currently available classification systems is not recommended for soil layers above the water table (suction controlled) or for very loose silt mixtures;
- the paper shows the possibility of estimating the effective stress state in the vadose zone by increasing (at various depths) the negative pore pressure until the I_c index matches that measured below the water table. This approach requires further verifications. Moreover, it is only applicable to homogeneous layers;
- the empirical correction of the I_c index is only applicable to the studied cases, but the proposed methodology could be extended to other contexts. This approach guarantees the possibility of continuing to use the currently available commercial program for CPTu interpretation

Acknowledgements

Thanks are due to Mrs. Marguerite Jones for reviewing the paper from an English point of view. The Authors would also like to thank Mr. P. Barsanti, Mr. M. Cosco, Mr. F. Spadaro and Prof. C. Meisina for having supplied the data.

References

- AGI (1997) – *Raccomandazioni sulle Prove Geotecniche di Laboratorio*. <http://www.associazionegeotecnica.it/pubblicazioni/raccomandazioni>. 56pp
- AUBERTIN M., MBONIMPA M., BUSSIÈRE B., CHAPUIS R. P. (2003) – *A model to predict the water retention curve from basic geotechnical properties*. Canadian Geotechnical Journal, n. 40, pp. 1104-1122.
- AUBERTIN M., RICARD J.-F., CHAPUIS R.P. (1998) – *A predictive model for the water retention curve: application to tailings from hard-rock mines*. Canadian Geotechnical Journal, 35, pp. 55-69 (with Erratum, 36, 401)
- BEGEMANN H.K.S. (1965) – *The Friction Jacket Cone as an Aid in Determining the Soil Profile*. Proc. 6th ICSMFE, 1, pp. 17-20.
- BELLOTTI R., CRIPPA V., PEDRONI S., GHIONNA V.N. (1988) – *Saturation of Sand Specimen for Calibration Chamber Tests*. Proc. ISOPT-1, Orlando, 2, pp. 661-672.
- BARSAANTI P. (2016) – *Indagini Geotecniche in Località Porcari (Lucca)*. Personal Communication to the first Author.
- BUSONI D. (2016) – *Procedura innovativa per la determinazione dell'OCR da prove CPTu in terreni parzialmente saturi*. B.Sc. Thesis University of Pisa.
- COSANTI B., SQUEGLIA N., LO PRESTI D.C.F. (2014) – *Analysis of existing levee systems: the Serchio river case*. Rivista Italiana di Geotecnica, n. 4, pp. 47-65.
- COSCO M., SPADARO F. (2014) – *Database of CPTu in the Pisa Area*. Personal communication to the first Author
- DOUGLAS J.B., OLSEN R.S. (1981) – *Soil Classification Using Electric Cone Penetrometer*. Symposium on Cone Penetration Testing and Experience, Geotechnical Engineering Division, ASCE, St. Louis, pp. 209-227.
- ELMGREN K. (1995) – *Slot-Type Pore Pressure CPTu Filters*. Proc. Int. Symposium on Cone Penetration Testing, Swedish Geotechnical Society Report, n.3, 95, Linköping, Sweden, n.2, pp.9-12.
- ESLAMI A., FELLENIUS B.H. (1997) – *Pile Capacity by Direct CPT and CPTu Methods Applied to 102 Case Histories*. Can. Geotech. J., n.34, pp. 886-904.
- FULCINITI N. (2016) – *Interpretazione della prova penetrometrica statica (CPT) su terreni parzialmente saturi e comprimibili (sedimenti di colmata)*. B. Sc. Thesis University of Pisa
- GEOLOGISMIKI (2007) – *Geotechnical Software, CPeT-IT v 1.6*. CPT interpretation software, <http://www.geologismiki.gr/Products/CPeT-IT.html>.
- JAMIOLKOWSKI M., LO PRESTI D. C. F., MANASSERO M. (2001) – *Evaluation of Relative Density and Shear Strength of Sands from CPT and DMT*. Invited Lecture Ladd Symposium, GSP n.119, ASCE, pp. 201-238.
- JEFFERIES M.G., DAVIES M.P. (1993) – *Use of CPTu to Estimate Equivalent SPT N60*. Geotechnical Testing Journal, vol. XVI, n. 4, pp. 458-468.
- KOVÁCS G. (1981) – *Seepage Hydraulics*. Elsevier Science Publishers, Amsterdam.
- LARSSON R. (1995) – *Use of a Thin Slot as Filter in Piezocone Tests*. Proc. Int. Symposium on Cone Penetration Testing, Swedish Geotechnical Society Report, 3, n. 95, Linköping, Sweden, 2, pp.35-40.
- LO PRESTI D., JAMIOLKOWSKI M., PEPE C. (2002) – *Geotechnical Characterization of the Subsoil of the Pisa Tower*. Invited Lecture International Workshop on Characterization and Engineering Properties of Natural Soils (National University of Singapore, Dec. 2002), Balkema, vol. II, pp. 909-946.
- LO PRESTI D., MEISINA C., SQUEGLIA N. (2009) – *Applicabilità di prove penetrometriche statiche nella ricostruzione del profilo stratigrafico* Rivista Italiana di Geotecnica, n. 2, pp.9-33.
- MARCONCINI M. (2016) – *Procedura Innovativa per la Determinazione dei parametri di Resistenza da Prove CPTu in Terreni Parzialmente Saturi*. B. Sc. Thesis, University of Pisa.
- MBONIMPA M., AUBERTIN M., CHAPUIS R.P., BUSSIÈRE B. (2000) – *Développement de fonctions hydriques utilisant les propriétés géotechniques de base*. Proc. 1st Joint IAH-CNC and CGS Groundwater Specialty Conference, 53rd Canadian Geotechnical Conference, Montreal, Quebec, Canada, pp. 343-350.
- MBONIMPA M., AUBERTIN M., CHAPUIS R.P., BUSSIÈRE B. (2002) – *Practical pedotransfer functions for estimating*

the saturated hydraulic conductivity. Geotechnical and Geological Engineering.

MEISINA C. (1996) – *Criteri e metodi per la valutazione della capacità di rigonfiamento di alcuni terreni e suoli affioranti nel territorio pavese*. Tesi di Dottorato in ricerca in Scienze della Terra, VIII° ciclo, Università di Pavia.

PONZANELLI M. (2014) – *Ricostruzione del profilo stratigrafico tramite prove penetrometriche statiche*. B. Sc. Thesis University of Pisa.

ROBERTSON P. K., CAMPANELLA R. G., GILLESPIE D., GRIEG J. (1986) – *Use of Piezometer Cone Data*. Proc. ASCE, Geotechnical Special Publication GSP n. 6, pp.1263-1280.

ROBERTSON P.K. (1990) – *Soil classification using the cone penetration test*. Canadian Geotechnical Journal, n.27, pp. 151-158.

ROBERTSON P.K., WRIDE C.E. (1998) – *Evaluating Cyclic Liquefaction Potential Using the Cone Penetration Test*. Canadian Geotechnical Journal, vol. XXXV, n.3, pp.442-459.

ROSIGNOLI L. (2014) – *Uso della Prova Penetrometrica Statica (CPT) nelle Analisi di Stabilità dei Pendii*. M. Sc. Thesis. University of Pisa.

SCARDIGLI A. (2014) – *Interpretazione della prova penetrometrica statica in terreni comprimibili (argille e torbe)*. B. Sc. Thesis University of Pisa.

SCHMERTMANN J.H. (1976) – *An Updated Correlation between Relative Density DR and Fugro-Type Electric Cone Bearing, qc*. Contract Report DACW 39-76 M 6646 WES, Vicksburg, Miss., 1976

SCHMERTMANN J.H. (1978) – *Guidelines for cone penetration test performance and design*. US Dept. of Transportation, FHWA, R.78-209. Washington D.C.

SEARLE J.W. (1979) – *The Interpretation of Begemann Friction Jacket Cone Results to Give Soil Types and Design Parameters*. Design Parameters in Geotechnical Engineering, BCS London. 2, pp. 265-270.

TATSUOKA F. (2015) – *Compaction Characteristics and Physical Properties of Compacted Soil Controlled by the Degree of Saturation*. Proc. Sixth International Symposium on Deformation Characteristics of Geomaterials. Buenos Aires, Nov. 2015.

ZACCAGNINO C. (2014) – *Interpretazione della prova penetrometrica statica (CPT) su terreni parzialmente saturi e comprimibili*. B. Sc. Thesis University of Pisa.

Interpretazione di prove CPTu in terreni atipici

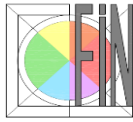
Sommario

Il lavoro riguarda l'interpretazione delle prove CPTu eseguite in terreni inusuali come quelli sopra falda, influenzati dalla suzione, o i terreni di intermedia permeabilità allo stato sciolto.

Per i terreni sopra falda l'articolo mostra un possibile approccio per ricavare la tensione verticale efficace (comprensiva della suzione) dall'indice I_c . Questo approccio è stato verificato rispetto ad un numero molto limitato di evidenze sperimentali. Il metodo consiste nel correggere il valore dell'indice incrementando arbitrariamente a diverse profondità il valore della pressione interstiziale (negativa) in modo da ottenere un incremento della tensione efficace. L'obiettivo è quello di ottenere un valore dell'indice corrispondente a quello misurato sotto falda. Il metodo può essere applicato a strati omogenei. Viene avanzata l'ipotesi che la tensione così determinata rappresenti la tensione di preconsolidazione.

Inoltre viene fornita una correzione empirica dell'indice I_c , applicabile solamente ai casi di studio. La metodologia seguita può essere replicata e calibrata in situazioni differenti.

La correzione offre il vantaggio di poter continuare a interpretare le prove CPTu utilizzando i software comunemente utilizzati.



Differences between mechanical and electrical cone penetration test in the liquefaction hazard assessment and soil profile reconstruction

Claudia Meisina¹, Maria Giuseppina Persichillo¹, Matteo Francesconi², Marco Creatini²,
Diego Carlo Lo Presti²

¹Department of Earth and Environmental Sciences, University of Pavia, Pavia, Italy

²Department of Civil and Industrial Engineering, University of Pisa, Pisa, Italy

Abstract

Liquefaction - hazard assessment is often accomplished by means of simplified procedures, which are based on CPT. The CPT liquefaction procedures, generally, require cone penetration test with electrical tip or the measure of u (CPTu); however, in most countries, as Italy, penetrometric tests are carried out with mechanical tip (CPTm). Generally, CPTm leads to an estimate of the Liquefaction Potential lower than that inferred from CPTu. Moreover, CPTm has a reduced resolution in soil profiling. While the cone – shape effects on q_c are not very relevant, those on f_s can strongly influence the FS_L calculation, especially in the case of silty sands. Within this framework, the main aim of this work is to identify the differences in liquefaction - hazard evaluation and soil profile interpretation in pairs of CPTm/CPTu. After that, two methodologies were used to correct CPTm results. At first, it was developed an empirical correlation between the sleeve friction measured with CPTm and that measured with electrical CPT/CPTu. After that, a method developed in literature was applied to the same CPTm/CPTu pairs. The two corrections were compared in order to see which one led to the best results in terms of enhancement of the liquefaction hazard assessment and soil profile reconstruction. Tests have been carried out in the area interested by the 2012 Emilia earthquake (Italy).

Keywords: Liquefaction hazard assessment, cone penetration test, Liquefaction Potential, soil profiling, 2012 Emilia Romagna earthquake.

1 INTRODUCTION

Liquefaction mainly occurs in saturated sandy soils and causes the loss of shear strength, which in turn leads to an almost complete loss of bearing capacity. As a consequence, the structures experience high differential settlements, tilting, or overturning. Eventually, in the free field conditions, sand ejecta and pore water pressure increase can damage infrastructures and lifeline systems. Recent examples of these effects include damage produced during the 2012 Emilia and 2010-2011 Canterbury earthquakes [1][2]. The identification of the area prone to liquefaction is therefore an important task for land use planning and provides decision makers useful information about the necessity of site-specific in-depth geotechnical investigation and the identification of areas requiring ground improvement.

The most known methods for liquefaction hazard assessment are simplified empirical (or semi – empirical) procedures (Liquefaction Evaluation Procedures – LEPs) [3][4][5].

Simplified procedures evaluate the liquefaction potential of soils computing the factor of safety (FS_L) against liquefaction at a given depth in the soil profile and consist of two steps: 1) to evaluate the earthquake-induced shear stress through an estimate of the cyclic stress ratio (CSR) [3] and 2) to evaluate the soil strength to liquefaction usually accomplished through an estimate of the cyclic resistance ratio (CRR). Because of the difficulty of sampling, CRR is



generally determined via in situ tests, such as standard penetration test (SPT) [3][6], cone penetration test (CPT) [7][8][9], shear wave velocity (V_s) [10], flat dilatometer tests (DMTs), and self-boring pressure meter (SBPT). Once the safety factor against liquefaction has been computed at various depths, numerical indicators or qualitative criteria to define the liquefaction severity at ground level can be used such as the LPI index [11] or the LSN parameter [12].

CPT based LEPs were developed with reference to the results of CPTu tests (i.e. cone tests with piezocone). On the other hand, in some countries, as Italy, huge databases of cone tests with mechanical tip (CPTm) are available.

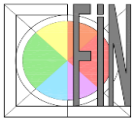
This paper is aimed at demonstrating that available CPTm databases can be used for the prediction of the liquefaction risk. The obtained risk estimate essentially coincides with that inferred by using CPTu if the results of CPTm are subjected to appropriate corrections of the measured sleeve friction and of the estimated I_c index. For the accomplishment of the final objective the following steps were developed:

- To identify the main differences between CPTm and CPTu results with special emphasis on the assessment of liquefaction hazard;
- To find an empirical correlation between the sleeve friction measured with mechanical tip and that measured with piezocone in order to correct CPTm results;
- To compare the SBT class, evaluated according to Robertson 1990 [13], to that given by Schmertmann (1978) [14] classification chart for a large CPTm database;
- To find an empirical correction of the I_c index [13], so that the Robertson SBT class coincide with that of Schmertmann (1978) [14];
- To apply both corrections to pairs of tests (CPTm and CPTu) realized at short distances from each other in order to verify the effectiveness of the proposed methodology.

2 CPTm - CPTu: MAIN DIFFERENCES

Main differences between CPTm and CPTu results and capabilities can be summarised as follows:

- CPTm measurements are carried out every 20 cm. On the contrary measurements with piezocone as well as those with electrical tip are repeated every 2 cm. Therefore, CPTu have a higher resolution and can detect even very thin liquefiable layers. Recently, the use of mini cones was suggested in order to increase the cone capabilities especially in thin layered soil deposits. Analysis of possible advantages of the use of mini cones is beyond the scope of the present paper. Actually, various producers offer mini cones (see as an example [15]);
- Use of piezocone enables us to measure the dynamic pore pressure during penetration and to check deviation from verticality. Pore pressure measurements are relevant for the assessment of total tip resistance which is not very relevant in sands. Deviation from verticality can provide a more accurate estimate of layer thickness and depth;
- Reduction of the diameter of the tip above the cone, as in the mechanical penetrometer, leads to q_c measurements lower than those obtained from piezocone. This aspect is especially relevant in very dense sands. On the contrary, the soil friction along the protective sleeve above the cone is responsible for q_c values greater than those obtained from CPTu. This is especially relevant in loose sand and soft clay;
- In the case of Begemann cone with sleeve not only do we measure the friction but, because of the union at the lower end of the sleeve, also a part of resistance at the base (return flow material after the cone has passed). For this reason f_s measured with the mechanical bit is always greater than the one measured with the electrical bit (the difference is practically



- negligible for clay). While the cone – shape effects on q_c are not very relevant, those on f_s can strongly influence the FS_L calculation, especially in the case of silty sands;
- On the whole, CPTm interpretation using SBT classes or I_c index that have been developed for the interpretation of CPTu tends to underestimate the grain size.

3 PROPOSED METHODOLOGY

3.1 Sleeve friction correction

Penetrometric tests CPTm and CPTu were carried out at a site in Pisa (central Italy) with the support of Pagani Ltd and Geoservizi snc (Figure 1) in order to find out an empirical correlation between f_s (CPTm) and f_s (CPTu).

This site was selected for various reasons: a) availability of a previous geotechnical campaign (boreholes), carried out in October 2009, and b) stratigraphic variability which includes various lithotypes. In fact the first 10 meters depth are characterized by silty, sandy and clayey layers. Three continuous boreholes S1, S2 and S3 were carried out in 2009 (Figure 1). Distances between these boreholes and CPTs are respectively of about 50, 80 and 90 meters. It is worth noting that the subsoil of the investigated area exhibits a very low horizontal variability. From a geological point of view the site consists of recent alluvial deposits. The subsoil is very similar to that existing beneath the leaning Tower of Pisa and consists of an upper thin layer of silty clay, a thick layer of marine soft clay with an interbedded layer of sand (in between 7 – 8 m depth). The piezometric surface is located about 1 meter below the ground level (GWT).

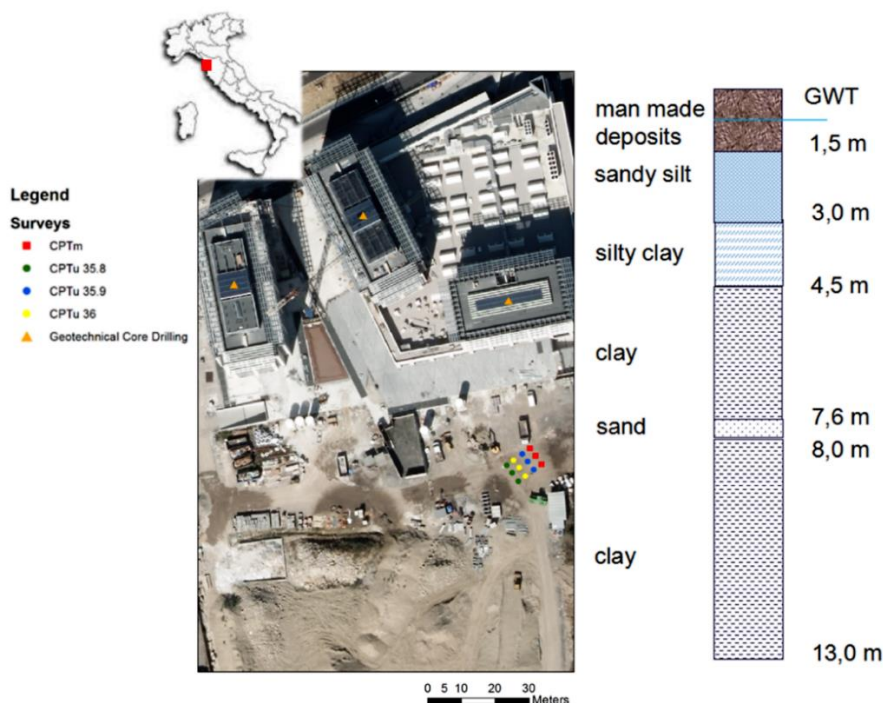
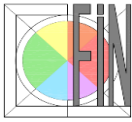


Figure 1 Location of CPTm and CPTu in Pisa (Porta a Mare)

Twelve penetration tests (3 CPTm and 9 CPTu) were carried out using a penetrometer Pagani TG 73/200. Three different sleeve diameters (35.8 mm, 35.9mm and 36mm) of piezocone were used in order to investigate a possible influence on the measured f_s parameter.



In fact the ASTM standard allows the use of sleeves having a diameter equal to that of the cone (35.7 mm) with a tolerance of 0 - 0.3 mm (sleeves with a diameter of 35.7 to 36.0 mm are then allowed). Test repetition was adopted in order to minimize differences due to soil heterogeneity.

The tests were performed following a regular square grid of 0.5 meter (Figure 2); this distance was chosen to minimize the reciprocal influence between near tests. For each test a pre-drilled hole of about one meter was performed due to the presence of very compact man-made deposits. The investigation depth varied from 7 to 11 meters.

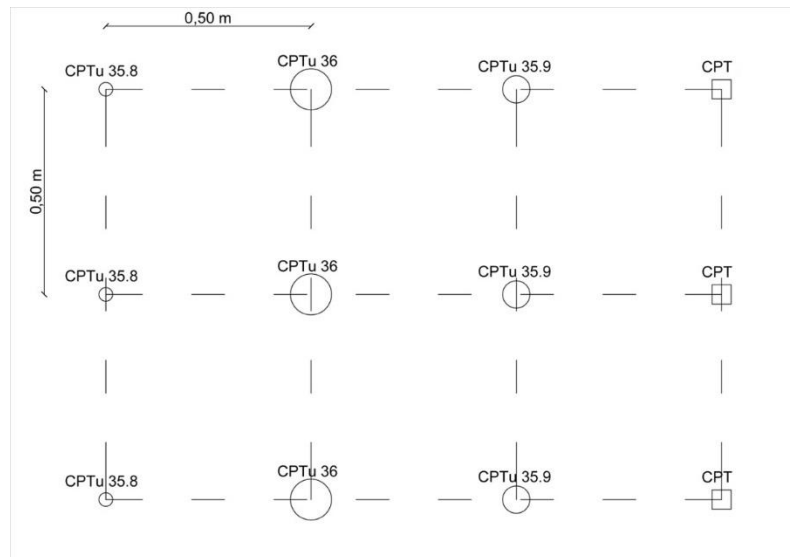


Figure 2 CPTm and CPTu scheme.

Figure 3 shows the results of the Pisa CPTm and CPTu surveys; the q_c and f_s values have been averaged for CPTm and for the different sleeve diameters of CPTu. It is evident that the q_c and f_s parameters do not depend on the diameter of the sleeve in the case of CPTu tests. The comparison shows that the differences in terms of tip resistance between CPTu and CPTm are negligible and can be mainly attributed to soil heterogeneity while $f_s(\text{CPTm})$ is systematically greater than $f_s(\text{CPTu})$. Finally, it can be observed how the overestimation of the f_s parameter during the survey with mechanical tip depends on the type of soil crossed.

Using the results of the tests that have been carried out at Pisa and those of four pairs of CPTm/CPTu from Emilia-Romagna Region database [16], a correlation function between the $f_s(\text{CPTm})$ and the $f_s(\text{CPTu})$ was found.

A depth correction for CPTm was necessary in order to correctly couple the tip resistance q_c and the sleeve friction f_s . More precisely the tip resistance of CPTm is measured after a penetration of 4 cm, while the sleeve friction is obtained by subtraction after a penetration of another 4 cm. During this second penetration both tip resistance and sleeve friction are measured. After that, the cone is moved for additional 12 cm and conventionally the measured q_c and f_s are associated to such a final depth (i.e. 20 cm below the beginning of the measurements). In order to correctly couple the measured values of f_s from the two different test types, each value of $f_s(\text{CPTm})$ was associated with the average of 5 values of $f_s(\text{CPTu})$ including that at the same height of the CPTm, the two values immediately above and the two values immediately below. Indeed, the depth of the $f_s(\text{CPTm})$ parameter has to take into account not only what has already been stated about the different depth associated with the tip resistance measurements, but also the relative distance between tip and mantle (and mantle length). In particular, the mid height of the mantle (CPTm) is located 20 cm above the tip base.



The data were finally evaluated on the basis of the differences between $q_c(\text{CPTm})$ and $q_c(\text{CPTu})$, taking into account the values of f_s that are associated to $\Delta q_c < 0,25 \text{ MPa}$ and excluding values that may be affected by horizontal soil variability.

The correlation between $f_s(\text{CPTm})$ and $f_s(\text{CPTu})$ was identified using the two separate variables and the ratio of the two variables. The best correlation was found placing the ratio of $f_s(\text{CPTu})/f_s(\text{CPTm})$ versus $f_s(\text{CPTu})$ as shown in Figure 4.

The obtained empirical equation is reported below. It is applicable only when $f_s < 65 \text{ kPa}$

$$f_s(\text{CPTu}) = [0,0797 \cdot f_s(\text{CPTm})]^{2,504} \text{ if } f_s(\text{CPTm}) < 65 \text{ kPa} \tag{1}$$

$$f_s(\text{CPTu}) = f_s(\text{CPTm}) \text{ if } f_s(\text{CPTm}) \geq 65 \text{ kPa} \tag{2}$$

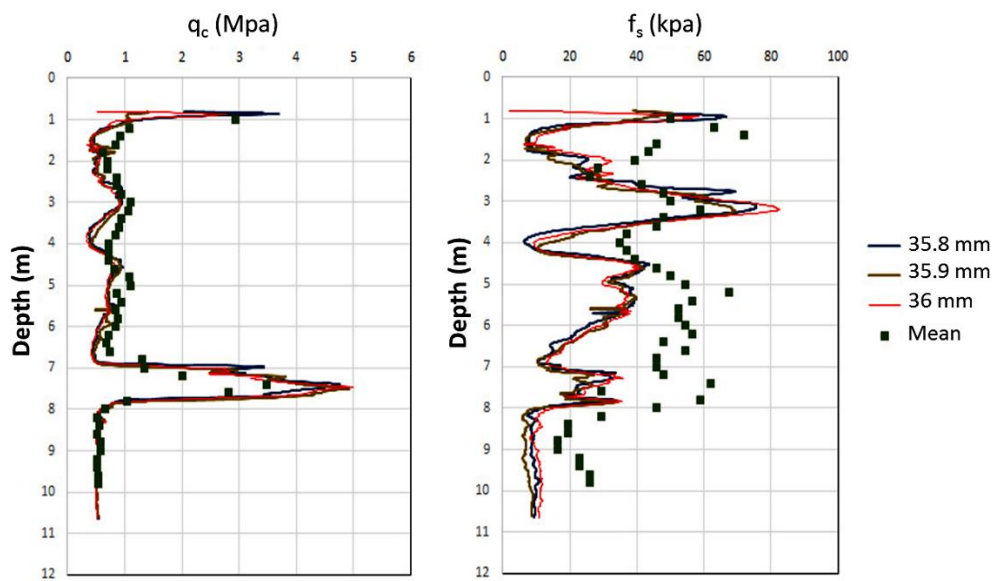


Fig.3 Comparison of CPTu and CPTm results at Pisa site

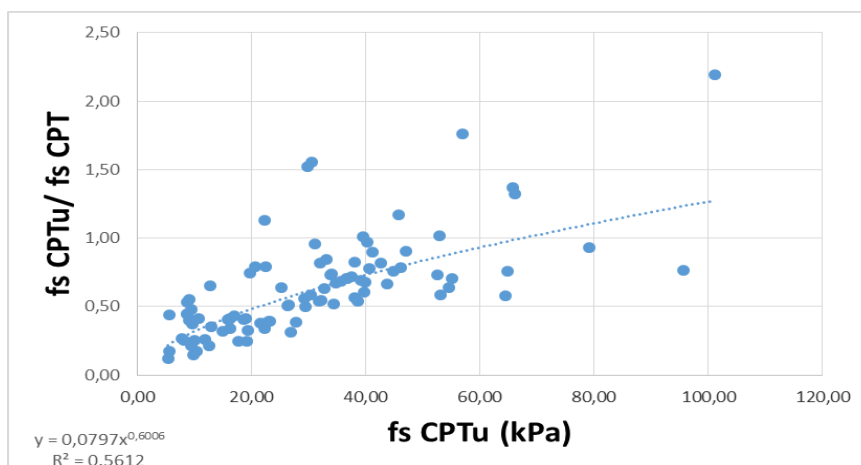
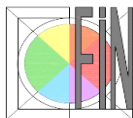


Figure 4 Correlation function between $f_s(\text{CPTm})$ and $f_s(\text{CPTu})$



3.2 SBT - Ic index correction

As a matter of fact, use of CPTu - based classification charts (see as an example [13]) for the interpretation of CPTm leads to erroneous evaluation. In particular, on the Authors experience, use of Robertson (1990) approach [13] to interpret CPTm gives an underestimate of the soil grain size. In order to compare the two approaches, which are different in principle, a correspondence among the lithotypes of the Schmertmann (1978) approach [14] and the SBTn classes by Robertson (1990) [13] was proposed (Table 1).

A database of 78 CPTm carried out in the urban area of San Carlo, Mirabello and Sant'Agostino, located in the Emilia Romagna Region (Italy) and hit by the 2012 Emilia Romagna Seismic Sequence, were interpreted by using both Schmertmann (1978) [14] and Robertson (1990) [13] approaches.

Table 1 Correspondence between [14]Schmertmann (1978) and [13]Robertson (1990) approaches (Classes 1 and 9 of Robertson approach were not considered)

Schmertmann (1978)	SBTn (Robertson 1990)	Normalized class description
Organic clay and mixed soils	2	Organic soils, peats
Insensitive non fissured inorganic clays	3	Clays: clay to silty clay
Sandy and silty clays	4	Silt mixtures: clayey silt to silty clay
Clayey sands and silts	5	Sand mixtures: silty sand to sandy silt
Silt - sand mixtures	5	Sand mixtures: silty sand to sandy silt
Sands	6-7	Sands: clean sand to silty sand; Gravely sands to sands
Dense or cemented sands	8	Very stiff sand to clayey sand
Very shell sands, limerocks	8	Very stiff sand to clayey sand

On the whole, over 6141 CPTm measurements, a perfect match between the two approaches was obtained for 2168 cases (35%). On the other hand [13]Robertson (1990) approach underestimated of one class the [14]Schmertmann (1978) classification in 1445 cases (24%) and of two classes in 963 cases (16%). Overestimate of one or two classes was obtained respectively in 1234 (20%) and 331 cases (5%). The perfect match between the two systems was mainly observed for classes 3-4 and 5. Organic clays (according to [14]Schmertmann 1978) are classified as clays (according to [13]Robertson (1990)). The Robertson overestimate (OE) mainly concerned this type of soils. On the other hand, the Robertson underestimate (UE) concerned the sandy soils. Figures 5a to 5b clearly show that the class 6 has a limited number of cases, while 7 and/or 8 are completely absent in the [13]Robertson 1990 chart. On the contrary, the [14]Schmertmann (1978) chart exhibit a relevant number of points in the sand and silt/sand areas.

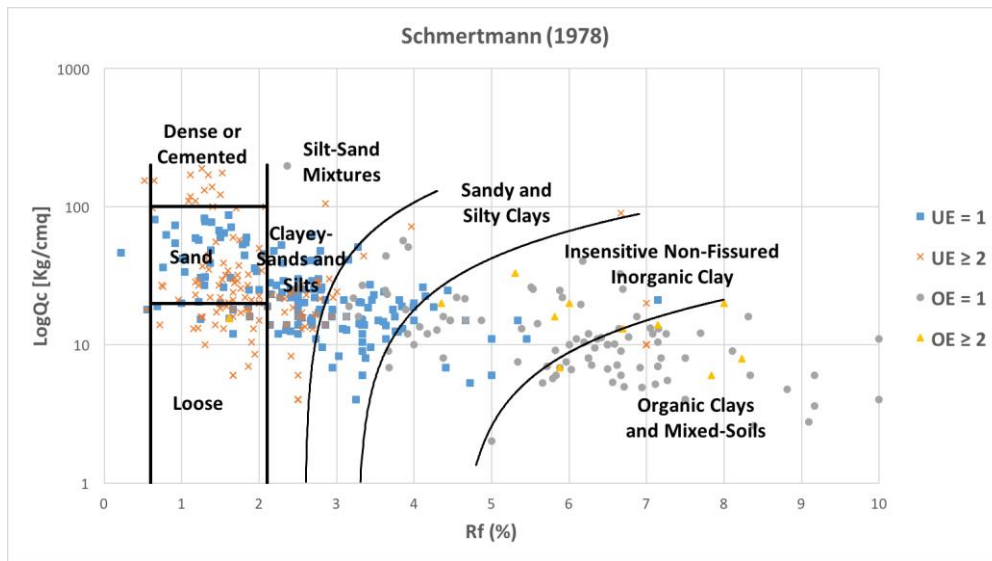


Figure 5a Schmertmann (1978) classification of CPTm

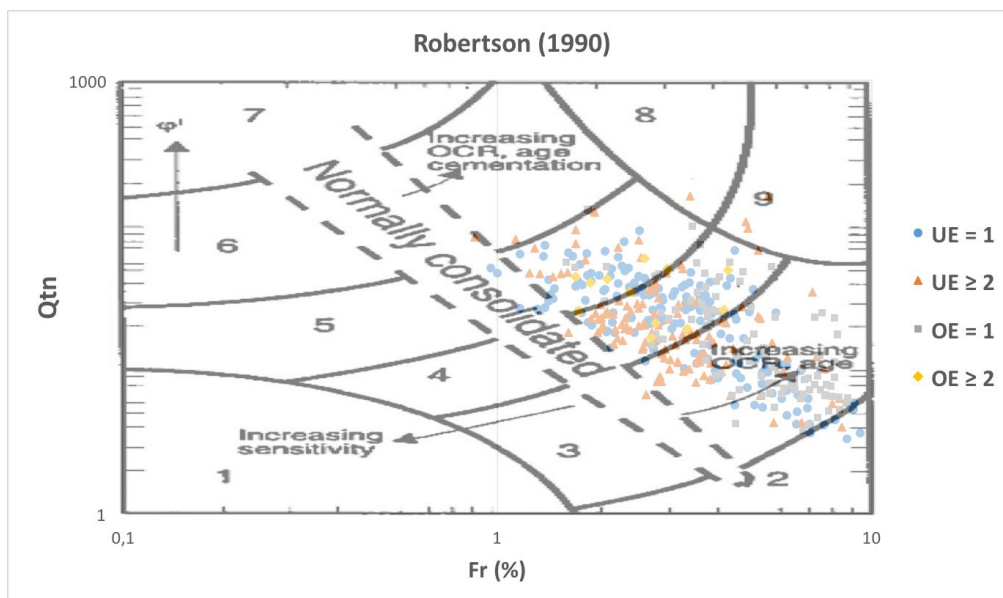


Figure 5b Robertson (1990) classification of CPTm

Application of fs correction, as stated in the previous section, did not modify the above discussed aspect. Therefore, it was decided to compute the necessary ΔI_c to have a correct match between the two classification systems.

$$\Delta I_c = I_c(\text{OV}) - I_c(\text{PM})$$

Where: $I_c(\text{OV})$ = is the I_c index from [13]Robertson (1990) classification; $I_c(\text{PM})$ = is the mean value corresponding to the SBTn class that matches the [14] Schmertmann (1978) classification.

This was done only for the potentially liquefiable layers (clayey soils were not considered). Figure 6 shows the variation of ΔI_c vs. the tip resistance expressed in MPa.

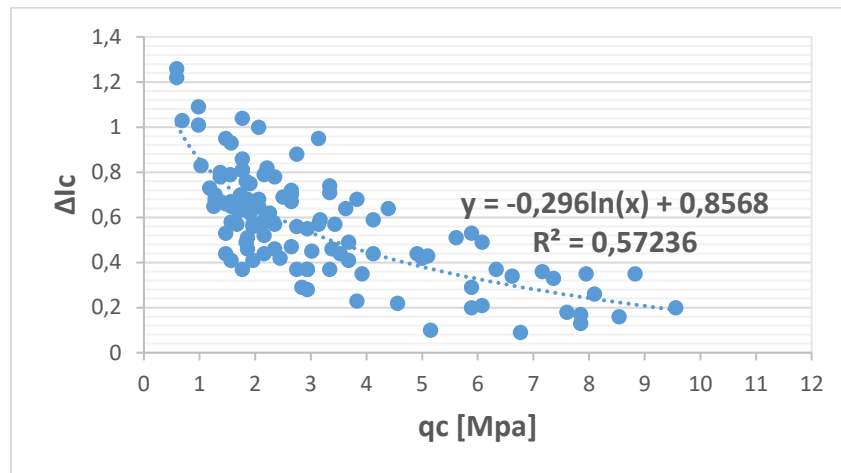
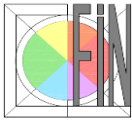


Figure 6 Variation of ΔI_c vs. the tip resistance

4. APPLICATION OF THE DEVELOPED METHODOLOGY

The proposed methodology was applied to the Emilia Romagna database. Nonetheless the considered database was huge, only four pairs of CPTm/CPTu tests were found within a relative distance CPTm-CPTu ranging from 13 to 36 m. For each pair of tests a reference borehole, with a maximum distance of 65 m from the considered CPT, was selected in order to define a reference stratigraphic profile.

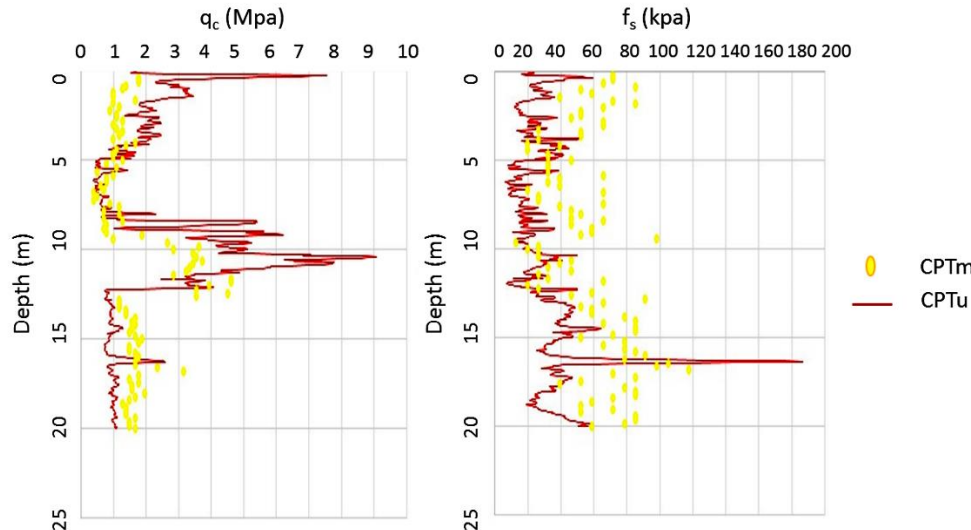


Figure 7 q_c -depth and f_s -depth (CPTm and CPTu).

Factors of safety against liquefaction were computed according to the procedures proposed by [17][18][19][4]. In this paper only the results obtained by the [4] Boulanger and Idriss (2014) method are shown.

Figures 7 compare the tip resistance and sleeve friction of one pair of penetration tests. It is possible to observe a certain heterogeneity. Therefore, it was decided to disregard the comparison if at a given depth, $q_c(\text{CPTu}) - q_c(\text{CPTm}) > 0.1$ MPa. Figure 7 clearly confirms (apart possible heterogeneity) that the tip resistance is not too much influenced by the type of tip, on the contrary it is always possible to observe that $f_s(\text{CPTm}) > f_s(\text{CPTu})$.



Figures 8 compares the SBT profile of CPTm and CPTu with the borehole profile. It is confirmed that the use of classification methods which were developed to interpret CPTu, mainly causes the loss of sandy to silty liquefiable layers.

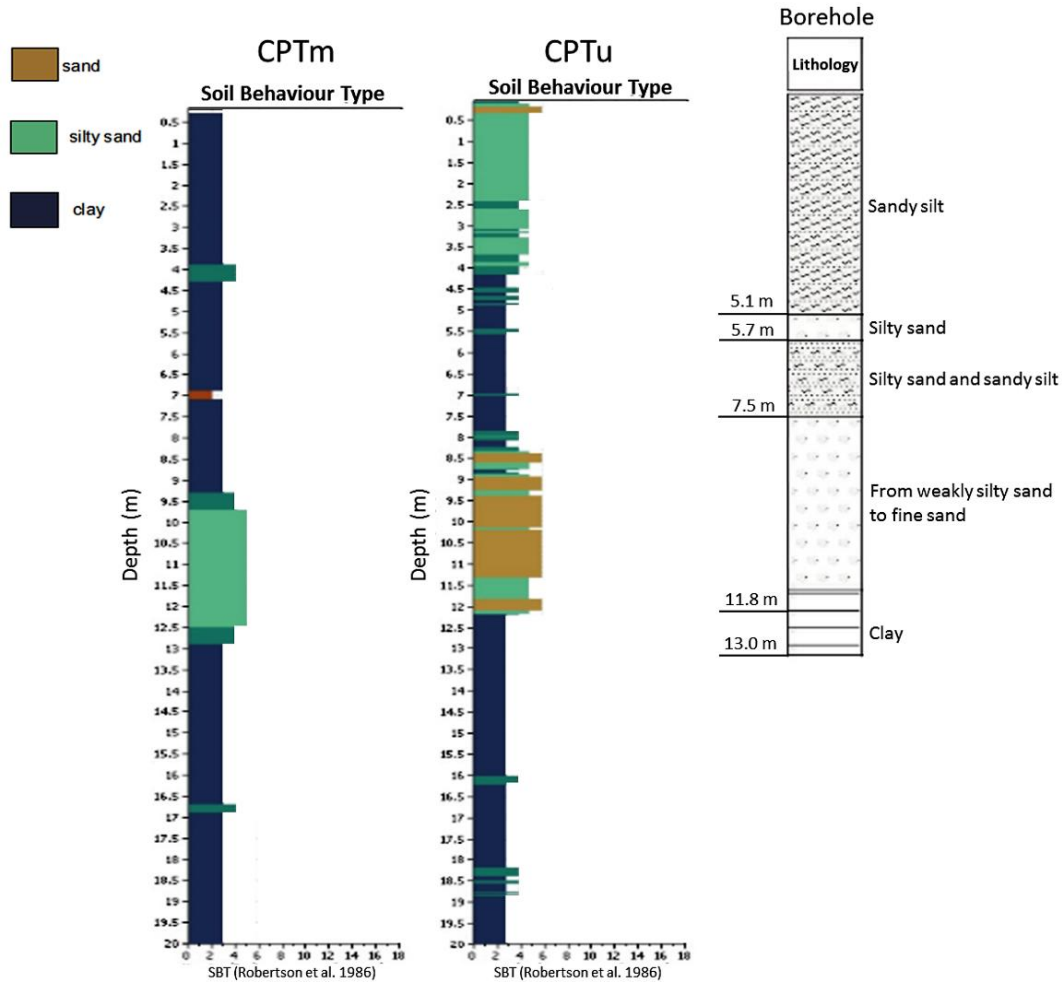


Figure 8 Comparison of the SBT graphics and the borehole.

The effectiveness of the proposed method is shown in Figures 9 where, for the considered pairs of penetration tests, the FS_L profile is shown. It is possible to notice that, after the application of the above described correction factors the FS_L profile from CPTm is very similar to that obtained from CPTu.

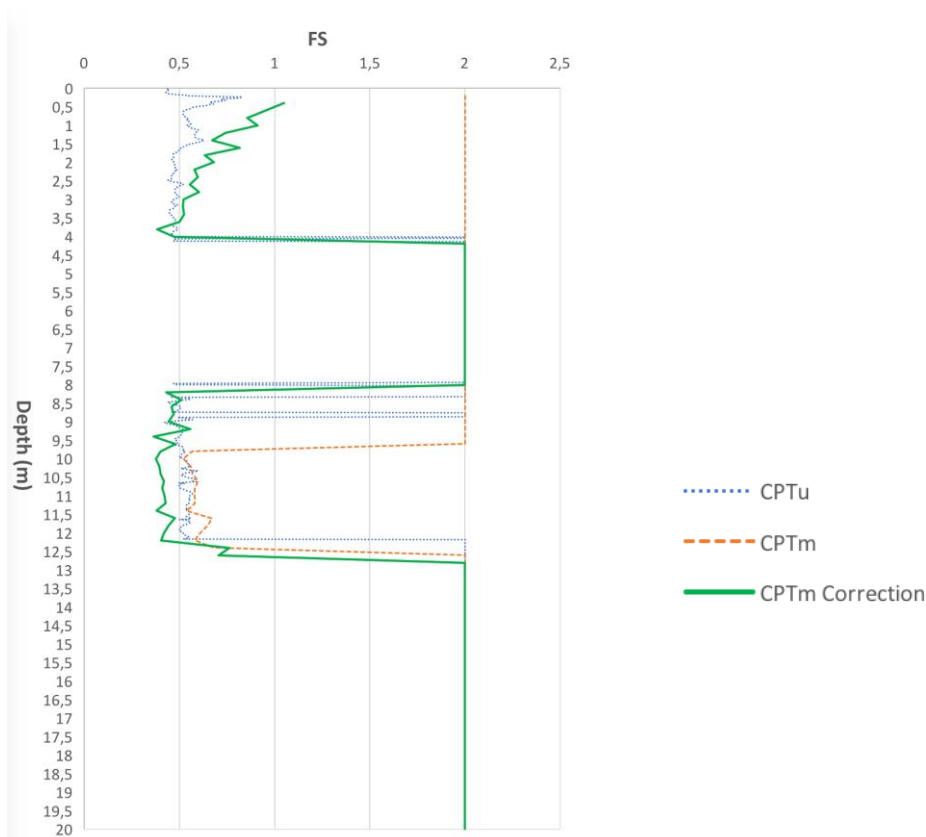
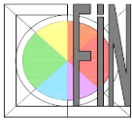


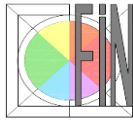
Figure 9 Comparison between the FS_L profiles

5. Conclusions

The paper demonstrates the possibility of using available database of CPTm for defining the liquefaction risk if appropriate correction factors are applied. The proposed correction factors should be calibrated in different context. Even though, the use of CPTu remains highly recommended for liquefaction hazard analyses, the proposed methodology is a very useful tool for those countries where CPTm databases are available.

6. Reference List

- [1] Lo Presti D. C. F., Sassu M., Luzi L., Pacor F., Castaldini D., Tosatti G., Meisina C., Zizioli D., Zucca F., Rossi G., Saccorotti G., Piccinini D. (2013). A report on the 2012 seismic sequence in Emilia (Northern Italy). *Seventh International Conference on case Histories in Geotechnical Engineering*, April 29-May 4, 2013 Chicago. ISBN 1-887009-17-5.
- [2] Bray J.D. , Zupan J.D., Cubrinovski M., Taylor M. (2014). CPT-based liquefaction assessments in Christchurch, New Zealand. *Papers of the 3rd International Symposium on Cone Penetration Testing*, Las Vegas, Nevada.
- [3] Seed, H. B. and Idriss, I. M. (1971). Simplified Procedure for Evaluating Soil Liquefaction Potential. *Journal of the Soil Mechanics and Foundations Division*, ASCE, Vol. 97, No SM9, Proc. Paper 8371, September 1971, 1249-1273.
- [4] Boulanger, R. W., and Idriss, I. M. (2014). CPT and SPT based liquefaction triggering procedures. *Report No. UCD/CGM-14/01*, Center for Geotechnical Modeling, Department of Civil and Environmental Engineering, University of California, Davis, CA, 134 pp



- [5] Robertson P.K. and Wride C.E. (1998). Evaluating Cyclic Liquefaction Potential Using the Cone Penetration Test, *Canadian Geotechnical Journal*, 35: 442-459.
- [6] Youd T.L. et al. (2001). Liquefaction resistance of soils: Summary report from the 1996 NCEER and 1998 NCEER/NSF workshops on evaluation of liquefaction resistance of soils, *Journal of Geotechnical and Geoenvironmental Engineering*, 127: 817-833.
- [7] Idriss, I. M., and Boulanger, R. W. (2006). Semi-empirical procedures for evaluating liquefaction potential during earthquakes, *J. Soil Dynamics and Earthquake Eng.* 26: 115–30.
- [8] Robertson, P.K. and Campanella, R.G. (1985). Liquefaction potential of sands using the cone penetration test, *Journal of Geotechnical Division of ASCE*, 22(3): 277-286.
- [9] Juang, C.H., Yuan, H., Lee, D.-H., and Lin, P.-S. (2003). Simplified Cone Penetration Test-based Method for Evaluating Liquefaction Resistance of Soils . *Journal of Geotechnical and Geoenvironmental Engineering*, 129: 66-80.
- [10] Andrus, R.D. and Stokoe, K.H., (2000). Liquefaction Resistance of Soils from Shear-Wave Velocity. *Journal of Geotechnical and Geoenvironmental Engineering*, 126 (11): 1015-1025.
- [11] Iwasaki, T., Tokida, K., Tatsuko, F., and Yasuda, S. (1978). A practical method for assessing soil liquefaction potential based on case studies at various sites in Japan. *Proceeding of the 2nd International Conference on Microzonation for Safer Construction-Research and Application*, San Francisco, California, Vol. 2, 885–896.
- [12] Tonkin e Taylor (2013). Liquefaction Vulnerability Study. Tonkin e Taylor Ltd.
- [13] Robertson P.K. (1990). Soil Classification Using the Cone Penetration Test. *Canadian Geotechnical Journal*, Vol. 27, pp. 151-158.
- [14] Schmertmann J.H. (1978). *Guidelines for Cone Penetration Test. Performance and Design*, U.S. Department of Transportation, Washington.
- [15] Pagani geotechnical equipment. 2017. <http://www.pagani-geotechnical.com/it>
- [16] Regione Emilia Romagna (Italy). 2011. La banca dati geognostica. See <http://ambiente.regione.emilia-romagna.it/geologia/cartografia/webgis-banchedati/banca-dati-geognostica>.
- [17] Robertson P.K. (2009). Interpretation of cone penetration tests – A unified approach. *Canadian Geotechnical Journal*, 46: 1337-1355.
- [18] Idriss I.M. e Boulanger R.W. (2008). Soil Liquefaction during Earthquakes. *Earthquake Engineering Research Institute*.
- [19] Moss R.E.S et al. (2006). CPT-based probabilistic and deterministic Assessment of in situ seismic soil liquefaction potential. *Journal of Geotechnical and Geoenvironmental Engineering*, 132: 1032-1051.